DISSERTATIONES
SCIENTIAE
MATERIALIS
UNIVERSITATIS
TARTUENSIS
**39**

ALEXANDRA NEFEDOVA

# Oxide nanostructures as antiviral coatings for textiles

DISSERTATIONES SCIENTIAE MATERIALIS UNIVERSITATIS TARTUENSIS
**39**

**ALEXANDRA NEFEDOVA**

# Oxide nanostructures as antiviral coatings for textiles

UNIVERSITY OF TARTU
Press
1632

This study was carried out at the Institute of Physics and Institute of Molecular and Cell Biology, Faculty of Science and Technology, University of Tartu.

The Dissertation was admitted on September 18th, 2025, in partial fulfilment of the requirements for the degree of Doctor of Philosophy in Materials Science and allowed for defence by the Scientific Council on Materials Science of the Faculty of Science and Technology of the University of Tartu.

Supervisors: Prof. Angela Ivask,
Institute of Molecular and Cell Biology, University of Tartu
Dr. Alexander Vanetsev,
Institute of Physics, University of Tartu
Prof. Vambola Kisand, Institute of Physics,
University of Tartu

Opponent: Dr. Nadiya M. Zholobak,
Zabolotny Institute of Microbiology and Virology,
National Academy of Sciences of Ukraine

Defence: November the 14th, 2025 at University of Tartu, Tartu, Estonia

This work was financially supported by Estonian Research Council Grants (COVSG2, PRG1496, TK210), the European Commission project STOP (Grant agreement ID: 101057961). This work was also supported by The Centre of Excellence project TK141 (2014–2020.4.01.15-0011), Functional Materials and Technology Doctoral School (FMTDK) (2014–2020.4.01.16-0027) and Estonian Doctoral School (2021–2027.4.04.24-0003), all co-funded by the European Union.


ISSN 2228-0928 (print)
ISBN 978-9908-57-033-4 (print)
ISSN 2806-2574 (pdf)
ISBN 978-9908-57-034-1 (pdf)



University of Tartu Press
www.tyk.ee

# TABLE OF CONTENTS

## LIST OF PUBLICATIONS INCLUDED IN THE THESIS

This thesis is based on three original publications listed below. The publications are reprinted in accordance with open-access license.

I. Nefedova, Alexandra; Rausalu, Kai; Zusinaite, Eva; Vanetsev, Alexander; Rosenberg, Merilin; Koppel, Kairi; Lilla, Stevin; Visnapuu, Meeri; Smits, Krisjanis; Kisand, Vambola; Tätte, Tanel; Ivask, Angela, Antiviral efficacy of cerium oxide nanoparticles, Scientific Reports, 2022, 12, 18746, https://doi.org/10.1038/s41598-022-23465-6.

II. Nefedova, Alexandra; Rausalu, Kai; Zusinaite, Eva; Kisand, Vambola; Kook, Mati; Šmits, Krišjānis; Vanetsev, Alexander; Ivask, Angela, Antiviral efficacy of nanomaterial-treated textiles in real-life like exposure conditions, Heliyon, 2023, 9 (9), e20067, https://doi.org/10.1016/j.heliyon.2023.e20067.

III. Nefedova, Alexandra; Svensson, Fredric G; Vanetsev, Alexander S; Agback, Peter; Agback, Tatiana; Gohil, Suresh; Kloo, Lars; Tätte, Tanel; Ivask, Angela; Seisenbaeva, Gulaim A; Kessler, Vadim G., Molecular Mechanisms in Metal Oxide Nanoparticle-Tryptophan Interactions, Inorganic Chemistry, 2024, 63 (19), 8556–8566, https://doi.org/10.1021/acs.inorgchem.3c03674.

## AUTHOR'S CONTRIBUTION

I. Synthesis and characterization of nanoparticles, analyzing and interpreting the data, writing and editing the text.

II. Synthesis and characterization of nanoparticles, antiviral tests on TGEV, analyzing and interpreting the data, writing and editing the text.

III. Synthesis and characterization of nanoparticles. FTIR characterization.

# OTHER PUBLICATIONS


Kaldvee, K.; Nefedova, A.V.; Fedorenko, S.G.; Vanetsev, A.S.; Orlovskaya, E.O.; Puust, L.; Pärs, M.; Sildos, I.; Ryabova, A.V.; Orlovskii, Yu.V., Approaches to contactless optical thermometer in the NIR spectral range based on $Nd^{3+}$ doped crystalline nanoparticles, Journal of Luminescence, 183, 2017, 478–485, https://doi.org/10.1016/j.jlumin.2016.11.061.

Vanetsev, A., Kaldvee, Kaarel, Puust, L., Keevend, K., Nefedova, A., Fedorenko, S., Baranchikov, A., Sildos, I., Rähn, M., Sammelselg, V., Orlovskii,Y., Relation of crystallinity and fluorescent properties of $LaF_3:Nd^{3+}$ nanoparticles synthesized with different water based techniques, ChemistrySelect, 2 (17), 2017, 4874–4871, https://doi.org/10.1002/slct.201701075.

Vihodceva, S.; Šutka, A.; Iesalnieks, M.; Orlova, L.; Pludonis, A.; Otsus, M.; Sihtmäe, M.; Vija, H.; Nefedova, A.; Ivask, A.; Kahru, A.e; Kasemets, K., Emerging investigator series: $CeO_2$/CuO nanostructured composite with enhanced antimicrobial properties and low cytotoxicity to human keratinocytes in vitro, Environmental Science Nano, 2025, 12 (1), 276–291, https://doi.org/10.1039/d4en00501e.

Greijer, B.; Nefedova, A.; Agback, T.; Agback, P.; Kisand, V.; Rausalu, K.; Vanetsev, A.; Seisenbaeva, G. A.; Ivask, A.; Kessler, V. G., Molecular mechanisms behind the anti corona virus activity of small metal oxide nanoparticles, Nanoscale, 2025, 17 (7), 3728–3738, https://doi.org/10.1039/d4nr03730h.

Vihodceva, S.; Šutka, A.; Iesalnieks, M.; Sihtmäe, M.; Nefedova, A.; Ivask, A.; Blinova, I.; Maiorov, M.; Vanags, M.; Eiduks, T. V.; Plūdons, A.; Kahru, A.; Kasemets, K., Synthesis and antimicrobial efficacy of magnetic CuO/$Fe_2O_3$/$CuFe_2O_4$ nanostructured composite: Mechanisms of action, cytotoxicity to human keratinocytes in vitro, and ecotoxicity towards *Vibrio fischeri* and *Daphnia magna,* Journal of Environmental Chemical Engineering, 2025, 13, (5), 117991, https://doi.org/10.1016/j.jece.2025.117991.

# ABBREVIATIONS AND SYMBOLS

| | |
|---|---|
| ANOVA | Analysis of variance |
| aq | aqueous |
| BSA | Bovine serum albumin |
| ccp | Cubic close packed (structure) |
| CLD | Coded letter display |
| CMC | Carboxymethyl cellulose, sodium salt |
| COVID-19 | Coronavirus disease 2019 |
| CTAB | Cetyltrimethylammonium bromide, also called cetrimonium bromide, hexadecyltrimethylammonium bromide |
| CTAB@$SiO_2$ | CTAB- loaded $SiO_2$ nanocontainers |
| DLS | Dynamic light scattering |
| ds | Double stranded |
| DSS | 2,2-Dimethyl-2-silapentane-5-sulfonate sodium salt (Preferred IUPAC name Sodium 3-(trimethylsilyl)propane-1-sulfonate) |
| HCV | Hepatitis C Virus |
| HIV | Human immunodeficiency Virus |
| HMTA | Hexamethylenetetramine |
| HRTEM | High Resolution Transmission Electron Microscopy |
| HT | Hydrothermal (conditions) |
| ICP-MS | Inductively coupled plasma mass spectrometry |
| ICP-OES | Inductively coupled plasma optical atomic spectroscopy |
| ICTV | International Committee on Taxonomy of Viruses |
| MOF | Metal organic framework |
| MW | Microwave(s) |
| NMR | Nuclear magnetic resonance |
| NP(s) | Nanoparticle(s) |
| NZCYM | New Zealand casein yeast magnesium sulfate (broth) |
| PBS | Phosphate buffered saline |
| PE | Polyethylene |
| PEG | Polyethylene glycol |
| PIC | 3-Hydroxypyrroloindol carboxylic acid |
| POM | Polyoxometalate. |
| PSSS | Poly(sodium 4-styrenesulfonate) |
| PVP | Polyvinylpyrrolidone |
| ROS | Reactive oxygen species |
| RSV | Respiratory syncytial virus |
| RT | Reverse-transcribing |

| | |
|---|---|
| rt | room temperature |
| SCDLP | Soya casein digest lecithin polysorbate broth |
| SEM | Scanning electron microscopy |
| ss | Single stranded |
| TEM | Transmission electron microscopy |
| TPCK | Tosyl phenylalanyl chloromethyl ketone |
| TRP | Tryptophan |
| TSB | Tryptic soy broth |
| W-POM | Phosphotungstic acid |

# 1. INTRODUCTION

Diseases caused by viruses may severely affect people's everyday life. According to World Health Organization [1], seasonal influenza alone infects ca. one billion people annually, of which 3–5 million cases are severe and 290 000 to 650 000 are mortal. Recent COVID-19 pandemics took away seven million lives [2] and caused global social and economic distress. One of the lessons of COVID-19 was that the appearance of novel highly contagious viruses has a high potential for causing new pandemics. Therefore, the prevention of viral infections spreading is and will stay an object of interest of researchers but also health officials.

Pathogens, including viruses, can be transmitted via various routes. Usually, the following main ways of contamination are considered: airborne (via aerosols and droplets), and by direct or indirect contact. Indirect contact includes infection by viruses deposited on objects called fomites [3, 4]. The importance of touch route of transmission varies for different viruses and different conditions but should never be excluded from consideration. An experiment [5] using bacteriophage φX174 as a model virus showed that at least 14 people can be infected by touching the same door handle. The touch transmission of norovirus [6] showed that although people's touch behavior has priority importance in virus transmission, disinfection of touched surfaces should not be neglected either. Potential for surface touch transmission has been also suggested for rhinovirus, coronavirus OC43, adenovirus, and influenza A due to the presence of the genetic material on high touch surfaces in schools, kindergartens and airports [7, 8]. Considering this evidence on possible surface transfer, the ways of elimination of viruses from the surfaces of contaminated objects have attracted significant interest of researchers in the field.

Taking into account the constant evolution of viruses leading to new strains and increase in resistance, the importance of non-pharmaceutical interventions, especially at the early stages of pandemics, when medical treatment nor vaccines are not yet available, cannot be underestimated [3]. The most common solution remains disinfection, however, in many cases the lasting antiviral effect is necessary, which can be achieved only by modification of the surface with introduction of an antiviral function. Indeed, it has been clearly shown in laboratory conditions that hard surfaces and textiles with an intrinsic antiviral function can contribute to prevention of touch-mediated spread of viral infections [9]. Development of textiles with antimicrobial properties is especially compelling since soft surfaces are more difficult to clean and disinfect and at the same time pathogens can persist for a considerable amount of time on them. Application of antiviral surfaces is especially important in environments for people specifically vulnerable to microbial infections, e.g., in healthcare institutions, elderly care institutions, kindergartens and schools but also in food and packaging industry.

Materials used to create surfaces with antiviral activity include solid metals and metal alloys (copper, copper-nickel alloys, brass, silver in case of hard surfaces), polymers and biopolymers, and composites. The most frequently suggested

mechanisms of action of antiviral surfaces include absorption, pH regulation, metal ions release, reactive oxygen species (ROS) formation or direct bounding with viral particles [10]. The current work aiming to suggest a versatile approach for treating of hard to clean surfaces, mainly textiles, with antiviral compounds, initially started as a part of the project “Universal treatment method for antiviral protection of hard to clean surfaces” during COVID-19 pandemics. The main goal was to develop an antiviral treatment for textiles based on surface deposited oxide nanostructures and importantly, ensure their antiviral activity in close to real life conditions.

# 2. LITERATURE REVIEW

## 2.1. Viruses, their classification and replication cycle

The most common definition states that viruses are submicroscopic infectious agents that can only replicate inside a living cell, i.e. viruses are obligate intracellular parasites. More detailed definition was given by Lwov (1957): "strictly intracellular and potentially pathogenic entities with an infectious phase, and (a) possessing only one type of nucleic acid (DNA or RNA), (b) multiplying in the form of their genetic material, (c) unable to grow and to undergo binary fission, (d) devoid of a Lipmann system (an active metabolism)" [11].

In recent decades, these definitions have eroded facing findings that offer counterexamples to almost each of their key points (giant viruses, viroids etc.). A new definition considering evolutionary origin and functioning of viruses was proposed in 2020 [11]. It is as follows: "Viruses *sensu stricto* are defined as a type of MGE (mobile genetic element) that encodes at least one protein that is a major component of the virion encasing the nucleic acid of the respective MGE and therefore the gene encoding the major virion protein itself or MGEs that are clearly demonstrable to be members of a line of evolutionary descent of such major virion protein-encoding entities. Any monophyletic (i.e. descended from a common evolutionary ancestor) group of MGEs that originates from a virion protein-encoding ancestor should be classified as a group of viruses." In 2021, this definition was officially ratified by the International Committee on Taxonomy of Viruses (ICTV).

Virion mentioned above is a structurally complete viral particle. It is composed of a nucleic acid (either DNA or RNA) genome or core encased in a protein coat, capsid, made of virus-encoded proteins. Such viruses that only consist of genetic material and surrounding proteins are called **non-enveloped** viruses. Other types of viruses are surrounded by a lipid bilayer, called membrane, or envelope. The envelope consists of lipids derived from the host cell and membrane-associated proteins encoded by the virus [12]. The membrane-surrounded, or **enveloped** viruses are usually more susceptible to detergents, desiccation, heat and other factors limiting their preservation outside the host cell. On the other hand, envelope offers advantages in escaping immune response, i.e. inside the host cell [13].

The official taxonomic classification of viruses is the responsibility of ICTV (https://ictv.global). ICTV classification considers whether a virus is enveloped or not, the structure and shape of capsid, the composition of genome etc., paying much attention to the congruence with virus evolutionary histories [14, 15].

RNA viruses having genome single-stranded RNA with the same sense as messenger-RNA (mRNA) are called positive (+)-sense RNA viruses, if genome RNA is complementary (has the opposite sense) to mRNA, the virus is called negative (−) sense virus. [12, 16].

Along with ICTV classification of viruses, Baltimore classification is in use. It was proposed in 1971 by David Baltimore (1975 Nobel laureate in Physiology or Medicine) and, unlike the evolution-based approach of ICTV, divides viruses into seven groups according to their way of genome expression.

The seven Baltimore groups are:

Group I: double-stranded (ds) DNA viruses (e.g. Adenoviruses, Herpesviruses, Poxviruses)

Group II: single-stranded (ss) DNA viruses (e.g. Parvoviruses)

Group III: double-stranded RNA viruses (e.g. Reoviruses)

Group IV: positive sense (+) ss RNA viruses (e.g. Coronaviruses, Picornaviruses, Togaviruses)

Group V: negative sense (−) ss RNA viruses (e.g. Orthomyxoviruses, Rhabdoviruses)

Group VI: ss reverse-transcribing (RT) RNA viruses with a DNA intermediate in their life cycle (e.g. Retroviruses)

Group VII: ds RT DNA viruses with an RNA intermediate in their life cycle (e.g. Hepadnaviruses).

Some other unformal classifications may be used ad hoc, based on the nature of caused diseases, ways of transmission or host organisms (mammalian viruses, bacteriophages) etc.

The replication cycle of most, if not all, viruses include the following key events [12, 17]:

- Virus recognition, attachment and entry into the cell
- Viral gene expression and genome replication
- Viral capsid formation and virion assembly
- Release of virions.

Due to the general universality of the viral replication cycle, it is possible to find chemical compounds, which affect each of them. Table 1 presents information on drug type and specific drugs examples that could be used to target the different viral replication cycle stages as summarized in literature [12, 17].

**Table 1. Antiviral drugs targeting different stages of viral replication cycle**

| Targeted stage of replication cycle | Antiviral drugs | Example(s) |
|---|---|---|
| Virus attachment | Virion binding compounds (receptor analogues) | Enfuvirtide (against HIV) |
| Virus entry and uncoating | Fusion inhibitors | Amantadine, Rimantadine (against Influenza A) |
| Genome replication | DNA: chain terminating agents | Acyclovir (against herpesvirus) |
| | RNA: Viral RNA replicase inhibitors | Ribavirin (against HCV and RSV) |
| | Retroviruses: Reverse transcriptase inhibitors | Zidovudine, Zalcitabine, Didanosine (against HIV) |
| Assembly | Viral protease inhibitors, Capsid protein–protein interaction and budding inhibitors | Ritonavir, Saquinavir (against HIV) |
| Release of virions | Neuraminidase inhibitors | Oseltamivir, Zanamivir, Laninamivir (against influenza viruses) |

As seen from Table 1, although there are universal stages of viral replication cycle that can be targeted with specific drugs, those drugs differ between viruses due to the specificity of viral proteins. Therefore, finding a universal compound to influence one of the other replication cycle stages of all viruses is a rather rare possibility. While the drugs listed in Table 1 target specific processes in viral replication cycle, viral particles can be also inactivated before they infect the host cell and initiate the replication cycle. The selection of such virucidal compounds includes metals, but also cationic polymers and polyzwitterions. [18, 19, 20, 21].

Recent reports of virucidal compounds involve various nanoparticles, i.e., by definition small particles with one dimension less than 100 nm [22] being thus equal or smaller than the size of viral particles. The most widely studied virucidal nanoparticles are nanosized silver [23, 24, 25], copper [24, 25, 26], gold [25, 27], copper (II) oxide [24], zinc oxide [28, 29, 30], titanium (IV) oxide [26], but also organic nanomaterials such as tetraalkylammonium compounds, halamines, lipid-based dendrimers and polymers [19, 31].

## 2.2. Antiviral nanomaterials

### 2.2.1. Cerium dioxide nanomaterials

One of the main objects of this study is cerium (IV) oxide $CeO_2$ (also called cerium dioxide or ceria). Cerium is the second member of the lanthanoid series, the first to be discovered and the most abundant in the series. It has an electron structure of [Xe] $4f^1$ $5d^1$ $6s^2$ and, along with +3 oxidation state typical for

lanthanides ([Xe] $4f^1$), it has an even more stable +4 state ([Xe] $4f^0$) isoelectronic to $La^{3+}$. This feature facilitates the isolation and purification of cerium compounds from natural ores which always contain a mixture of rare earth elements, since +4 state for Ce is more stable in solid state compounds than +3 [32]. The natural abundance of cerium in Earth's crust is close to zinc and copper which makes cerium-based materials economically attractive [33, 34].

Cerium dioxide has a fluorite crystal structure with a space group F*m3m*, which can be also considered a ccp array of metal cations with oxygen anions occupying the tetrahedral voids. Each cerium cation is thus coordinated by eight oxygen anions at the corners of a cube, and each oxygen anion is tetrahedrally coordinated by four cerium cations [35].

Applications of cerium dioxide could be roughly divided into three groups: 1) abrasive materials, including polisher for glasses and other surfaces, such as silicon nitrides, sapphire and gallium nitride, 2) component for optical materials, including laser glasses and scintillators and 3) catalysts and active catalyst support (in particular, as three-way catalyst in automobile exhaustion systems), photocatalysts, electrolytes in solid-oxide fuel cells, sensors, sun-protecting cosmetics anti-corrosion additives and recently emerging biomaterials [33, 34, 36].

The first group of applications is related to the high mechanical stability and hardness of cerium dioxide, the second group is based on the strong f-d transitions of $Ce^{3+}$ ion, which are characterized by uniquely fast decay times among other rare earth ions. Third group contains rather diverse applications, but all of them are connected to the high oxygen mobility in the $CeO_2$ lattice even at relatively low temperatures and $Ce^{3+}/Ce^{4+}$ interplay. Due to comparable stability of Ce(III) and Ce(IV) oxidation states, a wide range of intermediate oxides can be formed depending on the partial oxygen pressure and temperature between $Ce_2O_3$ ($\Delta G^0_{298}$ = 1089 kJ $mol^{-1}$) and $CeO_2$ ($\Delta G^0_{298}$ = 1796 kJ $mol^{-1}$) being the extreme compositions. At higher temperatures oxides with lower oxygen content tend to form a series of fluorite-like phases with the general formula $Ce_nO_{2n-2m}$, however in the air close to room temperature the deviation from $CeO_2$ composition is relatively small and forming phase can be represented as $CeO_{2-x}$ [34]. Non-stoichiometry of cerium dioxide is connected to an easy and reversable release of the oxygen, which can be expressed by the following equation [35]:

$$2Ce_{Ce} + O_o = V^{\cdot\cdot}_o + 2Ce'_{Ce} + 1/2O_2$$

This feature of cerium dioxide is well-studied and even industrially used for catalysis of various redox processes and other applications based on consumption, release or transport of the oxygen species. However, in the last twenty years the biological potential of ceria redox activity has been intensively investigated. Antiviral [37], antibacterial [38], antioxidant [39], and enzyme-like properties [40, 41, 42] of multiple $CeO_2$ and $CeO_2$-based nanomaterials are reported. It is very important that in addition to remarkable redox activity at room temperature and availability, cerium dioxide nanoparticles exhibit low toxicity, which makes them an attractive candidate for biomedical applications.

### 2.2.1.1. Synthesis of ceria nanoparticles

Nano-ceria can be synthesized by a variety of methods depending on the intended use and desired characteristics of the final materials [43]. Particle size, morphology, crystallinity, surface charge and other properties are very sensitive to the synthetic conditions, so by adjusting composition of media, temperature, chemical nature and concentration of reagents, presence and type of stabilizers, etc., one can obtain ceria particles with various characteristics.

In this review we focus on low temperature water-based techniques, as they are used the most for the synthesis of $CeO_2$ for biomedical applications. These techniques allow to synthesize water-dispersible ceria nanopowders without the use of potentially toxic organic solvents and surfactants.

It is generally accepted that the driving force of formation of well-crystalline nanostructures of ceria in water solution is the extremely low solubility of $CeO_2$ [34]. The addition of any basic reagent into the water solution containing $Ce^{3+}$ or $Ce^{4+}$ ions leads to formation of the corresponding hydroxides, $Ce(OH)_3$ is quickly oxidized to $Ce(OH)_4$ by dissolved oxygen or directly by air, and $Ce(OH)_4$ readily loses water and transforms into $CeO_2$. The hypothesis that in case of $Ce^{3+}$ salts hydrolysis precedes oxidation was proved in [44]. The authors managed to isolate cerium (III) hydroxide formed as a result of hydrolysis of Ce(III) compounds before it was oxidized by air or dissolved oxygen. The obtained hydroxide underwent slow ageing in air with XRD control to obtain $CeO_2$. At the hydrolysis stage, the influence of various parameters on the reaction was studied, including the nature of the precipitating agent (NaOH vs KOH), its concentration, the reaction temperature (75 vs 100 °C), the nature of the gas phase in the vessel (air vs nitrogen), the nature of the cerium source ($Ce(NO_3)_3 \cdot 6H_2O$ vs $CeCl_3$), the reaction time and even the reaction vessel type and filling level. As expected, the composition of the gas phase was the most important factor.

A brief overview of water-based synthetic methods is summarized in Table 2. In all found literature, cerium (III) nitrate $Ce(NO_3)_3 \cdot 6H_2O$ was used as a precursor.

**Table 2. Water-based techniques of synthesis of $CeO_2$**

| Stabiliser/surfactant | Oxidizer | Precipitating agent | Temperature | Time | Size, nm DLS | Size, nm (microscopy) | ζ-potential, mV | Reference |
|---|---|---|---|---|---|---|---|---|
| sodium adenosine triphosphate or sodium citrate | air | ion-exchange resin | rt, then MW, 130–190 °C | 30–180 min | | 5.4–6.0 (TEM) | | [45] |
| PVP | air | HMTA | 180°C | 100 min | | 13–17 (SEM) | | [46] |
| no | air | NaOH, aq $NH_3$ | 140 °C | 20 min+1 hour | | 3 | | [47] |
| oleylamine, PhOPh | air | ethanol | rt, then 90°C, then 320°C | 2 hours | | 7 | | |
| no | air (no $CO_2$) | aq $NH_3$ | 60°C | 4.5 hours | | | 20.1 ± 6.8 at pH 5.5 | [48] |
| no | air | $(NH_4)HCO_3$ | rt | | | | −7.3 ± 5 at pH 5.5 | |
| no | air | HMTA | 70°C, then rt | 1 hour, then overnight | | | 13.2 ± 6.2 at pH 5.5 | |
| no | $H_2O_2$ | aq $NH_3$ | rt, then 0°C, then 100°C | 40+ hours | | | 30.6 ± 7.6 at pH 5.5 | |
| no | air | urea | 90°C | 6 hours | | | 2.4 ± 3.6 at pH 5.5 | |
| citric acid | $H_2O_2$ | aq $NH_3$ | 80 °C | 2+ hours | 5.3±1.4 | | −37±3.3 at pH 8.3 | [49] |
| sodium polyacrylate | $H_2O_2$ | no | 25°C<br>40°C<br>120°C HT | 5 min<br>1 hour<br>20 min | 2.6±0.7 | | −39±4.7 at pH 8.2 | |
| sodium polyphosphate | $H_2O_2$ | no | rt | overnight | 5.3±1.2 | | −44±6.4 at pH 8.3 | |
| dextran | air | aq $NH_3$ | rt<br>120°C HT | overnight<br>20 min | 3.2±0.9 | | −4.4±0.4 at pH 8.2 | |
| boric acid | air | NaOH | 25°C<br>rt °C<br>120°C HT | 10 min<br>overnight<br>20 min | 5.6±1.6 | | +53±2.0 at pH 4.5 | |

#### 2.2.1.2. Antiviral properties of cerium dioxide nanomaterials

Cerium dioxide nanomaterials have gained popularity for use in antimicrobial and biomedical applications just recently. The first report on antiviral activity of $CeO_2$ nanomaterials was published by Zholobak et al. [50] in 2010 when their inhibitory effect against vesicular stomatitis test-virus was reported. In 2012 Lozovski et al. [27] demonstrated antiviral activity of $CeO_2$ nanoparticles against herpes simplex virus and against influenza virus H1N1. Mohamed et al. [37] demonstrated that $CeO_2$ nanoparticles synthesized with the help of plant extract at concentrations between 20 and 125 μg/mL decreased the infectivity of Sabin-like poliovirus (type 1) even at 10 $TCID_{50}$ (i.e., at 10-fold virus concentration normally infecting 50% of the cells). A recent publication [51] also claims antiviral efficacy of boric acid stabilized $CeO_2$ nanoparticles that were used to treat nonwoven textile. Such textiles reduced the titer of mouse hepatitis virus (MHV), influenza A virus, and feline calicivirus by > 99% (i.e. >2 logs) within 2 h. Moreover, antiviral activity of those nanoparticles against MHV was demonstrated *in vivo* as well.

Although the mechanism of antiviral activity of $CeO_2$ nanoparticles has not been fully understood, some of the earlier studies suggest that crystal structure defects in $CeO_2$ may be responsible for their biological activity [50]. Those defects are likely to be responsible for redox activity of cerium (Ce(III) ⇔ Ce(IV)) on nanoparticles surface leading to the formation of oxygen vacancies [52], and finally, to the release of reactive oxygen species (ROS) from nanoparticles surface.

Notably, the formation of ROS on $CeO_2$ surface has been shown to depend on the acidity of the surrounding environment. At low pH values ROS formation has been shown to increase the toxicity of $CeO_2$ on bacteria [53], but also on cancer cells [37]. Interestingly, towards normal mammalian cells which tests have been carried out at less acidic pH, no notable cytotoxicity of $CeO_2$ nanoparticles has been observed. Instead, protective effects, expressed as better survival and promotion of growth have been demonstrated in cytotoxicity studies [54, 55]. As proposed by those authors these protective effects may be due to the entrapment of reactive radicals by $CeO_2$ and thus, reduction of ROS-induced oxidative stress [56, 57].

This interesting dual effect, likely driven by the surrounding environment and depending on the biological target suggest that $CeO_2$ materials may be indeed considered as potent antivirals with low side effects.

### 2.2.2. Other inorganic antiviral nanomaterials

A broad range of nanomaterials have been studied as potential antiviral agents. As the mechanism of action of inorganic nanomaterials on viruses is of a complex nature and not yet clearly understood [10], the main reason for the choice of potential antiviral agents usually is their antibacterial activity, which is better studied for most of the compounds.

The most popular and probably the most studied class of inorganic antiviral agents are metal nanoparticles and nanostructures, primarily based on copper and silver. The virucidal effect of these metals seem to have at least two contributing factors [58]: first, generation of reactive oxygen species [59], second, release of ions [60]. It has been shown that metal ions, especially copper, nickel and zinc ions, can efficiently bind biomolecules, including viral metalloproteins [61], as they form more stable complexes than original metal ions present. One can note that both these mechanisms are not very specific to the chemical compound, which contains active metal, as they are both mostly related to the action of the released ions. Therefore, nanomaterials based on various compounds, including oxides and salts of the mentioned metals, exhibit similar antiviral effects [62].

Another class of nanomaterials that can be used as antiviral agents are photocatalytic nanoparticles, mainly $TiO_2$ and ZnO [19]. Under UV and sometimes even visible [63] irradiation, photocatalytic nanomaterials, both in the form of colloids and coatings, are found to inactivate viruses. In this case, the mechanism of antiviral action is the formation of ROS on the surface of nanomaterials. However, it must be noted that some reports state the activity of such materials even in the dark [64, 65], suggesting that other mechanisms are also involved. For ZnO the leaching of material with formation of $Zn^{2+}$ also must be considered, as $Zn^{2+}$ ions possess high biological activity [66]. Formation of ROS in the case of photocatalytic nanomaterials occurs on their surface. This is rather different from copper or silver-based nanomaterials, which tend to produce ROS via Fenton-like mechanism involving redox reactions of ions in solution. For example, it has been reported that antiviral and in general antimicrobial activity of ZnO strongly depends on its morphology [67, 68, 30].

Recently a lot of works appeared on antibacterial and antiviral effects of graphene-based materials [10]. Especially graphene oxide and reduced graphene oxide attract attention due to better dispersibility in water [69, 70]. The antiviral activity of graphene-based nanoflakes is generally attributed to sharp edges, disrupting the virus membrane [10]. Moreover, graphene-based nanostructures can be very easily modified with molecules with known antiviral activity, for example polyglycerol sulfate [71].

Nanocontainers loaded with antiviral agents, or simply with immobilized active nanoparticles on their surface, are another important class of antiviral nanomaterials. The most popular hosts are polymeric capsules and films and mesoporous silica, all of which allow for controlled release of the incapsulated agent. Silver nanoparticles and silver ions loaded into silica [72], polylactide [73], chitosan [74] or chitin [75] matrices are shown to have antiviral activity with the main advantage being the controlled release and stabilization of silver nanoparticles on the surface to prevent washing off. Apart from inorganic nanoparticles, mesoporous silica can be loaded or coated with molecular antiviral agents also with the aim of controlled release and immobilization [76, 77].

In general, the antiviral nanomaterials can be divided into several groups by their mechanism of action [10]: 1) direct chemical interaction of metal ions with the biomolecules comprising the virus, 2) indirect damage via ROS production,

3) mechanical interaction causing membrane disruption by sharp edges or blocking by strong absorption forces, and 4) controlled release of virucides from nanocontainers, with some nanomaterials combining several modes of action.

### 2.2.3. Antiviral surfaces

The formulation of the concept of antiviral surfaces is relatively new as for the first time 'antiviral surfaces' appeared in an article's title in 2020 [78, 79, 9]. However, with SARS-CoV2 pandemic during 2020–2022 the concept has been relatively well explored. The purpose of developing and using antiviral surfaces is to decrease the contact transmission of infectious viral particles and such surfaces are expected to have the highest impact in case of enteric (e.g., gastroenteritis-causing norovirus, rotavirus, adenovirus, or other enteroviruses such as hepatitis viruses) and respiratory viruses (e.g., influenza virus, rhinovirus, coronavirus) [80]. While enteric viruses are well known to be transferred by fecal-oral route and thus, prone to be transferred also to touch surfaces by contaminated hands or other parts of the body, respiratory viruses may end up on surfaces via respiratory droplets from infected people [81]. Depending on the viruses, such surface-deposited viral particles may remain infectious over several hours to even months [80].

Antiviral surfaces can be largely divided into active and passive surfaces, although also intermediate variants exist. Essentially, active surfaces are those containing a functional antiviral agent that can either inhibit viruses upon direct contact or be released, while passive surfaces usually inhibit surface attachment of viral particles. In terms of their mode of action, Lishchynskyi et al [82] have divided the potential antiviral effects to five categories: direct action originating from immediate contact with antiviral agents, indirect action resulting from surface-mediated formation of highly reactive species such as ROS, blocking interaction of virus with host receptors, photothermal effect, and antifouling.

The most widely used compounds in active antiviral surfaces overlap largely with the most popular antiviral agents. Silver, copper, zinc but also aluminum, gold and selenium, have been most often used to create antiviral surfaces, usually incorporated inside a stable coating [83]. According to common understanding, active surfaces release the incorporated antiviral agent at least to a certain extent and this released agent is capable of affecting viral membranes, membrane proteins [83] or even nucleic acids. For example, $Cu^{+}$ and $Cu^{2+}$ ions releasing from copper alloy surfaces were shown to destroy the genetic material of human coronavirus [60]. Analogous effects have been suggested for silver containing surfaces [10].

Another class of popular antiviral agents incorporated onto the surface are cationic polymers such as chitosan, polyethyleneimine (PEI) or quaternary ammonium compounds, [84, 85, 86], which are expected to bind viral particles through electrostatic interactions via interactions with negatively charged viral membranes. However, due to the presence of membranes only in enveloped viruses, such a mode of action eliminates their effect against non-enveloped viruses [83].

Several papers have suggested also natural compounds such as plant extracts, animal products like propolis or exopolysaccharides as active agents in surface coatings [87]. However, the efficacy of such compounds may remain relatively low. In addition to the described relatively broad-spectrum compounds, very specifically acting small molecules binding to e.g., surface proteins or viruses, may be applied to antiviral surfaces [9].

Photocatalytic materials, e.g., ZnO and $TiO_2$, permanently disintegrating viral particles due to light (usually UVA)-induced reactive oxygen species (ROS) production [82, 88, 89, 90] have used in antiviral coatings. The important issue to consider in case of such light-activated surfaces is the antiviral activity of light itself. Viral particles have been clearly shown to be more sensitive towards short wavelength light than bacteria and so, UVA and UVB have been effectively inactivating SARS-CoV2 virus but also shown to play the role in seasonal occurrence of influenza virus [91, 92].

Among passive antiviral surfaces are surfaces that avoid the attachment or preservation of viruses on surfaces [82]. Such surfaces are usually acting by reducing the difference of electrostatic interactions between viruses and surfaces, van der Waals interactions between viral particles and surfaces, or changing the wettability of surfaces e.g., to superhydrophobic, to prevent interactions between the surface and viral proteins. Another extreme example to avoid viral attachment to surfaces is the use of superhydrophobic surfaces with minimized interactions between the surface and liquid droplets containing viral particles [93, 94]. Also, micro- and nanostructured surfaces have been shown to decrease viral adhesion and stay on surfaces, although the exact mechanism behind this phenomenon are not fully clear [83]. The most likely scenario seems to be viral deformation and damage on patterned surfaces due to their relatively low Young's modulus [83, 95].

In search for the best-acting antiviral agents and surfaces, one would like to compare the antiviral effects reported in different studies. However, such comparisons are rather complicated due to the differences in test formats, viruses used, as well as in methods used to calculate results. The most widely used method for surfaces testing is ISO 21702:2019 (Measurement of antiviral activity on plastics and other non-porous surfaces) that foresees spreading of a small aliquot of virus on surface, covering it with plastic foil to ensure even distribution and following quantitative determination of viral infectivity. However, several studies have emphasized the importance of carrying out surfaces antiviral testing using application-relevant conditions. One major factor affecting viral infectivity is relative humidity (RH), which at a higher level usually improves the survival of viruses but in case of some viruses and surfaces combinations may also decrease it [96].

Also, temperature is playing a role as viruses have been shown to persist better at rather low temperatures than higher ones [97]. One additional important factor potentially affecting the antiviral efficacy of surfaces is their soiling, i.e., the presence of unwanted organic residues that are highly likely to mask the desired effect. As demonstrated with antibacterial activity [98], surface soiling may also significantly affect viral persistence on surfaces, but up to date this effect has not

been thoroughly studied. Comparison of different studies is also hindered by the different ways of expressing test results. Some studies have chosen to express antiviral activity as % of initial infectivity while log10 decrease of infectious units should be used instead [99]. The use of log10 transformed values is important to ensure the statistical significance of the results, considering that infectivity tests data may be highly variable. While standard methods exist to analyze the effect of surfaces to viral infectivity, no methods have been standardized to study other mechanisms that may lead to antiviral activity, e.g., anti-attachment activity.

#### 2.2.3.1. Antiviral textiles

While there is an increasing interest towards antiviral materials, antiviral textiles are much less studied than antiviral surfaces in general. A query on Clarivate Web of Science carried out in August 2025 with keywords “antiviral, surface” resulted in 9980 articles (from which 1697 were reviews), and with keywords “antiviral, textile” resulted only 225 results, including 63 review articles. Between the years 2007–2019 the annual number of articles on antiviral textiles did not exceed 5 (usually 1 or 2) with a rapid growth from the year 2020 and a maximum of 48 articles in 2022. According to a recent review article [100], the number of patents in the field grew in the similar way (being higher in absolute values), but the number of successful commercialization is low.

The reports and reviews on antiviral textiles reveal that in general, the antiviral compounds added to textiles are overlapping with those described under general antiviral applications and antiviral surfaces. The most used are metal-based antiviral additives containing silver, copper or zinc [87]. Apart from metals, other known antimicrobials, e.g., triclosan combined with sodium pentaborate, have been used to create antiviral effect on textiles [101].

Another group of compounds used in antiviral textiles are those enabling photodynamic therapy, i.e., increase of temperature or ROS production under light illumination. Examples of those are graphene oxide, carbon nanotubes and natural photodynamic agents [102]. Graphene oxide has been coated as layers on textile fibers with a goal to increase the temperature of the textile up to 80 °C under illumination and with that, achieve antiviral activity [103].

Carbon nanotubes have been added to textiles with the goal to attract viruses by electrostatic interactions and to locally achieve temperature increase upon light illumination [94, 100, 104, 105].

The fibers used most frequently to produce antiviral textiles are synthetic polymers: polyvinyl chloride, polyacrylonitrile, or polyamide. However, also natural cotton fibers have used to create antiviral textiles [87, 100, 101].

In general, the application of antiviral textiles has been rather limited with face masks, the development of which peaked during SARS-CoV2 pandemic between 2020 and 2022. Some of the textile treatments proved indeed rather effective against viruses. Copper oxide treatment on an intermediate layer of a face mask used by Borkow et al. showed a strong antiviral activity against influenza [106]. Similarly, copper oxide impregnated textiles showed also their inhibitory activity

against HIV [107]. Face masks treated with photosensitizer molecules (rose Bengal and sodium 2-anthraquinone sulfate) showed expectedly a high efficacy under sunlight by decreasing the infectivity of T7 phage by 5–6 log10 during 1 h incubation [102]. Filtration of poliovirus and adenovirus through cotton textile treated with boron and triclosan showed up to 3 logs decrease of the virus titers [101].

Although up to date antiviral textiles have not seen much use outside face masks, the need is certainly there also in other application areas such as in public transportation, catering industry, medical procedures, farms etc. Adding antiviral properties to seat fabrics, seat belts, interior textiles, tablecloths, carpets, towels, medical and working clothes could significantly reduce the risk of viral cross-infection, especially in infectious diseases hotspots [87].

As in case of antiviral surfaces, one important issue to be considered for antiviral textiles is the method of their efficacy testing. ISO has published a standard ISO 18184:2025 (Textiles – Determination of antiviral activity of textile products) which foresees exposure of viral particles to a known size and weight textile pieces in liquid media; however, such a method does not necessarily reflect a real situation in case of face masks or other textiles that are mostly used in dry or semi-dry environments. Therefore, for more real-life relevant testing, application of virus-loaded aerosols or touch transferred viruses to textiles would be more representative.

#### 2.2.3.2. Preparation of antiviral textiles

The methods of preparation of antiviral textiles, as well as any other type of functionalized textile, fall into two major categories [87]: 1) mixing of the antiviral compound or nanomaterial into the initial polymer spinning solution and spinning a thread of a future textile with already introduced antiviral function and 2) finishing of the already existing textile using various procedure that depend on the nature of both textile material and the finishing agent.

Textile manufacturers prefer the first option; however, it is only possible for synthetic fibers [108]. This ensures durability of antiviral function, so it does not deteriorate during washing and handling. The most common methods for direct production of the antiviral thread are wet spinning and melt spinning, which mainly differ in the temperature of the process and whether the solvent is used or not [87]. During wet spinning precursors are dissolved, and the fiber is spun at room or slightly elevated temperature, while during the melt spinning the precursors are mixed and melted to form a resin, which is spun at high temperatures. The melt spinning is faster and allows finer threads but requires a certain thermal stability for both the polymer and the additives. This approach has been used to introduce several antiviral nanomaterials into textile, including silver nanoparticles [109] and MOF nanoparticles [110], but it is much more applicable to the soluble compounds rather than nanoparticles, as nanoparticles, even the smallest, are negatively affecting mechanical properties of the fiber. This is the reason why in commercial antimicrobial textiles soluble organic compounds or

metal ions are used almost exclusively, like “Permafresh” (Dimethyloldihydroxyethyleneurea or $Ag^+$ ions), “Amicor AB” and “Silfresh” (triclosan), etc. However, some commercial products are based on incorporation of zeolites containing metal ions, usually silver (“Livefresh N Neo” or “Bactekiller”) [108].

On the contrary, researchers prefer the second option – finishing, as it does not require expensive and complicated equipment for fiber spinning and allows the use of existing textile material. On of the most common ways of finishing is padding. In the case of nanomaterials attachment to the textile for padding can be used either colloid of existing nanoparticles [111] or the dissolved precursor with nanoparticles forming in situ, during the impregnation process [107, 112]. The latter approach allows for better attachment of nanoparticles, as they grow on textile fibers.

The usual routine is described as “pad-dry-cure”, involving impregnation of textile in the colloid, rolling and drying it, then application of a curing procedure – usually just heating, though sometimes microwave [113] or UV-irradiation is used. However, especially if pre-synthesized nanoparticles are used, a more complex approach may be needed to properly fix nanoparticles on textile fibers. One of the ways is to use a binder – usually a polymeric compound, that fixes nanoparticles on the surface of the textile. Several commercial binders for textiles based on polysiloxanes, ionic polyacrylates, butadiene copolymers were successfully used to attach antimicrobial nanoparticles [114, 115, 116]. Another way, which is applicable to cellulose and other natural textiles, is modification of their surface by oxidation or functionalization to increase its reactivity towards the surface of dispersed nanoparticles [117]. This procedure can be used instead [118] or together with a binder [119].

More sophisticated techniques, such as layer-by-layer coating [120, 121] or magnetron sputtering [122] can also be applied to ensure a more homogeneous distribution of the antimicrobial nanoparticles. For deposition of in situ forming CuO and ZnO nanoparticles on textile, an ultrasonic treatment was successfully used [123, 124]. The highly energetic microjets formed during sonication hammer nanoparticles onto the textile surface ensuring strong attachment.

# 3. MOTIVATION AND AIM OF THE WORK

The aim of this work is to develop an antiviral treatment for textiles based on surface deposited oxide nanomaterials, and to study the efficacy of the obtained textile surfaces in semi-dry conditions approximating real-life usage of textiles. To achieve this aim, the following tasks were pursued.

1) To synthesize a series of nanostructures varying chemical composition and study their morphological characteristics relevant to the possible antiviral activity.
2) To develop a method of spray deposition of synthesized nanostructures on the surface of the model textile, allowing to achieve adhesion and uniform distribution on textile fibers.
3) To test the reduction of infectivity of a range of viruses by synthesized nanostructures both in wet (colloids) and semi-dry (textile surface) conditions to assess their antiviral activity in different environments and applications.
4) To study the possible mechanism of the oxidative activity of ceria nanoparticles responsible for virus deactivation using tryptophan as a model molecule.

# 4. MATERIALS AND METHODS

This chapter is a brief overview of our experimental methods. For more detailed information see our articles [**I, II, III**].

## 4.1. Synthesis of nanomaterials

In this work, several types of nanoparticles and nanocontainers were used for antiviral purposes. Nanoparticles of Ag, $CeO_2$, and nanocontainers based on mesoporous $SiO_2$ microparticles with cetrimonium bromide (CTAB) loading were synthesized in house and nanoparticles of $TiO_2$ were obtained from our collaborator at Swedish University of Agricultural Sciences (Sveriges lantbruksuniversitet, SLU), Sweden. Phosphotungstic acid $H_3PW_{12}O_{40}$, which was used to obtain a model "smallest nanoparticle" – polyoxometalate (POM) ion, was purchased from Sigma Aldrich.

For synthesis of nano-Ag a two-step seed-mediated technique was adopted from [125] and modified to simplify the composition of reaction mixture and avoid toxic reagents. For the latter, poly(sodium styrene sulfonate) (PSSS) was replaced with polyvinylpyrrolidone (PVP). At the first stage, silver nitrate is reduced with freshly prepared sodium borohydride in aqueous trisodium citrate/PVP solution at room temperature to form seeds. The second stage is seed-catalyzed reduction of silver nitrate with trisodium citrate at 85 °C.

To synthesize nano-$CeO_2$ with positive surface charge (nano-$CeO_2$(+)), we used microwave-assisted hydrolysis of diammonium cerium (IV) nitrate $(NH_4)_2[Ce(NO_3)_6]$ at 200 °C in the presence of hexamethylenetetramine (HMTA) [46]. The product was washed with DI water and centrifuged thrice and then redispersed in fresh water by ultrasonication. A stable opalescent pale-yellow colloid was obtained. For the synthesis of nano-$CeO_2$(−) nanoparticles we used a modified method from [126]. Cerium (III) nitrate was hydrolyzed with aqueous ammonia at room temperature with oxidation by oxygen from the air in the presence of citric acid. The product was washed as described above for nano-$CeO_2$(+) and resuspended in DI water by ultrasonication to obtain a transparent dark yellow colloid.

Both $SiO_2$ [127, **I**] and CTAB-loaded $SiO_2$ (also designated as CTAB@$SiO_2$) [128, **II**] particles were synthesized using a modified Stöber technique. In both cases, tetraethyl orthosilicate (TEOS) was hydrolyzed by aqueous ammonia in water-ethanol mixture under vigorous stirring at room temperature. Pristine silica was synthesized in the presence of polyethylene glycol (PEG) as surfactant, for CTAB-loaded silica CTAB was used as surfactant and template. After washing, $SiO_2$ was redispersed in water to obtain a stable colloid, and CTAB-loaded $SiO_2$ was washed several times with ethanol and dried at 40 °C. Details are given in the corresponding papers [**I, II**].

Two types of titanium dioxide nanoparticles were used in this work. The first variety, triethanolamine stabilized titania ($TiO_2$–I), was obtained by the modification of titanium ethoxide with dry triethanolamine with subsequent dropwise addition on vigorous stirring of a hydrolyzing solution (mixture of $HNO_3$with ethanol). This procedure resulted in the NP starting solution with a $TiO_2$ concentration of 120 mg/g as established by TGA. The other applied sample, lactate-stabilized titania ($TiO_2$–II), was produced by dilution with Milli-Q water of the solution of the commercially available titanium(IV) bis(ammonium lactato)dihydroxide (TiBALD) solution. The initial concentration of $TiO_2$ was estimated as 45 mg/mL. [129, 130].

## 4.2. Antiviral tests with colloidal nanoparticles and solutions

The main characteristics of tested viruses are presented in Table 3. All the experiments were performed in sterile conditions. The tests with SARS-CoV-2 were carried out in a BSL-3 certified laboratory. (We sincerely thank Dr. Andres Merits, Dr. Eva Zusinaite and Dr. Kai Rausalu from the Institute of Bioengineering of the University of Tartu for our collaboration).

The antiviral testing carried out during this study concerned virucidal testing: eliminating the viruses before they may infect host cells. The most widely used test for virucidal activity testing is probably 50% tissue (cell) culture infectious dose or $TCID_{50}$ $CCID_{50}$ [131]. However, this approach is semi-quantitative and half-manual. As an alternative to that test, plaque assay which is more accurate and less subjective, can be used [131]. The drawback of this assay is the fact that not all test viruses may readily form plaques. All the viruses used in this study were successfully able to form plaques and therefore, plaque assays were used.

For plaque assay of chemicals and materials, their aqueous solutions or suspensions at selected concentrations were mixed with an equal volume of bacteriophages in water or mammalian viruses in 1/10 water-diluted cell culture medium. The mixtures were incubated for 1 h at room temperature after which these were diluted in tenfold series using SM buffer (bacteriophages) or virus growth medium (mammalian viruses). One hour incubation between viruses and test compounds was chosen to follow the requirements of European Biocidal Products Regulation requirements [132] for antimicrobial efficacy testing of treated articles.

In plaque assay with mammalian viruses viral wash-off dilution series in virus growth medium were used to infect 100% confluent host cells grown on 12- or 96-well plates and previously washed with phosphate buffered saline (PBS). Virus growth medium was added to cells in negative control. The infection was carried out for 1 h at 37 °C, 5% $CO_2$, in humidified atmosphere for 1 h with gentle rocking every 10–15 min. Then the infection medium was removed, the cells washed with PBS, and 3:2 mix of virus growth medium with 2% carboxymethyl cellulose (CMC) was added (in case of influenza virus the mix was supplemented

with 1 μg/ml TPCK-trypsin). Cells were grown in respective growth media for 96 h (as an exception 48 h in case of EMCV and Vero E6) at 37 °C, 5% $CO_2$, humidified atmosphere. For plaque counting in ST, MDCK-2 and BHK-21 cells, the virus growth medium was removed, and plates were dyed with crystal violet (0.25% crystal violet, 1.85% formaldehyde, 10% ethanol, 35 mM Tris, 0.5% $CaCl_2$). Plaques were identified as clear plaques within the cell layer.

In Vero E6 cells, immuno mini-plaque method was used in which case infection of cells was carried out as previously described. After infection microplate wells with cells were fixed with ice-cold 80% acetone in 1× PBS at – 20 °C for 1 h. Then the plates were dried for at least 3 h. The dried plates were treated with a blocking buffer diluted in PBS/0.05% Tween20 (PBS-T) for 60 min at 37 °C. Then probing with rabbit monoclonal anti-SARS-CoV-2 nucleocapsid antibody 82C3 diluted in PBS-T was carried out during 1 h at 37 °C. The plates were washed with PBS-T and treated with secondary goat anti-rabbit IRDye800CW antibody diluted in blocking buffer for 1 h at 37 °C. Plates were again washed with PBS-T, dried and scanned using LI-COR Biosciences Odyssey Infrared Imaging System and application software, to identify fluorescent focuses (mini-plaques).

Minimum of 3 plaques and maximum of 30 plaques per well were counted and PFU value was calculated according to the dilution and the volume of the inoculum. Each concentration of a compound or suspension was tested in three replicates and at least three independent experiments were performed. Antiviral activity was calculated as a difference between log-transformed plaque forming unit (PFU) counts in negative control and the test sample. 2-log decrease in PFU counts during 1 h was considered as the lowest biologically meaningful threshold in potential applications according to EU legislation [133].

To conduct a plaque assay with bacteriophages, after exposure to tested materials bacteriophage-compound mixtures were dropped as ~0.5 cm wide circles onto 10 cm diameter Petri dishes that contained agarized bacterial growth medium with freshly plated host bacteria. Phages incubated in water without compounds were dropped onto bacterial plate for negative control. Plaques (areas with no visible growth of the host bacterium on agar plates) within the circles were counted after overnight incubation to obtain the plaque forming units PFU/mL. Minimum of 3 plaques were counted per circle. Each concentration of a compound or suspension was tested with two technical replicates and at least three independent experiments were performed. To mitigate nano-Ag toxicity in antiviral assay with bacteriophages these nanoparticles were tested in combination with threefold molar excess of l-cysteine (see [**I**] for details).

Assays with bacteriophages were performed by Merilin Rosenberg and Kairi Koppel at the University of Tartu Institute of Molecular and Cell Biology, as well as testing of bactericidal activity of studied materials [**I**].

## 4.3. Toxicity testing of nanomaterials and compounds to viral host organisms

Prior to antiviral experiments, the toxicity of studied materials in colloids or solutions was tested against host organisms of those viruses—cell lines in case of mammalian viruses and bacteria in case of bacteriophages (Table 3). Those tests were carried out in conditions similar to antiviral tests. Viral host cells or bacteria were exposed to the exact concentrations of chemicals, nanomaterial colloids or textile wash-offs as in antiviral or anti-bacteriophage assays. Concentrations of compounds or wash-offs causing visual signs of toxicity in mammalian cells as observed under light microscope, or no growth of bacterial hosts on agar plates were not tested.

In [**I**] more in-depth toxicity analyses were carried out. For cytotoxicity analysis with host cells of mammalian viruses, the cells were seeded onto 96-well plates and grown in specified medium (Table 3) to reach 70% confluency. After this the growth medium was removed and the tested compounds at different concentrations were added. The cells were incubated for 1 h at 37 C, 5% $CO_2$, humidified atmosphere, the test compounds were removed, fresh growth medium was added, and cells were incubated for 48 h. Cell viability was measured using Cell Proliferation Reagent (WST-1) (Roche) by reading absorbance at 450 nm. Cell viability was calculated by subtracting from each measurement the value of a blank (no cells); viability of cells without a test compound was considered as 100%. Three replicates were tested for each compound and concentration. For bacterial toxicity testing the host bacteria were exposed to the test substances in plaque assay format omitting the bacteriophage.

**Table 3. Characteristics of tested viruses and test conditions**

| Virus | Family | Characteristics | Titer in exposure, PFU/ml | Host cells (growth conditions) | Maintenance/growth conditions | Test method | Tested | |
|---|---|---|---|---|---|---|---|---|
| | | | | | | | in colloid/ solution | on textile |
| **Enveloped viruses** | | | | | | | | |
| **Mammalian viruses** | | | | | | | | |
| Influenza virus A/WSN/1933ϭ | Ortho-myxo-viridae | Seasonally important to cause flu in Northern hemisphere | $6.65\times10^4$ | MDCK-2 cells (DMEM, 10% heat-inactivated fetal bovine serum (FBS), 100 U/mL penicillin, 100 µg/mL streptomycin, 37 °C 5% $CO_2$) | Virus growth medium: DMEM, 0.2% BSA, 100 U/mL penicillin and 100 µg/mL streptomycin, 1 µg/mL TPCK-treated trypsin | Plaque assay | yes | no |
| Transmissible gastroenteritis virus, TGEV | Corona-viridae | Causes a highly mortal gastro-enteritis in pigs. | $8.35\times10^6$ | ST cells (DMEM, 10% heat-inactivated FBS, 100 U/mL penicillin, 100 µg/mL streptomycin, 37 °C 5% $CO_2$) | Virus growth medium: DMEM, 0.2% BSA, 100 U/mL penicillin and 100 µg/mL streptomycin | Plaque assay | yes | yes |
| SARS-CoV-2 | Corona-viridae | Causes COVID-19 | $5\times10^5$ | Vero E6 cells (DMEM, 10% heat-inactivated FBS, 100 U/mL penicillin and 100 µg/mL, streptomycin; 37 °C and 5% $CO_2$) | Virus growth medium: DMEM, 0.2% BSA, 100 U/mL penicillin, 100 µg/mL streptomycin | Immuno mini-plaque method | yes | yes |

| Virus | Family | Characteristics | Titer in exposure, PFU/ml | Host cells (growth conditions) | Maintenance/growth conditions | Test method | Tested | |
|---|---|---|---|---|---|---|---|---|
| | | | | | | | in colloid/ solution | on textile |
| **Bacteriophages** | | | | | | | | |
| ϕ6 | Cysto-viridae | Enveloped bacteriophage of Pseudomonas sp | $1\times10^7$ | *Pseudomonas* sp. (Tryptone Soy Broth TSB: 17 g/L casein peptone, 3 g/L soy peptone, 2.5 g/L glucose, 5 g/L NaCl, 2.5 g/L $K_2HPO_4$; 25 °C; for solid medium 15 g/L agar added) | Phage maintenance medium: SM buffer (0.1 M NaCl, 8 mM $MgSO_4$, 50 mM Tris–HCl; pH 7.5) Semisolid TSB top agar used for infection: 7 g/L agar added to TSB | Plaque assay | yes | no |
| **Non-enveloped viruses** | | | | | | | | |
| **Mammalian viruses** | | | | | | | | |
| Encephalo-myocarditis virus, EMCV | Picorna-viridae | Rodent-borne virus, causative agent for neurological disorders in mammals | $2.5\times10^7$ | BHK-21 cells (GMEM, 10% heat-inactivated FBS, 2% TPB, 2% 1 M Hepes (pH 7.2), 100 U/mL penicillin, 100 µg/mL streptomycin, 37 °C, 5% $CO_2$) | Virus growth medium: GMEM, 0.2% BSA, 2% 1 M Hepes (pH 7.2), 100 U/mL penicillin, 100 µg/ml streptomycin | Plaque assay | yes | no |
| **Bacteriophages** | | | | | | | | |
| MS2 | Fiers-viridae | Non-enveloped bacteriophage of Escherichia coli | $1\times10^7$ | Escherichia coli (Growth medium NZCYM broth: 10 g/L, casein hydrolysate, 5 g/L NaCl, 1 g/L casamino acids, 5 g/l yeast extract, 2 g/L $MgSO_4{\cdot}7H2O$, 2 g/L maltose 37 °C; for solid medium 15 g/L agar added) | Phage maintenance medium: SM buffer (see above). Semisolid NZCYM top agar for infection: 7 g/L agar added to NZCYM | Plaque assay | yes | no |

## 4.4. Finishing of textiles

The textile used in the study was a knitted fabric for mattress covering "Sareaux-C 24" (100% polyester, specific weight 240 g/m$^2$) (provided by TAD Logistics OÜ, Estonia). The textile was cut to 15×15 cm pieces and solutions or suspensions of tested materials were sprayed onto a vertically placed piece of knitted polyester fabric (15 mL of concentrated solution of the compound or suspension of nanomaterials was sprayed onto 0.0225 m$^2$) (Figure 1). Then the textiles were left to dry in air at room temperature.

Figure 1. The process of spraying

After drying the treated fabric was cut into 2×2 cm (0.045 ±0008 g) pieces, which were stored in zipped PE bags and sterilized by autoclaving before antiviral tests. Table 4 introduces all the prepared textiles. The distribution and quantity of antiviral agents on the surface were evaluated using SEM and ICP-MS (see paragraph 4.6.3.1 and 4.6.3.2). To determine the concentration of CTAB, bromine concentration was measured, since it was reasonable to assume the absence of any other Br sources in the samples. To assess the stability of textile coating, wash-offs were collected during antiviral tests, and the release of active components was evaluated using ICP-MS and ICP-OES (see paragraph 4.6.3.2).

**Table 4. Treated textiles and their characterization**

| Substance sprayed onto textile | Purpose | Characterization |
|---|---|---|
| Nano-$CeO_2$(+) and nano-$CeO_2$(−) | Antiviral textile | SEM<br>ICP-MS (Ce analysis)<br>Leachate ICP-MS (Ce analysis) |
| $SiO_2$ nanocontainers loaded with CTAB (CTAB@$SiO_2$) | Antiviral textile | SEM<br>ICP-MS (Br analysis),<br>ICP-OES (Si analysis)<br>Leachate ICP-MS (Br analysis),<br>ICP-OES (Si analysis) |
| CTAB | Comparison for CTAB@$SiO_2$ | SEM<br>ICP-MS (Br analysis)<br>Leachate ICP-MS (Br analysis) |
| $Cu(NO_3)_2$ | Positive control | SEM<br>ICP-MS (Cu analysis)<br>Leachate ICP-MS (Cu analysis) |

## 4.5. Antiviral testing of textiles

For antiviral testing of textiles, ISO 18184:2019 “Textiles – Determination of antiviral activity of textile products” guidance was used. This standard specifies the essential steps related with preparation of textiles for antiviral testing, virus loading and exposure conditions, and is one of the main international standards in this area. Exposure time for viruses on textiles varied and was selected based on initial experiments in which persistence of viruses on the textile was tested after 24, 48 and 72 hours.

Antiviral activity of nano-$CeO_2$(+), nano-$CeO_2$(−), CTAB@$SiO_2$ and copper nitrate treated textiles against two mammalian coronaviruses, SARS-CoV-2 and TGEV was tested. Testing samples of textile were sterilized by autoclaving. Autoclaved 2×2 cm pieces of untreated textile were used as negative control. Virus without textile exposure was used as no textile control. Virus stocks in growing medium were mixed 10:1 with 10x soil load (1x soil load: 1 g/L BSA, 1 g/L yeast extract, 0.08 g/L porcine gastric mucin in PBS). A piece of textile was placed into a 50 mL screw cap tube; soil load supplemented virus stock was applied to the textile surface in ten uniformly distributed 2 µL droplets (20 µL per piece in total) and the tube was closed and left for selected time interval. In no textile control the drops of virus were pipetted onto the surface of 50 mL screw cap tube. Aluminum foil was used to protect the tubes from light. Viruses were washed off from textiles using 10 mL of SCDLP (30 g/L TSB, 1 g/L lecithin, 7 g/L Tween 80) by vortexing at 0, 1 and 24 h after exposure. For 0 h timepoint, virus was washed off from textile immediately. The wash-offs were either directly or after diluting in virus growth medium used to infect the cells for plaque assay or immuno-plaque assay as described above. Before counting the plaques,

the plates were checked for any cytotoxicity or other interfering effects by visually checking staining of the cell layer. Wells with visual signs of cytotoxicity were not counted. Plaques were counted only if their count fell between 3 and 30. PFU count was calculated according to the dilution and the volume of the inoculum. Considering the minimum of 3 plaques per assay, 110 infectious virus particles ($log_{10}$=2.04) per textile piece was the limit of detection (LOD). Each textile was tested in three replicates and at least three independent experiments were performed. Antiviral activity was calculated as a difference between log-transformed plaque forming unit (PFU) counts in negative control and the test textile. 2-log decrease in PFU counts during 1 h was considered as the lowest biologically meaningful threshold in potential applications [133].

After antiviral tests on textiles with TGEV, 1 mL aliquots of selected wash-offs were collected and used to determine the leaching of the active compound by ICP MS (see Section 4.6.3.2) after UV inactivation of the viruses. For inactivation, 1 mL of SCDLP after washing the textile samples was placed in an open 1.5 mL Eppendorf vial into a Hoefer UV Crosslinker UVC-1000 device and exposed to UV light for 10 minutes. The results are presented in Table 10, Section 5.4.

## 4.6. Overview of physico-chemical methods of characterization

### 4.6.1. Size measurement of nanoparticles

The size and size distribution of synthesized nanoparticles was evaluated using dynamic light scattering (DLS) and transmission electron microscopy (TEM).

#### 4.6.1.1. Hydrodynamic size measurement with dynamic light scattering

The DLS method [134, 135], based on scattering of light on constantly moving (Brownian motion) particles, is used to measure particles' hydrodynamic size. Since the velocity is higher for smaller particles, the particles size can be determined based on the changes in frequency and intensity of the light after passing through the reader. DLS is a reliable method for samples of good quality, i.e., samples showing sufficient stability, relatively low particle concentration, and no interfering color or bubbles.

For hydrodynamic size measurement, relevant concentrations of nano-$CeO_2$(+), nano-$CeO_2$(−), CTAB@$SiO_2$ and nano-Ag were dispersed in water (to resemble the actual exposure condition in antiviral and bacterial assays) and Malvern Zetasizer Nano ZSP was used. The chosen nanoparticle concentrations included at least the highest antivirally tested ones and, in the case of nano-$CeO_2$, all antivirally tested concentrations.

#### 4.6.1.2. Transmission electron microscopy

TEM has been considered as the best technique for characterization of micro- and nanomaterials. This method is based on the detection of an electron beam passed through a sample, it enables a quantitative measure of particle size, grain size, size distribution, size homogeneity, lattice type, morphological information and crystallographic details [136].

For TEM analysis a drop of nanoparticle suspension with suitable concentration (e.g., 100 mg/L) was deposited onto a 400-mesh holey carbon coated copper grid (Agar scientific AGS147-4) or Lacey Carbon Copper grid, and the sample was dried. TEM images were acquired using JEOL JEM-2200FS with field emission gun and 200 kV acceleration voltage. The mean size and size distribution of the nanoparticles were determined by statistical analysis of at least 300 nanoparticles per sample using ImageJ software.

### 4.6.2. Surface characterization of nanoparticles

The surface of nanoparticles was analyzed for surface charge and surface-related functional groups.

#### 4.6.2.1. Surface charge measurement with dynamic light scattering

The DLS method described above was also used to measure particles' surface ζ potential or surface charge. This measurement is based on Brownian motion of the particles in an electric field. ζ potential reflects the potential difference between the electric double layer of electrophoretically mobile particles and the layer of dispersant around them at the slipping plane. In nanoparticles studies ζ potential is interpreted as a measure of the particles' surface charge.

#### 4.6.2.2. Infrared Spectroscopy

Fourier transformed infrared (FTIR) spectroscopy was used to assess the chemical composition of synthesized samples. For FTIR analysis, spectral analysis mode of Bruker Vertex 70 or a PerkinElmer Spectrum 100 FTIR spectrometers were used. Samples were analyzed in attenuated total reflectance (ATR) configuration with diamond crystal, and mercury cadmium telluride detector was used. Data was collected at pre-determined wavelengths.

#### 4.6.2.3. UV-Vis absorption spectroscopy

The UV-Vis absorption was used to assess the fundamental absorption edge for $CeO_2$ nanoparticles in water colloids, which provides information on the state of surface and concentration of defects. Agilent Cary 5000 UV–Vis–NIR device or Thermo Scientific Multiskan SkyHigh microplate spectrophotometer were used in transmission regime.

### 4.6.3. Analysis of nanoparticles and chemicals on textile

Visualization of nanoparticles sprayed onto the textiles was carried out under scanning electron microscope while quantitative composition of nanoparticles and compounds on textile was determined by their chemical analysis using ICP-MS or ICP-OES.

#### 4.6.3.1. Scanning electron microscopy

SEM is a popular method for visualization of micro- and nanomaterials due to its relative simplicity, theoretical nanoscale resolution and capability for three-dimensional analysis [137]. As SEM is based on scanning a sample with an electron beam, it requires samples to be conductive and therefore, non-conductive samples should be covered with a conductive layer. This along with the difficulty in obtaining true nanoscale resolution in case of certain samples could be considered as disadvantages of SEM.

Imaging of textile surfaces was performed with Thermo Fisher Scientific Helios 5 scanning electron microscope after fixing the surfaces or nanomaterial suspensions onto sample holder using conductive carbon tape.

#### 4.6.3.2. Elemental composition analysis using ICP-MS or ICP-OES

Inductively coupled plasma (ICP) based methods such as ICP mass spectrometry are becoming increasingly popular over other analogous methods such as atomic absorption and atomic emission [138]. The ICP-MS method is based on high-temperature plasma atomizing and ionizing the sample and generating ions that will be analyzed using mass-spectrometry. Also, other detection methods can be attached to ICP and, for example, ICP optical emission spectrometry measures the emission of light after the excited ion transfers back to its ground state.

Agilent 7700 ICP-MS and Agilent 5100 ICP-OES instruments were used to determine the elemental concentrations in this study. Concentrations of selected elements were analyzed before the addition of nanoparticles and chemicals to textiles, on textiles and in textile wash-offs.

In [**I** and **II**] the concentration of elements in nanoparticles and nanocontainers was analyzed. Ce, Cu and Br (as an indication for CTAB concentration) were analyzed using ICP-MS and Si was analyzed with ICP-OES. Before measurements the colloids of particles were mixed with diluted $HNO_3$ and directly loaded into the device. In [**I**] also release of ions from nanoparticles was analyzed, for which before the analysis the particles were removed by ultracentrifugation (Optima XE-90 Ultracentrifuge device) 300,000×*g* for 2 h.

To extract the compounds and particles from textile samples in [**II**], textile was incubated with 3:1 mixture of $HNO_3$ and HCl ("reversed aqua regia") and treated using Berghof Speedwave Xpert device until full decomposition. Then, analysis of elements was carried out using ICP-MS. The leaching of elements from textiles was measured after collecting the textile wash-offs from antiviral tests, mixing with diluted $HNO_3$ and analyzed using ICP-MS.

### 4.6.4. Characterization of tryptophan interactions with materials by NMR

The interaction between nanoparticles and tryptophan as a model amino acid was studied using NMR in [**III**]. NMR, although challenging to interpret spectra, is the main method to analyze protein-ligand interactions [139].

The suspensions of $TiO_2$ or $CeO_2$ particles at specified concentrations were mixed with tryptophan and chemical shift standard sodium trimethylsilylpropanesulfonate (DSS), then ultrasonicated in an ultrasonic bath for 10 min at 25 °C and thereafter transferred into 5 mm NMR tubes. NMR analysis was performed by using Bruker Advance III spectrometer operating at 14.1 T, equipped with a cryo-enhanced QCI-P probe at a temperature of 298K. For assignment of NMR the chemical shifts of tryptophan peaks, Bruker standard pulse sequences of 2D TOCSY, HSQC, HMBC, and NOESY were used. Spectra were processed with TopSpin 4.2.0 software. All spectra where tryptophan was titrated with $TiO_2$ or $CeO_2$ particles with the internal $^{1}H$ chemical shift standard, 0.1 mM DSS, and $^{13}C$ chemical shifts were referenced indirectly to the $^{1}H$ standard using a conversion factor derived from the ratio of NMR frequencies.

## 4.7. Statistical analysis

Statistically significant differences in antiviral experiments were confirmed by one-way ANOVA analysis for repeated measurements and post-hoc Tukey's range test with CLD output. P-values of less than 0.05 were considered statistically significant. Statistical analysis was carried out using GraphPad prism or Origin.

# 5. RESULTS AND DISCUSSION

## 5.1 Synthesis and characterization of potentially antiviral nanoparticles

### 5.1.1. Silver nanoparticles

Silver nanoparticles were obtained by seed-mediated citrate route [125]. Average particle size according to HRTEM was 15.3 ± 3.0 nm (Figure 2), hydrodynamic size measured by DLS was 18.5 ± 3.0 nm, and ζ-potential was − 52 ± 5 mV. The maximum concentration reached was 480 mg/L (4.4 mM). Due to the small and uniform size of the particles combined with high negative surface charge, the resulting yellow colloid was extremely stable, and silver concentration could not be increased by centrifugation. HRTEM images show high crystallinity and low degree of aggregation of spherical particles.

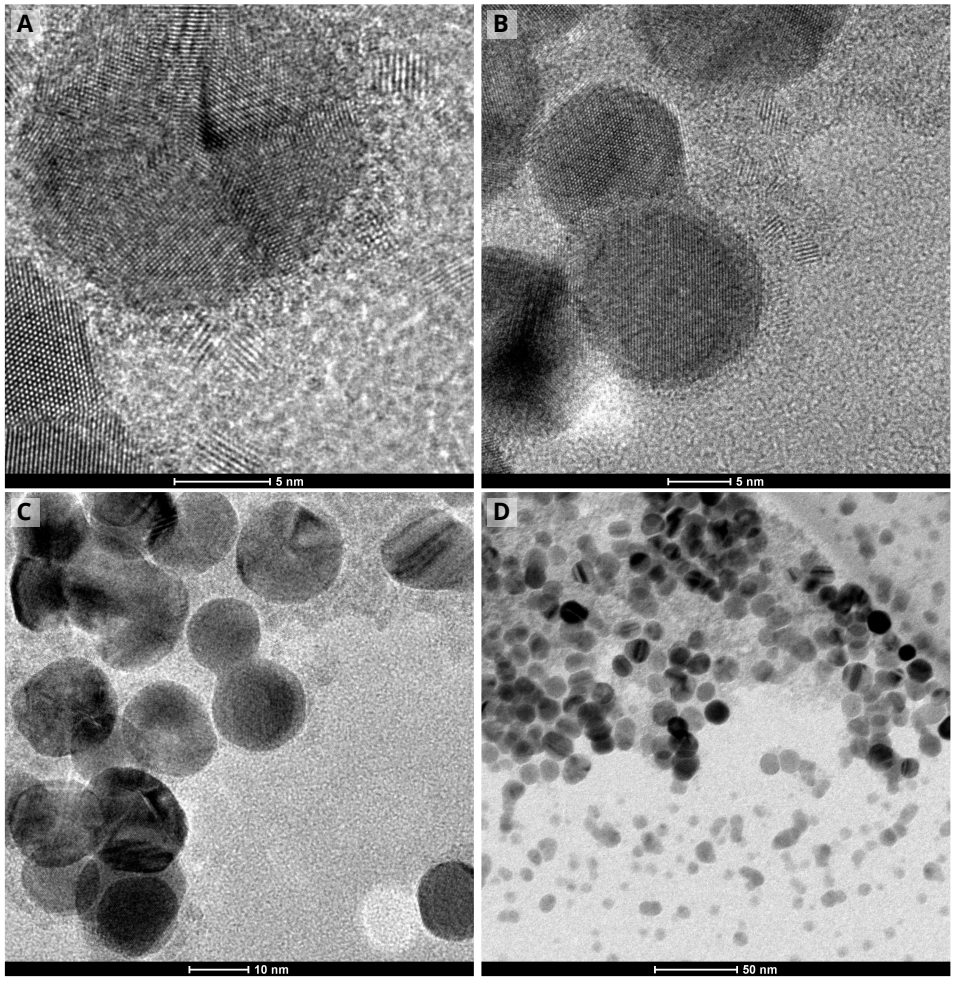


**Figure 2**. HRTEM-images of obtained Ag nanoparticles at various magnifications (scale bar size: A, B – 5 nm, C – 10 nm, D – 50 nm) [**I**]

### 5.1.2. Cerium dioxide nanoparticles

Since the surface interactions play an important role in biological effects of nanoparticles, two types of nano-$CeO_2$ with different states of surface were synthesized: positively charged nano-$CeO_2$(+) with nearly "bare" surface and nano-$CeO_2$(−) particles stabilized by citric ions and thereby carrying a negative surface charge.

To synthesize positively charged ceria nanoparticles, we modified the technique suggested by [46], i.e. microwave-assisted hydrolysis of diammonium cerium (IV) nitrate in the presence of HMTA under hydrothermal conditions. Cerium (III) nitrate used in [46] was replaced with diammonium cerium (IV) nitrate to avoid oxidation-reduction process and thus simplify the composition of the reaction mixture and obtained particles. In original method PVP was added to the reaction mixture as a stabilizer, we did not use it, first, to obtain particles with a positive surface charge, while PVP stabilized particles are frequently negatively charged [139, 140, 141] second, to avoid interference of PVP and its possible derivates in tests on viruses and cells. Due to the absence of a stabilizer, we had to reduce the concentration of cerium in reaction mixture ca. 8 times compared to [46] to obtain a stable colloid solution. The maximal concentration of synthesized $CeO_2$(+) colloid was 6500 mg Ce/L (ca. 45 mM).

Nano-$CeO_2$(−) nanoparticles were synthesized following the modified technique from [126]. The synthesis was carried out in the presence of citric acid, so the obtained ceria nanoparticles were stabilized with citrate ions and carried a negative surface charge. We adjusted the synthetic conditions by reducing citric acid concentration ca. 5 times to obtain dispersible stable colloids and avoid gelation of citric acid. Our target was also to minimize the amount of impurities on the ceria surface caused by decomposition and polymerization of citric ion in concentrated solutions. $CeO_2$(−) nanoparticles colloid solution was obtained with maximal concentration of 8200 mg Ce/L (ca. 60 mM).

Both nano-$CeO_2$(+) and nano-$CeO_2$(−) formed stable aqueous colloids due to their large (+ 41 mV or – 53 mV, respectively) ζ-potential (Table 5). According to high resolution transmission electron microscopy (HRTEM) (representative TEM images of $CeO_2$ nanoparticles are shown in Figure 3), the average particle size of both nano-$CeO_2$(+) and nano-$CeO_2$(−) was close to 3 nm.

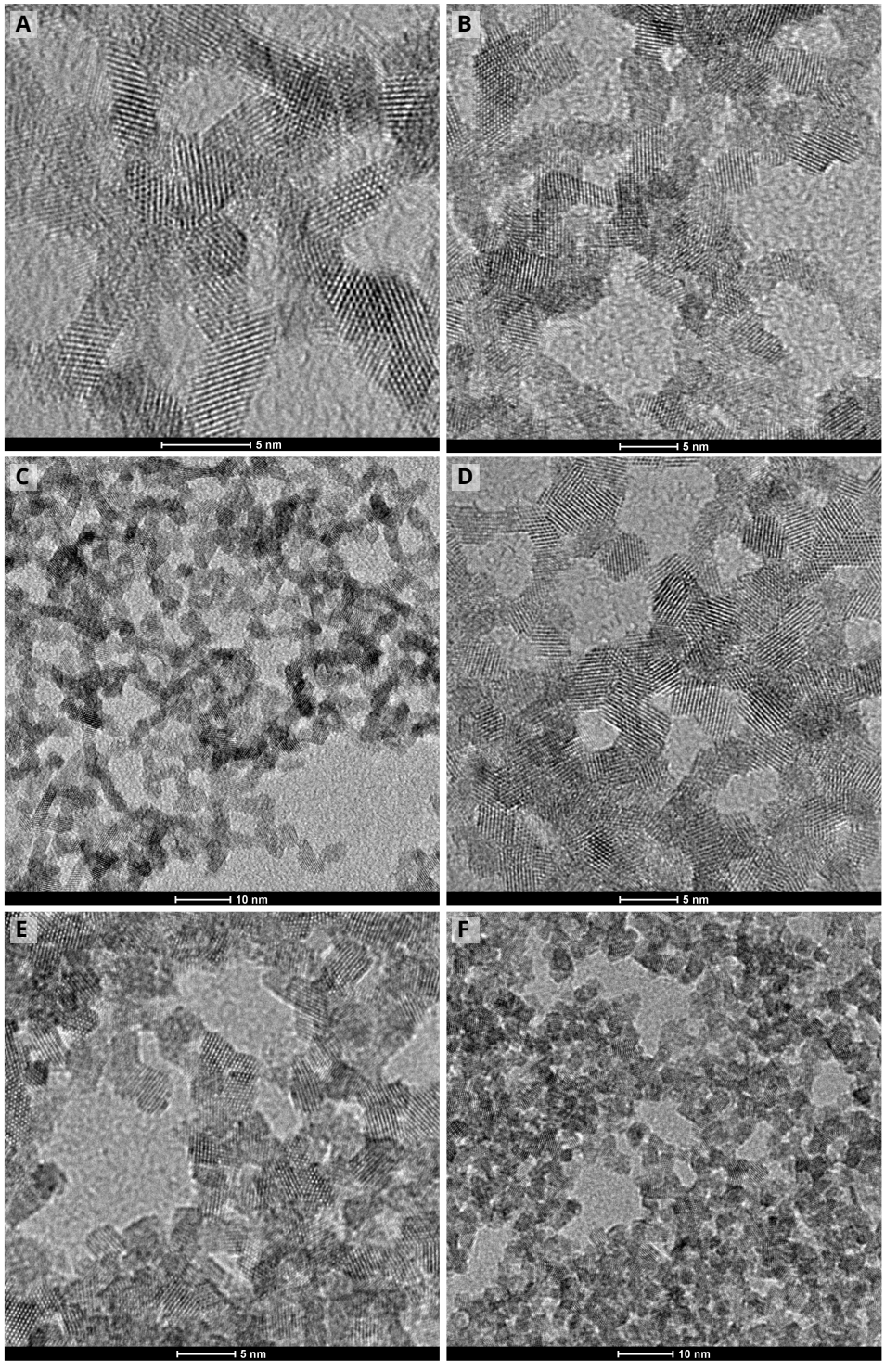


**Figure 3**. HRTEM-images of obtained $CeO_2$ NPs at various magnification (left column (A–C) – $CeO_2$(+), right column (D–F) – $CeO_2$(−)). Scale bar size: A, B, D, E – 5 nm, C, F – 10 nm [**I**]

The hydrodynamic size of nano-$CeO_2$(−) obtained at highest tested antiviral concentration was relatively close to the particles TEM size (Table 5), while nano-$CeO_2$(+) showed some aggregation (hydrodynamic size approximately corresponding to double aggregates). With decrease of nano-$CeO_2$ concentration in colloids an increase in measured hydrodynamic size was observed, i.e. both nano-$CeO_2$(+) and nano-$CeO_2$(−) are more likely to aggregate with dilution of colloids, the latter being more sensitive to dilution-induced instability (Figure 4). This decrease in colloidal stability may be caused by desorption of citric ions from the surface upon dilution of colloid and, thus, the decrease of the surface charge of the nanoparticles. It is worthy to note, that behavior of nano-$CeO_2$(+) and nano-$CeO_2$(−) with dilution is different. Nano-$CeO_2$(+) tends to form particle agglomerates with a relatively narrow size distribution. The mean size of these agglomerates remains almost unchanged with dilution, while only its share is growing compared with the individual particles, which almost disappear after dilution reaches 20 mg/mL. While dilution of nano-$CeO_2$(−) leads to formation of several fractions of agglomerates, which size and share changes non monotonously with concentration of colloid.

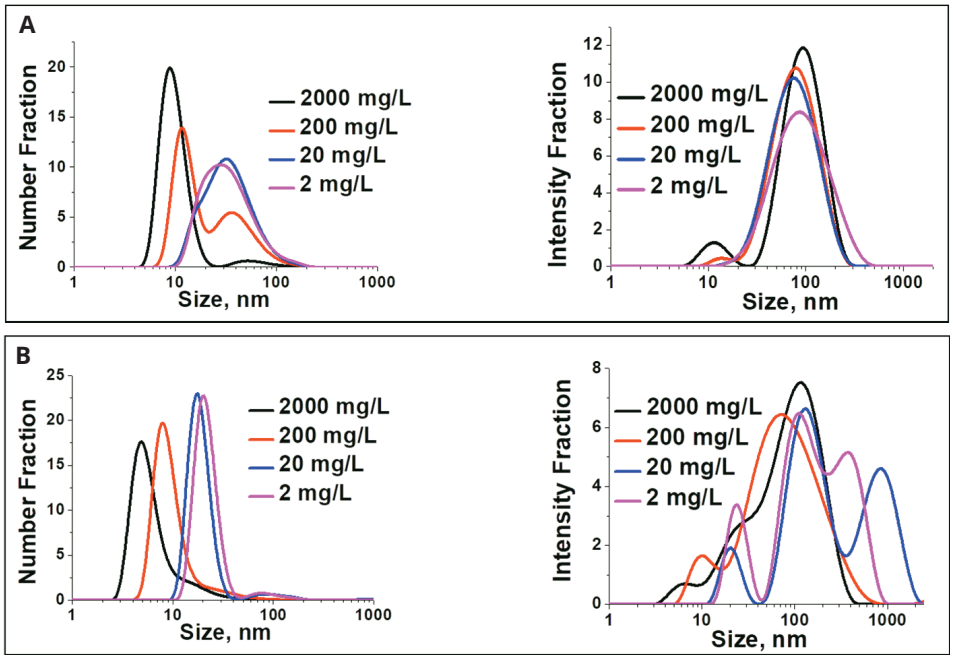


**Figure 4.** Hydrodynamic particle size at various concentrations of nano-$CeO_2$(+) (A) and (−) (B) colloids. The number fraction is shown on the left and intensity fraction on the right. In both nano-$CeO_2$(+) and nano-$CeO_2$(−) colloids individual particles aggregate upon dilution [**I**].

UV–Vis absorption spectra of $CeO_2$ nanoparticles in colloid are shown in Figure 5. The fundamental absorption edge of nano-$CeO_2$(−) is ca. 10 nm red shifted compared to nano-$CeO_2$(+). This shift may be due to the different Ce(III)/Ce(IV) ratio on the surface or may be caused by the presence of products of oxidation and polymerization of citrate ions formed on the surface of nano-$CeO_2$(−) particles during the synthesis. Visually, the colloid of nano-$CeO_2$(−) is more deeply yellow than nano-$CeO_2$(+). The apparent decrease of the absorption in the nano-$CeO_2$(−) colloid below 300 nm is related to the compensation error caused by the absorption of the mother solution (it is symmetrical to the increase of the absorption in mother solution, see Figure 5A, black line). The latter is probably related to the products of citric ion decomposition and/or complexation with cerium ions (or cerium atoms on the surface of nanoparticles).

Infrared (IR) spectrum of the synthesized nano-$CeO_2$ (Figure 5B) agrees with the literature data [143]. Peaks in the region between 3600 and 3200 $cm^{-1}$ correspond to –OH stretching of absorbed water and surface OH-groups. Peaks around 1600 $cm^{-1}$ are H–O–H deformational vibrations, and the signals at 1400 $cm^{-1}$ correspond to C–O stretching vibrations of carbonate ions. The peaks in the region from 700 to 500 $cm^{-1}$ are due to Ce–O stretching vibrations. FTIR of both types of ceria nanoparticles are rather similar. The greater intensity of the bands around 1400 $cm^{-1}$ and 1600 $cm^{-1}$ is most likely due to a higher concentration of sorbed species on the surface of nano-$CeO_2$(−), mainly the citrate ions showing the characteristic band of COO– group [144]. A small blue-shift of the band from 1539 $cm^{-1}$ nano-$CeO_2$(+) to 1546 $cm^{-1}$ for nano-$CeO_2$(−) is probably due to overlapping of H–O–H deformational vibrations with anti-symmetric COO– group stretching band with maximum around 1585 $cm^{-1}$ [144]. In summary, synthesized nano-$CeO_2$(+) and nano-$CeO_2$(−) nanoparticles possess significantly different properties according to DLS data, UV–Vis and IR-spectroscopy. The charge of the nanoparticles and the chemical composition of their surface differ significantly, which may lead to different behavior in biological systems.

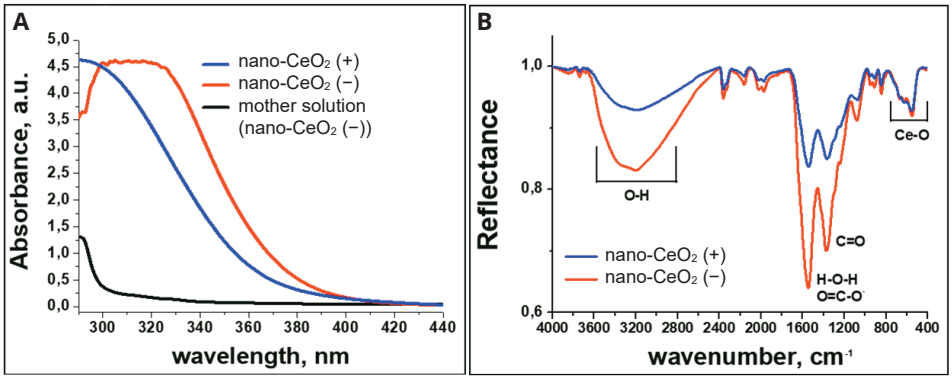


**Figure 5.** Characteristics (A) UV–Vis absorption spectra and (B) infrared reflection spectra of nano-$CeO_2$(+) and nano-$CeO_2$(−). On (A) also the UV–Vis absorption spectrum of nano-$CeO_2$(−) mother solution is shown.

To estimate the possible degree of solubility of synthesized colloids and therefore, assess the possible activity of $Ce^{3+}/Ce^{4+}$ ions apart from nanoparticles, the $CeO_2$ colloids were ultracentrifuged and the concentration of cerium in obtained mother solution was determined by ICP-MS. The concentrations of cerium in supernatants from $1.4 \times 10^{-2}$ M (2000 mg Ce/L) $CeO_2$ colloids were rather low: $8 \times 10^{-5}$ M (12 mg Ce/L) for $CeO_2$(+) and $1.7 \times 10^{-4}$ M (24 mg Ce/L) for $CeO_2$(−). According to the literature data [145], solubility of $CeO_2$ in water at neutral pH range is in the range of $10^{-7}$–$10^{-8}$ M, which is much lower than the value obtained in our experiment. This difference is probably due to incomplete separation of the nanoparticles, but even the measured concentration is too low to affect the treated viruses.

### 5.1.3. Silicon dioxide-based nanomaterials

In this work two types of silica nanostructures were produced: 1) small silicon dioxide nanoparticles acting as a negative control (nanoparticles with no activity) for other antiviral nanoparticles, 2) larger mesoporous silica nanocontainers with the solution of CTAB loaded in mesopores with pronounced antiviral activity.

The negative control small silica nanoparticles (nano-$SiO_2$) were synthesized using the modified Stöber technique. The small size of the silica nanoparticles was achieved by using a larger quantity of ammonia and the addition of the non-toxic PEG as a surfactant. The synthesized nanoparticles had a mean size of 16.6±1.9 nm according to TEM (Figure 6), hydrodynamic size 45±5 nm and ζ-potential −34±3 mV.

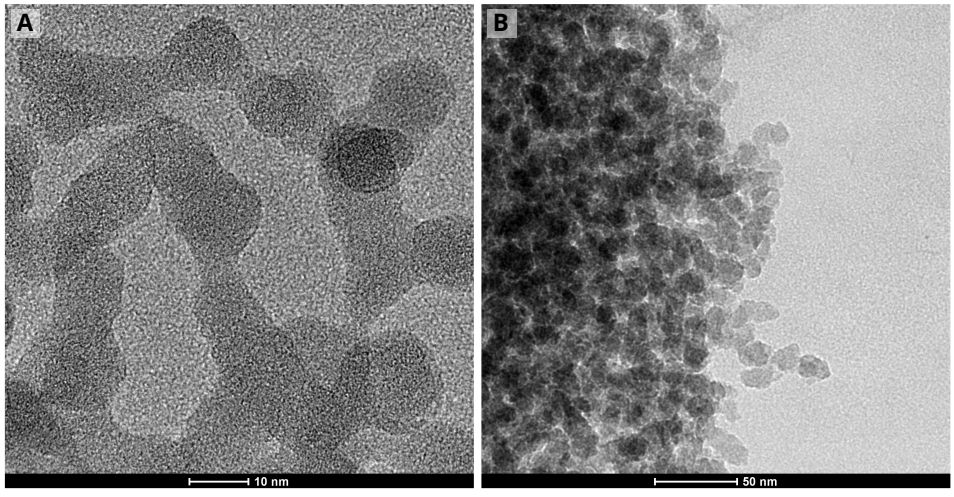


**Figure 6.** HRTEM images of $SiO_2$ nanoparticles. Scale bar size: A – 10 nm, B – 50 nm [**II**]

For the synthesis of antiviral CTAB-loaded silica nanocontainers, a different modification of the Stöber technique was used. The amount of ammonia was crucially reduced compared to the previously described small silica NPs synthesis and CTAB was added to the reaction mixture instead of PEG to serve both as a template for mesopores formation and as an active antiviral component loaded into mesopores in the form of a solution. The mean size of synthesized nanocontainers according to TEM was 59 ± 14 nm with mesopores size of ca. 2 nm (Figure 7). From TEM images it is seen that the pores are closed and have a rather uniform size distribution. Hydrodynamic size (320 ± 90 nm) is significantly larger, indicating that nanocontainers are agglomerating in the colloid, probably due to lower surface charge (−29 ± 3 mV) compared with others synthesized nanomaterials. Unlike the other synthesized NPs, which consist of active antiviral materials, nanocontainers are loaded with the active component, while the main body of nanocontainer is inert towards viruses. Therefore, the concentration of the tested colloids in this case is defined as a concentration of CTAB, which was determined using ICP-MS technique.

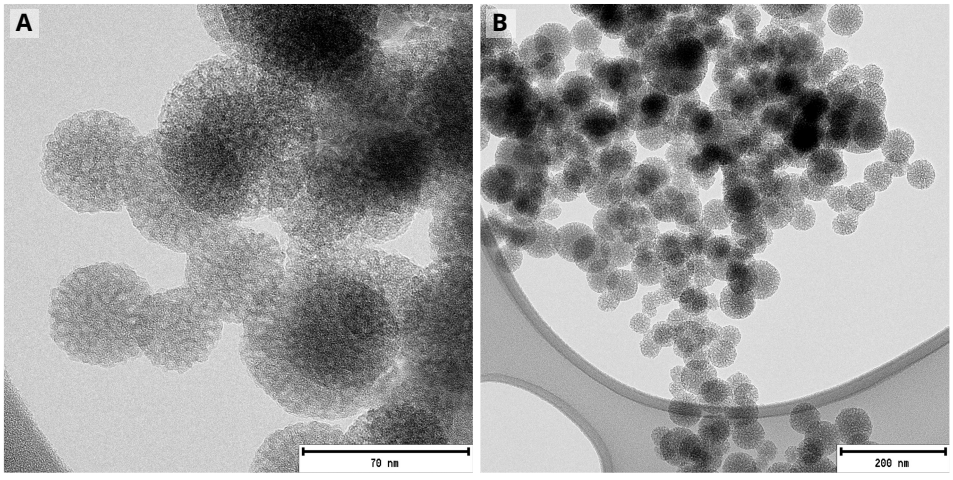


**Figure 7.** HRTEM images of CTAB@$SiO_2$ nanocontainers. Scale bar size: A – 70 nm, B – 200 nm [**II**]

The key characteristics of the synthesized nanomaterials are summarized in Table 5.

**Table 5. Main characteristics of tested nanomaterials**

| Nanomaterial | TEM size, nm | Hydrodynamic size, nm[a] | ζ potential, mV | Tested concentrations |
|---|---|---|---|---|
| Ag | 15.3 ± 3.0 | 18.5 ± 3.0 | − 52 ± 5 | 0.0015–1500 μg Ag/mL |
| $CeO_2$ (+) | 3.3 ± 0.4 | 7.0 ± 3.0 | + 41 ± 2 | 0.002–2000 μg Ce/mL |
| $CeO_2$ (−) | 3.2 ± 0.4 | 4.5 ± 2.0 | − 53 ± 4 | 0.002–2000 μg Ce/mL |
| $SiO_2$ | 16.6 ± 1.9 | 45 ± 5 | − 34 ± 3 | 0.0004–400 μg Si/mL |
| CTAB-loaded $SiO_2$ | 59 ± 14 nm | 320 ± 90 nm | −29 ± 3 | 0.1–10000 μg NPs/mL, i.e. 0.067–667 μg CTAB/mL |

[a] Number-based hydrodynamic size according to DLS (dynamic light scattering) measurements.

From comparison of TEM and hydrodynamic mean sizes it can be noted, that depending on the surface charge nanoparticles tend to either exist in colloid individually (Ag and $CeO_2$(−)) or form two-particle aggregates ($CeO_2$(+) and $SiO_2$) or even larger agglomerates (CTAB@$SiO_2$).

## 5.2. Antiviral properties of studied materials in colloids

In order to select nanomaterials for antiviral treatment of textiles, several types of nanoparticles in the form of colloids were tested against a wide range of viruses, including enveloped and non-enveloped mammalian viruses and bacteriophages.

In total, we tested four potentially antiviral nanomaterials [**I, II**]: nano-Ag, nano-$CeO_2$ (+), nano-$CeO_2$ (−) and CTAB-loaded $SiO_2$ nanocontainers.

- Silver nanoparticles are generally considered as antimicrobial material, antiviral properties of nano-Ag were reported in the literature [145, 146, 147].
- Cerium (IV) oxide is a widely studied material with established bioactivity and antiviral potential (see Section 2.2.1.2 for literature review on antiviral activity of ceria). Since surface properties play a crucial role in particle-virus interactions, we synthesized two types of $CeO_2$ nanoparticles with positive and negative surface charge (nano-$CeO_2$(+) and nano-$CeO_2$(−), see Section 5.1.2).
- CTAB@$SiO_2$, i.e. silica nanocontainers bearing cetrimonium bromide (CTAB) in their mesopores. CTAB is a widely studied antimicrobial agent [149].

Four additional materials served as controls [**I, II**]:

- Nano-$SiO_2$ was used as presumably inert material to control for possible effects of nanostructures per se independent of their chemical composition (e.g. due to high surface-volume ratio).
- Cerium (III) nitrate solution was tested at the same content of Ce per mL as ceria nanoparticles, to evaluate the possible role of $Ce^{3+}$ ions in the antiviral activity of $CeO_2$.
- CTAB solution was used as a comparison for CTAB@$SiO_2$.
- Copper (II) nitrate solution was used as positive control.

The following viruses were studied in this work [**I, II**] (see also Table 3, Section 4.2):

- A/WSN/1933, or Influenza virus, which is an enveloped virus from family Orthomyxoviridae, seasonally important to cause flu in Northern hemisphere
- SARS-CoV-2 that is an enveloped virus from Coronaviridae family, causes COVID-19
- TGEV, or Transmissible Gastroenteritis Virus of pigs, an enveloped virus from family Coronaviridae
- EMCV, encephalomyocarditis virus, which is a non-enveloped virus from family Picornaviridae and a causative agent for neurological disorders
- Φ6, an enveloped bacteriophage of *Pseudomonas* sp.
- MS2, a non-enveloped bacteriophage of *Escherichia coli*

In addition to antiviral assays, the materials were tested on Gram-negative (*E. coli*) and Gram-positive (*Staphylococcus aureus*) bacteria. The studied combinations of tested objects are shown in Table 6.

**Table 6. The studied combinations of materials with viruses and bacteria**

| **Material** | **Influenza** | **SARS-CoV-2** | **TGEV** | **EMCV** | **Φ6** | **MS2** | ***E. coli*** | ***S. aureus*** |
|---|---|---|---|---|---|---|---|---|
| Nano-Ag | + | + | + | + | + | + | + | + |
| Nano-$CeO_2$(+) | + | + | + | + | + | + | + | + |
| Nano-$CeO_2$(−) | + | + | + | + | + | + | + | + |
| Nano-$SiO_2$ | + | + | + | + | + | + | + | + |
| $Ce(NO_3)_3$ | + | + | + | + | + | + | + | + |
| CTAB@$SiO_2$ | – | + | + | – | – | – | – | – |
| CTAB | – | + | + | – | – | – | – | – |
| $Cu(NO_3)_2$ | – | + | + | – | – | – | – | – |

Table 7 and Figure 8 represent the results of antiviral assessment of obtained materials. According to EU legislation [133] only products exhibiting more than 2 log virus titer reduction within up to 1 h in suspension test can be considered as virucidal. Therefore, in our assessment we primarily aimed at 2 log decrease of infectious virus titers as determined in plaque assay.

Later we mostly focus on the results obtained on two coronaviruses, TGEV and SARS CoV 2, since they were studied further on textiles. A more detailed discussion of other viruses and bacteria can be found in our publications [**I, II**]. The results of antiviral tests with two coronaviruses, TGEV and SARS-CoV-2 are summarized in Figure 8.

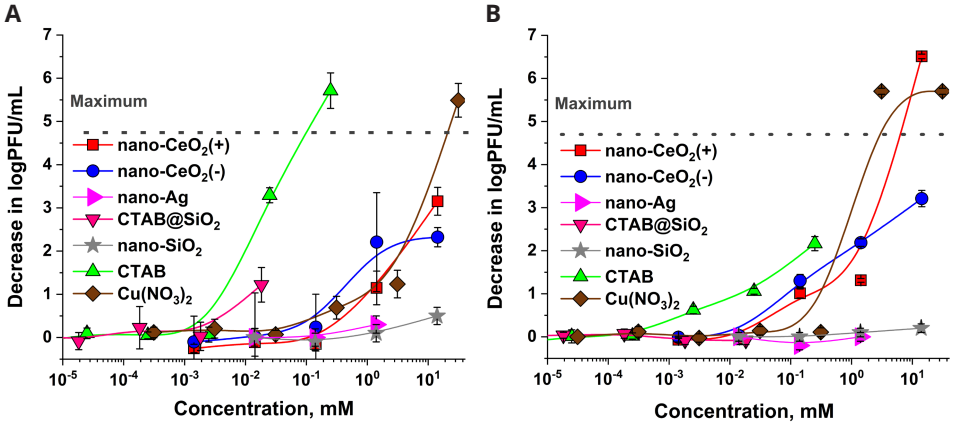


**Figure 8**. Effect of colloidal forms of nanostructures or solutions of compounds on two coronaviruses, TGEV (A) and SARS-CoV-2 (B). The average decrease in log plaque forming units (PFU)/mL from at least three independent experiments with standard deviation is shown. Dotted line represents the maximum decrease in log PFU/mL that could be reliably defined.

**Table 7. Antiviral and bactericidal activity of nanoparticles and $Ce(NO_3)_3$ at various concentrations.** Antiviral activity is expressed as log reduction in infectious viral titer compared to unexposed control after 1h. Bactericidal activity is expressed as log reduction in viable counts compared to unexposed control after 1h. Concentrations causing at least 1 log (90%), 2 logs (99%), 3 logs (99.9%) and 4 logs (99.99%) decrease are indicated with light to dark green color gradient. * p<0.05, ** p<0.01, *** p<0.001 and **** p<0.0001.

| **Concentration** mg/L (μM) | **Enveloped** | | | | **Non-enveloped** | | **Bacteria** | |
|---|---|---|---|---|---|---|---|---|
| | **Viruses** | | | **Bacteriophages** | **Viruses** | **Bacteriophages** | **Gram-negative** | **Gram-positive** |
| | SARS-CoV-2 | TGEV | Influenza virus | Φ6 | EMCV | MS2 | *E. coli* | *S. aureus* |
| **nano-$CeO_2$(+)** | | | | | | | | |
| 2 (14) | 0.0 | –0.1 | 0.1 | 0.2 | –0.2 | –0.2 | 0.32 | 0.14 |
| 20 (142) | 1.1 * | –0.2 | 1.5**** | 4.4**** | –0.3 | 0.1 | 0.94* | 0.07 |
| 200 (1427) | 1.4 ** | 1.1*** | 1.6**** | 6.4**** | –0.2 | 0.4 | 1.03* | 0.06 |
| 2000 (14 270) | 6.7 **** | 3.2**** | 4.3**** | 6.4**** | –0.3 | 0.4 | 0.43 | 0.11 |
| **nano-$CeO_2$(–)** | | | | | | | | |
| 2 (14) | 0.1 | 0.0 | 0.4 | –0.2 | –0.1 | 0.4 | 1.52**** | 0.10 |
| 20 (142) | 1.4 ** | 0.2 | 2.0**** | 0.0 | –0.1 | 1.6*** | 1.68**** | 0.13 |
| 200 (1427) | 2.3 **** | 2.2**** | 2.4**** | 2.9**** | –0.1 | 1.4** | 1.48*** | 0.02 |
| 2000 (14 270) | 3.3 **** | 2.3**** | 4.3**** | 2.8**** | 0.2 | 0.1 | 0.18 | –0.03 |
| **$Ce(NO_3)_3$** | | | | | | | | |
| 2 (14) | 0.0 | 0.1 | 0.4 | 0.1 | –0.4 | –0.2 | 1.68**** | 0.05 |
| 20 (142) | 0.9 | 0.2 | 3.3**** | 3.3**** | –0.3 | 0.0 | 2.83**** | 0.15 |
| 200 (1427) | 1.9 **** | 0.9 | 4.7**** | 6.0**** | –0.1 | 0.4 | 3.52**** | 0.25 |
| 2000 (14 270) | na | 1.2* | 4.7**** | 6.4**** | –0.1 | 0.8 | 6.76**** | 1.02** |
| **nano-Ag** | | | | | | | | |
| 1.5 (14) | 0.0 | 0.0 | 0.3 | 5.3**** | –0.1 | –0.2 | 6.70**** | 0.40 |
| 15 (140) | –0.2 | 0.0 | 0.2 | 6.3**** | 0.0 | –0.2 | 6.70**** | 7.29**** |
| 150 (1400) | 0.0 | 0.3 | 0.5 | 6.3**** | –0.2 | –0.2 | 6.70**** | 7.29**** |
| 1500 (14 000) | na | na | na | na | Na | na | na | Na |

Silica nanoparticles, as expected, showed no activity against viruses nor bacteria, confirming that just contact with nano-sized particles itself has no antimicrobial effect.

Silver nanoparticles in our experiment exhibited a significant activity only against enveloped bacteriophage Φ6 along with a high bactericidal activity. While the antimicrobial activity was anticipated, the lack of antiviral activity seemed rather surprising and contradictory to literature data. At a closer look, however, it becomes clear that the antiviral properties of silver are usually overestimated. Articles claiming antiviral activity of silver nanoparticles often demonstrate less than 90% (i.e. less than one log) decrease of virus titer. Thus, [150] reported the maximum of 92% of HBV inhibition after exposure to 50 μM 50 nm silver nanoparticles and [146] demonstrated up to 79% decrease in infectivity of monkeypox virus after 15 min exposure to nanosilver in the range 12.5–100 μg/mL. The replication of respiratory syncytial virus (RSV) decreased by 79% in A549 cells and 78% in HEp-2 cells upon 1 h exposure to 50 μg/mL PVP-stabilized Ag nanoparticles (the most effective dose in either cell type) [148]. Mycosynthesized silver nanoparticles were tested against herpes simplex and human parainfluenza virus type 3 with maximum inhibition of less than 90% at 5–10 μg/mL Ag [147].

Both nano-$CeO_2$ (+) and nano-$CeO_2$(−) demonstrated a promising activity against enveloped viruses. In case of $CeO_2$(+), the highest tested concentration of 2000 mg Ce/L (14 mM) was active against all the tested enveloped viruses with minimum log PFU decrease of 3.2 for TGEV and maximum of 6.7 for SARS-CoV-2. $CeO_2$(−) showed a significant activity against enveloped viruses already at 200 mg/l Ce (from 2.2 log for TGEV to 2.9 log for Φ6). In case of influenza virus, the threshold of 2.0 log PFU decrease was reached at 20 mg Ce/L (142 μM). No significant activity was detected against non-enveloped viruses. Interestingly, no significant bactericidal activity was detected either.

CTAB-loaded $SiO_2$ nanocontainers did not affect SARS-CoV-2; in the case of TGEV, ca. 1 log PFU reduction was obtained at the highest tested concentration (0.01 mM). CTAB solution exhibited activity against TGEV at lower concentration than against SARS-CoV-2 (one log decrease in PFU obtained at about 0.002 mM and 0.01 mM respectively).

Higher susceptibility of TGEV to CTAB was somewhat surprising. A possible explanation may be related to different cholesterol content in the viral membranes. A specific role of cholesterol in infections of cells with TGEV was demonstrated in [151]. Cholesterol content in SARS-CoV-2 membrane is relatively low [152]. It was shown [153] that cholesterol provides a negative charge to lipid membrane, so we can assume that higher cholesterol content promotes the interaction with cationic CTAB.

In addition, cytotoxicity of the investigated materials on host cells was studied and antiviral properties of citric acid were tested to exclude their possible influence on the experimental results.

## 5.3. An approach to the mechanism of action of nanoceria

To explain our finding on selective antiviral activity of nanoceria, a more detailed mode of action study was carried out. Due to fact that solubility of ceria is very low [145] we concluded that the antiviral effect of ceria nanoparticles could not be due to the release of $Ce^{3+}$ ions. Also, our experiments with solutions of $Ce(NO_3)_3$ had demonstrated that the antivirally active concentrations of $Ce^{3+}$ ions are several orders higher than achievable due to the release of ions from $CeO_2$ nanoparticles [**I**]. Therefore, our hypothesis was that the antiviral mechanism was related to $Ce^{4+}/Ce^{3+}$ redox process taking place on the surface of nanoparticles. We suggested a selective oxidative action of ceria on virus envelope (direct or via ROS formation). As a first approach to establishing the mechanism, we studied the interaction of ceria and other nanoparticles with tryptophan as a model amino acid [**III**]. Tryptophan (Trp, TRP) is a proteinogenic amino acid (Figure 9A) playing an important role in metabolism of various organisms, which is highly susceptible to oxidation and therefore presents a rather probable target for the redox activity of $CeO_2$ nanoparticles [154]. Moreover, our colleagues from Swedish University of Agricultural Science had previous experience in NMR studies of tryptophan.

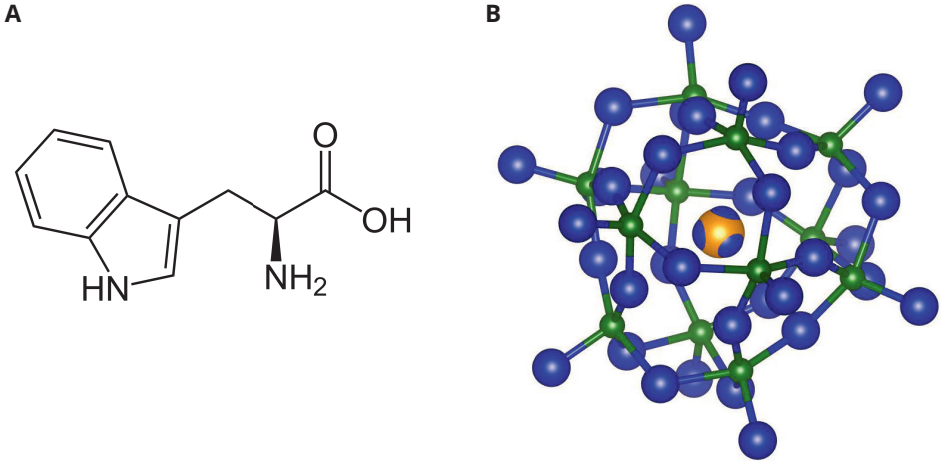


**Figure 9.** L-Tryptophan (A) and $H_3PW_{12}O_{40}$ (B). Blue spheres – oxygen, green spheres – tungsten, yellow sphere – phosphorus (protons are not displayed)

Along with nano-$CeO_2$(+) and $CeO_2$(−), the interaction of tryptophan with two types of titanium dioxide nanoparticles and phosphotungstic acid, $H_3PW_{12}O_{40}$ (W-POM) (Figure 9B), which are in the focus of interest of our collaborators, were studied. Characteristics of the studied particles are summarized in Table 8 (particles size and ζ potential measured by DLS).

**Table 8. Studied nanoparticles, methods of their synthesis and main characteristics**

| NPs | Size, nm | ζ, mV | Source |
|---|---|---|---|
| $CeO_2$(+) | 7.0 | +41 | $(NH_4)_2Ce(NO_3)_6$, HMTA, $H_2O$, MW, 180°C, 30 min |
| $CeO_2$(−) | 4.5 | −53 | $Ce(NO_3)_3$, $NH_4OH$, $O_2$ (air), sodium citrate |
| W-POM | 1.04 | | Phosphotungstic acid, $H_3PW_{12}O_{40}$ |
| $TiO_2$ I | 3.8 | −8 | $Ti(OEt)_4$ 1) $N(C_2H_4OH)_3$; 2) $HNO_3$/EtOH |
| $TiO_2$ II | 3.2 | −11 | Titanium(IV) bis(ammonium lactato)dihydroxide, $H_2O$ |

Screening of NMR spectra with variation of NP:TRP ratio was performed to detect interactions between them and, if possible, to identify the products of TRP transformation in the presence of nanoparticles. It was assumed that the identification of these products would help to understand the mechanism of TRP transformation in the presence of nanoparticles.

Detailed results for $TiO_2$ nanoparticles and W-POM are presented in the paper [**III**] and we're not reproducing them here, as both synthesis of nanoparticles and NMR experiments were performed by our Swedish collaborators. The main result was that in the absence of light, $TiO_2$ does not oxidize TRP molecule and only forms a strongly bound inner sphere complex with it by the replacement of the original ligands, stabilizing titania nanoparticles in the sol, which manifests with the constant width of the NMR lines during titration (Figure 10A, B). W-POM forms a charge transfer complex with TRP molecules, which structure is described in [**III**].

The behavior of $CeO_2$:TRP mixtures (both nano-$CeO_2$(−) and nano-$CeO_2$(+)) during NMR screening was characterized by the decrease of TRP lines intensities and the increase of broadening (Figure 10C, D) starting from very low concentrations of nanoparticles added. Another feature is the up-field chemical shifts of the lines corresponding to aromatic protons (Figure 10D) for TRP titrated with nano-$CeO_2$(+). A new set of resonances is observed in the 1D $^1H$ NMR spectra of TRP titrated with nano-$CeO_2$(−) suggesting formation of a new compound (Figure 11). The same compound was observed in the NMR spectrum of the mother solution after TRP reaction with W-POM. These results suggest the formation of the weakly bound (outer sphere) complexes of TRP with nano-$CeO_2$ accompanied by the chemical reaction leading to the transformation of TRP into a new compound in the case of nano-$CeO_2$(−).

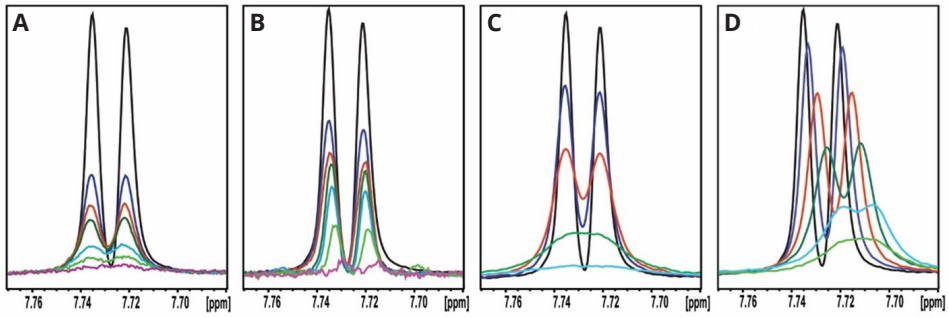


**Figure 10.** Titration of 0.5 mM TRP with $TiO_2$-I (A), $TiO_2$-II (B), $CeO_2$(−)(C) and $CeO_2$(+)(D) showing on H6 proton resonance of TRP at 7.728 ppm. The following colors of curves obtained at different rations of NP/TRP were used. (A), (B) TRP: $TiO_2$-I or $TiO_2$-II: 0.5 mM: 0 mM (black); 0.5 mM:0.031 mM (blue); 0.5 mM:0.0625 mM (red); 0.5 mM:0.125 mM (green); 0.5 mM:0.250 mM (light blue); 0.5 mM:0.5 mM (light green); 0.5 mM:1.0 mM (rose). (C), (D) TRP: $CeO_2$(−)(C)/or $CeO_2$(+)(D): 0.5 mM: 0 mM (black); 0.5 mM:0.0005 mM (blue); 0.5 mM:0.001 mM (red); 0.5 mM:0.002 mM (green); 0.5 mM:0.005 mM (light blue); 0.5 mM:0.007 mM (light green) [**III**].

Several different paths of oxidation of TRP are known and it is rather complicated to establish a product of oxidation without special analysis. Therefore, an additional study by means of series of 2D NMR experiments with support of LC-MC analysis was performed. Detailed results of these experiments can be found in supplementary to the [**III**]. The formed compound was identified as 3-hydroxypyrroloindol carboxylic acid (PIC).

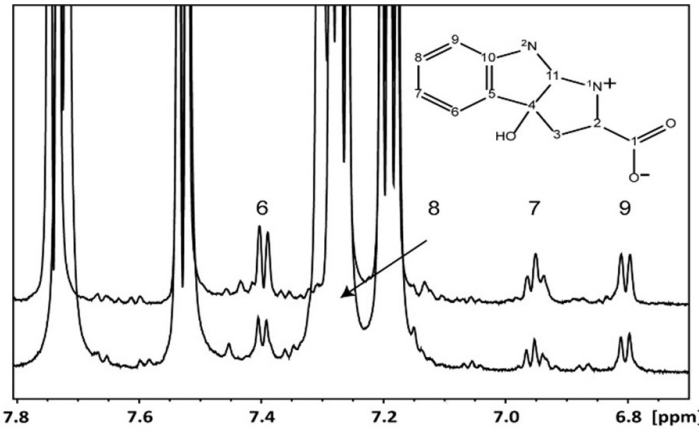


**Figure 11**. 1D $^1$H spectrum with assignment of the proton resonances of oxidized product of TRP obtained in mixture with nano-$CeO_2$(−) NP. Expanded spectra in the aromatic 8.0–6.5 ppm region are presented. The assignment and numbering are shown according to the structure on the panel. Lower normalized spectrum corresponds to overnight treatment of 1 mg/mL TRP in the presence of 8 mg/mL $CeO_2$(−) immediately after centrifugation and gives 2.9 ± 0.5% of the primary product by integration. Upper spectrum is for the sample after removal of ca. 90% $CeO_2$(−) by centrifugation and 1 month storage at 5 °C. The primary oxidized product content 6.4 ± 0.4% by integration [**III**].

Analysis of the NMR and LC-MC chromatography results allowed us to suggest the possible three stage mechanism of the TRP oxidation after formation of a complex with nano-$CeO_2$(−) (Scheme 1). The oxidation process is going in two stages, each of them involves proton-coupled electron transfer. On the first stage indole five membered ring loses aromaticity with formation of the radical cation and on the second stage radical cation transforms into cation and simultaneously the third ring closes with attachment of nitrogen from the amine group to the carbon of the indole five membered ring. On the third stage the formed carbocation attaches water and transforms into PIC. The process results in the formation of the excess of $Ce^{3+}$ ions on the surface of $CeO_2$ nanoparticles, which is oxidized back by the dissolved oxygen from the air to restore equilibrium $Ce^{3+}/Ce^{4+}$ ratio.

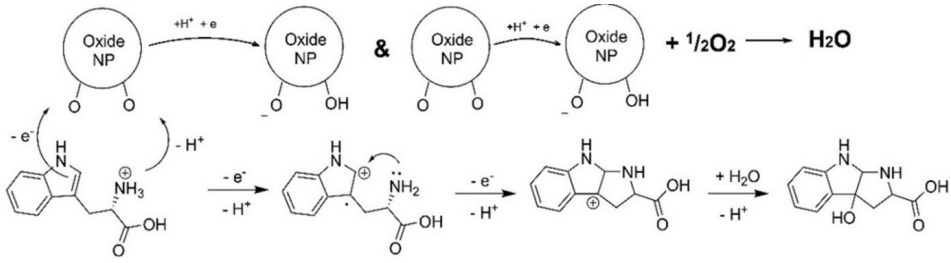


**Scheme 1.** Proposed molecular mechanism of TRP oxidation based on observed structural features of the POM-TRP complex, theoretical calculation and the identified nature of the reaction product. The latter is apparently generated in a neutral form, but will then, of course, transform into a zwitter-ion [**III**].

Oxidation of TRP was found to be not stereospecific – two stereoisomers of the product were detected by LC-MS in comparable quantities. After prolonged incubation (1 month) of TRP with nano-$CeO_2$(−) the second product – dioxoindolealanine – and the third product – kynurenine – become detectable also in the form of two stereoisomers. All the observed products are characteristic to the process of TRP photooxidation with the singlet oxygen [154]. It is important to note that PIC as the prevailing product of oxidation, was previously observed in rather acidic conditions [155], nano-$CeO_2$ allows to generate this compound in biologically compatible environment.

Thus, our study has shown that oxidation of tryptophan by cerium dioxide is not related to ROS formation but is based on a proton-coupled electron transfer mechanism leading to the formation of 3-hydroxypyrroloindol carboxylic acid.

## 5.4. Characterization of textiles finished with antiviral nanomaterials

For antiviral finishing we used knitted polyester fabric consisting of threads with a diameter of ca. 400–500 μm, which in their part are formed by densely packed fibers with a diameter of ca. 10 μm. General microstructure of the textile before treatment with nanomaterials is shown in Figure 12.

Spray-coating was selected as the simplest finishing method to avoid complicated experimental techniques before the antiviral potential of treated textile is assessed.

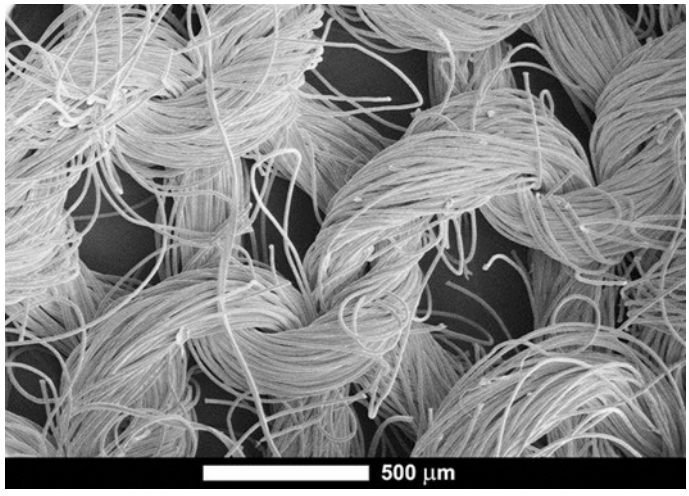


**Figure 12.** SEM microphotograph of the untreated polyester textile at low magnification [**I**]

The materials selected for textile treatment are presented in Table 9. Silver nanoparticles were not used to prepare antiviral textiles, as they were found to have little to none antiviral activity in colloids (see Section 5.2).

**Table 9. Materials deposited onto the textile**

| **Material** | **Function** | **Reasons for selecting** |
|---|---|---|
| $CeO_2$(+) | Potentially antiviral material | Promising antiviral properties in colloidal form [**I**] |
| $CeO_2$(−) | Potentially antiviral material | Promising antiviral properties in colloidal form [**I**] |
| CTAB@$SiO_2$ | Potentially antiviral material | Promising antiviral properties in colloidal form [**II**]. The gradual release of the active agent from the mesopores of silica could prolongate its activity. |
| CTAB | Comparison for CTAB@$SiO_2$ | Aqueous solution of CTAB with approximately the same concentration as in CTAB@$SiO_2$ was used |
| $Cu(NO_3)_2$ solution | Positive control | A source of $Cu^{2+}$ ions known for their antiviral activity [156] |

The microstructure of textile samples before and after the treatment with nanoparticles is shown in Figure 13. The SEM images show that the character of particles distribution on textile depends on their chemical composition and morphology. While $CeO_2$ tends to form a continuous layer on the surface of the fiber, CTAB-loaded $SiO_2$ forms islands of various sizes. Since polyester composing the textile has no surface functional groups capable of forming covalent bonds with nanoparticles under spraying conditions, we suggest that the attachment of the particles onto the textile is only due to adhesion, i.e. Van der Waals forces and weak hydrogen bonding. The main factor determining the efficiency of transfer of nanocontainers from colloid onto textile is thus the surface/volume ratio of the particles characterizing their surface activity, so during spraying the losses of smaller ceria particles are expected to be lower. A stronger aggregation in CTAB@$SiO_2$ colloid compared to nanoceria could also contribute to this effect.

To assess the durability of the textiles coating, during antiviral assay we measured the release of active components from treated textiles as described in Section 4.4. The release behavior of potentially antiviral agents from textile differs significantly depending on their chemical properties (Table 10). The sample treated with $Cu(NO_3)_2$ demonstrated the highest release rate: after 1 hour and 24 hours 23% and 50% respectively of the initial $Cu(NO_3)_2$ loading was leached out. In the case of $CeO_2$ NPs, only negligeable release was observed (0.16% and 0.32% of the initial loading after 1 and 24 hours, respectively). Since according to literature data, the solubility of $CeO_2$ is very low [145], this release was probably due to detachment of particles from textile surface. The release of CTAB from CTAB textile surface was unexpectedly low, reaching only 3.5% of the initial loading in both 1 hour and 24 hours experiments. Interestingly, CTAB@$SiO_2$ textile demonstrated a CTAB release of 5% of initial loading after 1 and 24 hours, comparable with that of CTAB textile. It can be assumed that CTAB trapped in $SiO_2$ mesopores could be released slowly but continuously. However, the result of our experiment is most likely due to dissolution of the CTAB sorbed directly on the surface of $SiO_2$ nanocontainers, while CTAB in the pores is not released during the antiviral experiment. It is worth noting that the $SiO_2$ content in the wash-offs from CTAB@$SiO_2$ textile was extremely low (0.04% of the initial load), i.e. $SiO_2$ nanocontainers were relatively tightly bound and did not detach from the textile surface. Those observations allow us to conclude that soluble copper salts such as $Cu(NO_3)_2$, despite their high antimicrobial activity, are not suitable for finishing of textile intended for use in moist environment, since the active component is leached very quickly and no long-lasting application is possible. Nanomaterials applied on textile surface are more durable and allow for the slower release of the active components. It must be admitted, however, that the nanomaterial loadings studied in this work are probably excessive for real-life application of textile materials. Thus, textile treated with both positively and negatively charged $CeO_2$ turned visibly yellowish. On the other hand, the CTAB@$SiO_2$ treated textile did not visibly change compared with untreated textile. Addition of pure CTAB on the surface of textile in the same quantities as in CTAB@$SiO_2$ changes the touching sensation of the fabric making

it “soapy”. Therefore, CTAB@$SiO_2$ appears to be the most promising candidate for textile treatment, as along with antiviral efficiency it imposes minimal changes on its appearance and tactual properties.

**Table 10. Characteristics of textiles tested for antiviral activity**

| **Applied material** | **Concentration in sprayed colloid solution** | **Active compound on textile, per piece[a]** | **Active compound in wash-off per piece[a] (% from initial quantity on textile)** | |
|---|---|---|---|---|
| | | | **1 hour[b]** | **24 hour[b]** |
| $CeO_2$ (+) | 21.5 mM | 8.7 µmol $CeO_2$ | 0.014 µmol $CeO_2$ (0.16%) | 0.028 µmol $CeO_2$ (0.32%) |
| $CeO_2$ (−) | 27.1 mM | 8.7 µmol $CeO_2$ | 0.014 µmol $CeO_2$ (0.16%) | 0.028 µmol $CeO_2$ (0.32%) |
| CTAB-loaded $SiO_2$ | 215 mM SiO2 and 0.0013 mM CTAB | 343 µmol $SiO_2$ and 0.04 µmol CTAB | 0.13 µmol $SiO_2$ (0.04%) and 0.002 µmol CTAB (5%) | 0.14 µmol $SiO_2$ (0.04%) and 0.002 µmol CTAB (5%) |
| CTAB | 0.005 mM | 0.05 µmol CTAB | 0.0015 µmol CTAB (3.5%) | 0.0015 µmol CTAB (3.5%) |
| $Cu(NO_3)_2$ | 62.5 mM | 7.5 µmol $Cu(NO_3)_2$ | 1.75 µmol $Cu(NO_3)_2$ (23%) | 3.75 µmol $Cu(NO_3)_2$ (50%) |

[a] 4 $cm^2$ or 0.045 ± 0.008 g textile piece
[b] See Section 4.5. for more detailed procedure of wash-offs collection

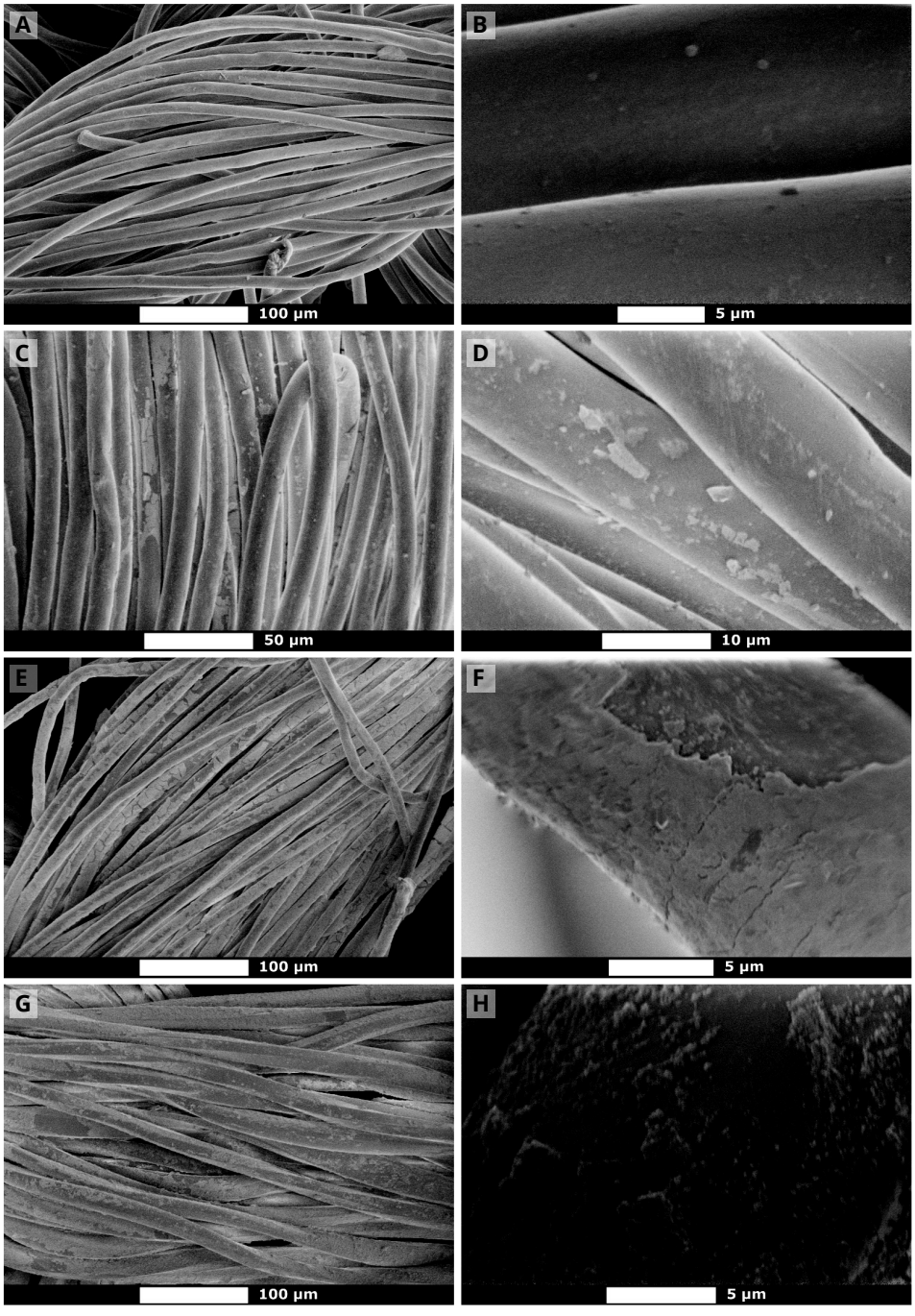


**Figure 13.** SEM images of textiles sprayed with nanomaterials. (A–B) untreated textile, (C–D) $CeO_2$(+) textile, (E–F) $CeO_2$(−) textile, (G–H) CTAB@$SiO_2$ textile. Scale bar size: A, E, G — 100 µm, C – 50 µm, D – 10 µm, B, F, H – 5 µm [**II**]

## 5.5. Antiviral properties of nanomaterial-treated textiles

Based on the antiviral assessment of colloids, the following materials were used for textile treatment in this experiment [**II**]: $CeO_2$(+) and (−) nanoparticles and silica nanocontainers loaded with CTAB as potentially antiviral materials, CTAB solution as comparison for CTAB-loaded silica and copper nitrate solution as a positive control. Two coronaviruses, namely TGEV and SARS-CoV2, were selected for the assessment of the antiviral activity of prepared textiles. Characteristics of treated textiles are summarized in Table 10, Section 5.4.

To mimic the real-life virus transmission, in our experiments we selected semi-dry exposure conditions. Virus stock was evenly applied to a textile sample in 2 μL droplets imitating real-life conditions of virus transmission, left for selected time interval in closed light-protected plastic tube at room temperature, then washed with SCDLP to neutralize after-effects of antiviral materials and used to infect cells. Before the test, virus stock was supplemented with soil load containing mucin, a gel-forming product of animal epithelial tissues, imitating saliva, nasal or gastrointestinal mucosa to make experimental conditions closer to airborne (SARS-CoV-19) or fecal-oral (TGEV) ways of transmission.

Prior to testing antiviral activity of treated textiles, a persistence experiment on untreated textile was performed to determine the meaningful duration for the antiviral test. According to the literature data on persistence of viruses on textiles [157], some coronaviruses may preserve their infectivity for ca. 1 day on cotton, with a general tendency to persist longer on synthetic fabrics. For the persistence test, the virus stock with the same initial titer as in antiviral tests was applied as described above to a sample of untreated textile or directly onto the walls of the tube (no textile control) and then either immediately washed with SCDLP (0 h) or kept for 1, 24, 48 and 72 h and then washed and used to infect cells.

Both tested coronaviruses demonstrated a very low to no decrease of infectivity after 0 and 1 hour of exposure to non-treated (control) textile. After 24 hours, infectivity of SARS-CoV-2 decreased by ca. 1.5 log, while log reduction for TGEV was less than one. For both viruses there were no significant differences between samples with and without textile, so the inactivation of virus on control textile was caused rather by simple drying than by any specific interaction with textile. After 48 hours, SARS-CoV-2 was completely inactivated on control textile, but still persisted in “no textile” control samples, although titer reduced by 2 logs. Log decrease for TGEV after 48 hours on either control textile or without textile was still less than 2. After 72 hours, SARS-CoV-2 was completely inactivated on control textile and in no textile conditions, while TGEV showed approximately 2 log reduction of titer (Figure 14). This result demonstrates that antiviral agents providing an effect before 24 and even 48 hours could be applicable and 0, 1 and 24 hours would be reasonable timepoints.

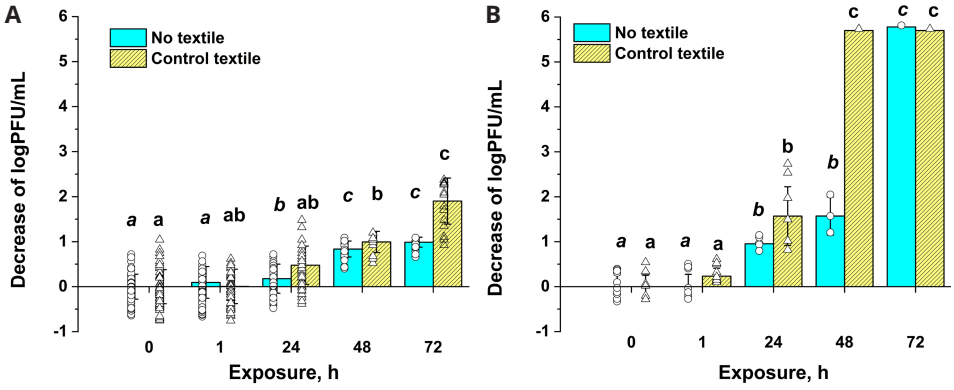


**Figure 14**. Infectivity of TGEV (A) and SARS-CoV-2 (B) expressed as log plaque forming units (PFU)/mL after semi-dry exposure to untreated (control) textile or in a similar exposure without textile during 1–72 hours. Lower case letters indicate statistically independent groups, as according to Tukey range test with P-value <0.05 [**II**].

The results of textile antiviral assessment are shown in Figure 15. As expected, textile treated with copper nitrate showed the most significant antiviral activity with more than 3 logs decrease in infectivity after 1 hour of exposure. After 24 hours exposure, the decrease in infectivity reached 4 logs for SARS-CoV-2 and was close to 3 logs for TGEV. Unlike copper nitrate, both (+) and (−) $CeO_2$, although exhibited a promising antiviral activity when tested in colloidal form, provided no significant activity when applied on textile. The maximum decrease in infectivity (TGEV, 24 hours exposure) was less than 1.5 logs, while minimal biologically meaningful activity requires at least 2 logs reduction. These results are comparable, as loading of nano-$CeO_2$ and copper nitrate on textile was very similar (7.5 µmol of $Cu(NO_3)_2$ vs. 8.7 µmol of $CeO_2$ per textile piece, see Table 10, Section 5.4). A possible explanation could be that due to high solubility, the release of copper ions was significant even in semi-dry conditions of the test on textile, while $CeO_2$ nanoparticles were not released from the textile surface. In other words, activity is related to the release of the noticeable amount of active agent and in the case of very low or no release, the antiviral activity will also be very low.

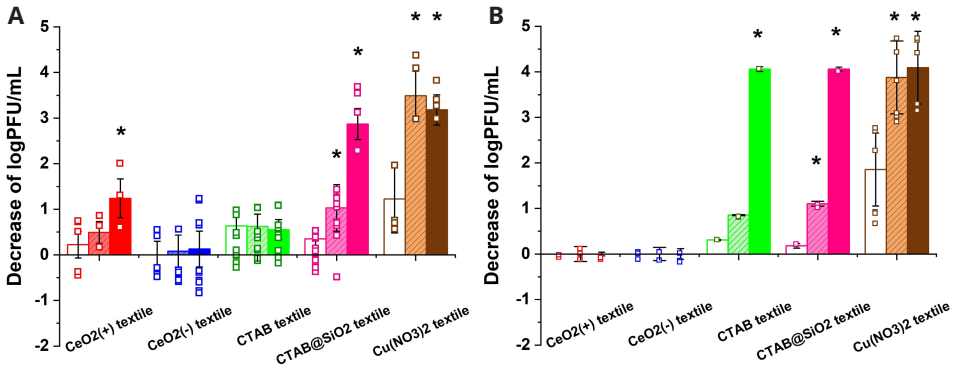


**Figure 15**. Decrease in log plaque forming units (PFU)/mL of TGEV (A) and SARS-CoV-2 (B) on treated textiles as compared with control non-treated textile at the same timepoint. White-out columns represent 0 hours exposure, light colored and textured – 1 hours exposure and dark colored – 24 hours exposure. The results that are statistically different from the corresponding control textiles according to Tukey range test with P-value <0.05 are marked with asterisk [**II**].

CTAB@$SiO_2$ on textile also demonstrated a noticeable antiviral activity, however a significant titer decrease (> 3 log reduction) was achieved only after 24 hours of exposure. As CTAB release from CTAB and CTAB@$SiO_2$ treated textile was comparable (Table 10, Section 5.4), a similar antiviral behavior would be expected for both of those textiles. Indeed, it was the case of SARS-CoV-2, however in case of TGEV CTAB textile showed a lower efficiency than CTAB@$SiO_2$ textile (Figure 15). Considering the activity of CTAB@$SiO_2$ treated textile against both tested viruses and its relative stability manifested by low levels of silicon and CTAB in the wash-offs (Table 10), this textile shows a strong application potential. Considerable antiviral activity combined with durability makes CTAB@$SiO_2$ coated textile an attractive candidate for antiviral use.

It must be noted that earlier studies on antiviral textiles reported in the literature generally do not consider a potential loss of antiviral activity of their agent after loading onto the textile. In our study we compared, without going deeply into details, the efficacy of antiviral compounds before and after their incorporation into the textile. The efficacy decreased upon textile attachment, which may be due to variation in contact area between virus and surface, spatial differences, masking of antiviral nanostructures by textile fibers and other factors. It is worth noting, however, that the decrease is not independent of the nature of the antiviral agent. Thus, CTAB@$SiO_2$ exhibited less antiviral activity than nano-ceria in colloid form but was found to be more efficient on textile. Based on antiviral profile of CTAB@$SiO_2$ treated textiles we can suggest that in semi-dry experimental conditions intrinsic moisture of the particles, i.e. water in form of aqueous CTAB solution entrapped in their mesopores plays a crucial role in the antiviral activity of textiles. According to our rough estimation, aqueous CTAB solution comprises about 50% of the particles' weight. The presence of water in the particles has no impact on their activity as colloids, i.e. in aqueous medium, but becomes

important under the deficiency of solvent. Apparently, the amount of water from the particles and from virus stock (20 μL per piece) is enough to provide a release of the active compound and its contact with virus. Unlike silica-based nanoparticles, both (+) and (−) nano-$CeO_2$ are highly crystalline and contain only a negligible amount of intrinsic moisture.

The textile treated with $Cu(NO_3)_2$ demonstrated considerable virucidal activity due to high and rapid solubility of copper nitrate in water. On the other hand, such a high solubility sets limitations on the durability of the material; that is $SiO_2$ nanocontainers with their tight attachment to the surface and gradual release of active component are the most promising option among the studied materials.

Putting our results into a wider context, two closely connected problems must be taken into consideration while developing antimicrobial textiles: finding appropriate antiviral material and selecting proper application-relevant testing conditions. It is safe to assume that the majority of known antiviral materials require water to achieve their full functionality, i.e., to enable a contact between virus and antiviral agent, and to participate in virus-agent chemical interactions. Many inorganic materials exhibiting antiviral properties under wet testing conditions (copper and silver metal nanoparticles, zinc, titanium and copper oxides nanoparticles, etc.) apparently would not demonstrate any significant activity in dry or semi-dry conditions. Nanocontainers, on the other hand, in a form of porous inorganic or polymeric nanoparticles, hydrogels, activated carbon, etc., can contain significant amount of internal moisture to enable the antiviral interaction. This opens a perspective for their usage in the antiviral treatment of textiles that are not in direct contact with water and are operated under average or low humidity conditions. The importance of proper experimental design and application relevant testing conditions has been widely discussed in literature in recent years [156–159]. Even the commercial products claimed antibacterial demonstrate no effect when tested under realistic conditions [159]. Our results demonstrate a dramatic difference between antiviral profile of tested materials in wet and semi-dry testing conditions and put forward the role of application-relevant experimental setup.

# 6. CONCLUSIONS

The main goal of this work was to develop an antiviral treatment for textiles based on nanomaterials deposited on their surface and to study their efficacy in semi-dry conditions approximating real-life usage of textiles. In accordance with the aims of the work, we synthesized a series of nanomaterials and studied their antiviral activity in various experimental setups.

1) We produced a series of $CeO_2$ nanoparticles with minimal concentration of foreign surface groups influencing the biological activity using a synthetic approach based on well-known precipitation and hydrothermal methods. We developed a technique for loading antiviral organic compound (CTAB) into silica nanocontainers for controlled release in semi-dry conditions. [**I**, **II**]

2) Our study demonstrated a significant antiviral activity of both positively and negatively charged cerium dioxide nanoparticles in colloidal form against several enveloped viruses (coronaviruses SARS-CoV-2 and TGEV, influenza virus and bacteriophage Φ6). In contrast, non-enveloped viruses were not susceptible to nano-ceria. Interestingly, both types of ceria nanoparticles exhibited almost no bactericidal activity and cytotoxicity, which makes them highly promising for targeted antiviral treatment against enveloped viruses. CTAB-loaded mesoporous silica nanocontainers demonstrated considerable activity against two coronaviruses as well. Unexpectedly, silver nanoparticles synthesized in the same conditions exhibited significant bactericidal activity and cytotoxicity, but almost no pronounced antiviral properties. [**I**, **II**]

3) As an approach to the mechanism of specific antiviral activity of ceria nanoparticles, their interaction with a model amino acid (tryptophan, selected as a protein component prone to oxidation) was studied using NMR spectroscopy. It was shown that oxidation of tryptophan by cerium dioxide is not related to ROS formation but is based on a proton-coupled electron transfer mechanism leading to the formation of 3-hydroxypyrroloindol carboxylic acid, a product characteristic for the tryptophan oxidation in living organisms. [**III**]

4) A range of potentially antiviral textiles was prepared using a simple spray-coating technique. The study of the microstructure of treated textiles revealed the dependence of the uniformity of nanomaterial distribution on the size of its particles. While $CeO_2$ tends to form a continuous layer on the fiber surface, CTAB-loaded $SiO_2$ forms islands of various sizes. Since polyester composing the textile has no surface functional groups capable of forming covalent bonds with nanoparticles under spraying conditions, we suggest that the attachment of the particles onto the textile occurs solely via adhesion. [**II**]

5) The antiviral activity of coated textiles against two coronaviruses (SARS-CoV-2 and TGEV) was evaluated in semi-dry experimental conditions imitating the transmission of a virus during the real-life textile use. Prior to the antiviral test, it was demonstrated that TGEV stays infectious for up to

48 hours on the untreated textiles, and SARS-CoV-2 even longer. The textile treated with CTAB-loaded silica nanocontainers exhibited significant activity against both tested viruses after 24 hours of exposure. In contrast, both types of cerium dioxide nanoparticles deposited on textile, unlike colloidal form, showed little to no antiviral activity. [**II**]

6) Obtained results suggest that in semi-dry experimental conditions intrinsic moisture of the particles, i.e. water in the form of aqueous CTAB solution entrapped in their mesopores, plays a crucial role in the antiviral activity of textiles. The presence of water in the particles has no impact on their activity as colloids, i.e. in aqueous medium, but becomes important under the deficiency of solvent. Unlike silica-based nanoparticles, both (+) and (−) nano-$CeO_2$ are highly crystalline and contain only negligible amount of intrinsic moisture. [**II**]

7) Elemental analysis of wash-off solutions during our antiviral tests demonstrated a low level of silicon and bromine, which means that textiles treated with CTAB-loaded silica nanocontainers are firmly attached to the textile fibers. This fact, in addition to a significant antiviral activity in reasonable exposure time, makes silica-based nanocontainers a promising material for the development of antiviral textiles. [**II**]

# 7. SUMMARY IN ESTONIAN

**Oksiidsed nanostruktuurid tekstiilide antiviraalseks töötluseks**

Viiruste põhjustatud haigused võivad mõjutada negatiivselt inimeste igapäevaelu, mistõttu on viirusnakkuste leviku ennetamine oluline uurimisteema. Üks viiruste olulistest levikuviisidest on puutepindade kaudu. On teada, et viirused võivad pikemalt püsima jääda ning ka nakkusvõimelistena püsida pehmetel pindadel ja seetõttu võiksid viirusvastased tekstiilid olla üheks oluliseks abivahendiks viirusnakkuste ennetamisel. Selliste tekstiilide kasutusala võiks olla üsna laialdane alates toiduainete pakendamisest kuni tihti puudutatavate pindadeni ühistranspordis, koolides ja lasteaedades, hooldekodudes ja tervishoiuasutustes. Käesoleva doktoritöö peamine eesmärk oli disainida viirusvastaseid tekstiilmaterjale, mille antiviraalsed omadused säiliksid ka madala õhuniiskusega keskkonnas, kuna ühiskasutatavates ruumides on tekstiilid, nt pehme mööbli katted, kardinad jne, kasutuses enamasti just sellistes tingimustes. Tekstiili antiviraalse töötluse vahenditeks valiti metalsed ja oksiidsed nanoosakesed, kuna varasemalt oli teada nende võimalik viirusvastane mõju, samuti on võimalik selliseid nanostruktuure kasutada ka mõne alternatiivse antiviraalse molekuli kandjana. Töö esimeses faasis sünteestiti väljavalitud nanostruktuurid, need iseloomustati ning testiti nende antiviraalseid omadusi suspensioonis. Seejärel valiti välja perspektiivsed ühendid ja järgnenud tekstiilide viirusvastane testimine viidi läbi juba poolkuivades tingimustes, kus viirusosakesed kanti tekstiilidele aerosoolina. Antud töö olulisemad järeldused on:

1) Tseeriumdioksiidi nanoosakesed, mida antud töös sünteesiti nii positiivse kui ka negatiivse pinnalaenguga, omavad kolloidses vormis olulist aktiivsust meie poolt testitud ümbrisega (membraaniga) viiruste vastu, nagu koroonaviirused SARS-CoV-2 ja TGEV, gripiviirus ja bakteriofaag Φ6. Ümbriseta (membraanita) viiruste vastu tseeriumoksiidi nanoosakesed kolloidses vormis aktiivsed ei olnud. Viirusvastaste omaduste kõrval ei omanud $CeO_2$ nanoosakesed ei tsütotoksilisust ega bakterivastast aktiivsust, mistõttu võiks neid nanostruktuure kasutada spetsiifiliselt viirusvastasel eesmärgil. Huvitav oli leid, et hõbeda nanoosakesed ei omanud kolloidses vormis mingit viirusvastast toimet, kuid samas olid bakterivastased ning samuti tsütotoksilised. Sünteesiti veel üks oksiidne nanostruktuur, mis mõjus kolloidses olekus viirusvastasena – mesopoorne ränidioksiidi ja kvaternaarse ammooniumiühendi CTABi komposiit. Ülalmainitud kahte viirusvastast oksiidset nanostruktuuri testiti edaspidi kui võimalikke viirusvastaseid katteid tekstiili pinnal.
2) $CeO_2$ nanoosakeste viirusvastase mõjumehhanismi uurimisel selgus, et tõenäoliselt toimivad need nanostruktuurid läbi aminohapete spetsiiflise oksüdeerimise, kahjustades selliselt viiruse valkude struktuuri.

3) Väljavalitud kahe nanomaterjali – tseeriumoksiidi ja CTABi ning ränidioksiidi komposiidi osakeste pihustamisel tekstiili pinnale selgus, et kui tseeriumoksiid moodustab tekstiili pinnale ühtlase katte, siis mesopoorne ränidioksiidi ja CTABi komposiit kinnitus tekstiili pinnale paiguti. Kuna kasutatud polüestertekstiilil puuduvad spetsiifilised funktsionaalsed grupid, siis toimus nanoosakeste tekstiili pinnale kinnitumine ainult läbi adhesiooni, mis toimis kahe kasutatud nanomaterjali tüübi puhul erinevalt.

4) Poolkuivades tingimustes läbi viidud viirusvastane test näitas, et kuigi kolloidses vormis toimisid antiviraalsena nii $CeO_2$ kui ränidioksiidi ja CTABi komposiitsed nanoosakesed, siis tekstiilile pihustatuna toimis viirusvastasena vaid mesopoorse ränidioksiidi ja CTABi komposiit. Võib arvata, et selle põhjuseks oli erinevus nende materjalide sisemises veesisalduses: tseeriumoksiidi veesisaldus on madal, kuid ränidioksiidi pooridesse on arvatavasti lukustatud mingi hulk vett, mis ka poolkuivades tingimustes võimaldas tekstiilil antiviraalsena toimida. Viirusvastasena toimis ka positiivse kontrollina kasutatud vasknitraadi lahusega immutatud tekstiil, kuid kuna sellisest tekstiilist leostus aja jooksul välja suures hulgas vaseioone, siis võib eeldada, et sellise tekstiili antiviraalne toime kaob peale esimest kokkupuudet vedelikega. Samal ajal ei leostunud tekstiilidest mesopoorse ränidioksiidi ja CTABi komposiit ning sellise tekstiili viirusvastane toime oleks seetõttu pikaajalisem.

Kokkuvõttes näitasid meie tulemused, et nanostruktuuride viirusvastased omadused sõltuvad oluliselt testitingimustest, mis viitab sellele, et materjalide antiviraalseid omadusi tuleb testida nende päriselu rakendusele lähedastest tingimustes. Antiviraalsetes rakendustes on soovitatav kasutada kõrge sisemise veesisaldusega nanostruktuure, mis võimaldavad efektiivset kokkupuudet viirustega. Arvestades tekstiilile kaetud mesopoorse ränidioksiidi ja CTABi komposiidi viirusvastast mõju ning selle materjali püsivust tekstiili pinnal võiks ränidioksiidi ja CTABi komposiitseid nanostruktuure kaaluda sobiva materjalina antiviraalsete pinnakatete arendamisel.

# 8. ACKNOWLEDGEMENTS

I am profoundly grateful to my supervisors Angela Ivask, Vambola Kisand and Alexander Vanetsev for their constant guidance, support and patience. I feel lucky to be a member of our team and work under your supervision.

I sincerely thank Dr. Andres Merits, Dr. Eva Zusinaite, Dr. Kai Rausalu from the Institute of Bioengineering of the University of Tartu for our collaboration. I would like to express my special gratitude to Kai who gave me my first unforgettable lessons in work with cell cultures and viruses. It is my pleasant duty to mention here as well Dr. Alla Piirsoo, Dr. Krystyna Naumenko, Yevheniia Zholudenko, Dr. Sandra Koit, Dr. Sainan Wang, Dr. Nastassia Shtaida, Galina Halus, Regina Virre, Artemi Maljavin, who generously shared with me their experience, time, reagents and working space and were always willing to help.

I am grateful to my colleagues from the Institute of Physics Mati Kook and Dr. Dmytro Danilian who taught me and helped me with instrumental methods, and Dr Tanel Tätte who brought us all together.

Thanks to Dr. Merilin Rosenberg, Dr. Hanna Ainelo, Harleen Kaur, Sandra Park, Brenda Raid (Institute of Molecular and Cell Biology).

I thank all my coauthors. It was a pleasure to work together and to contribute to the collaborative research.

My PhD journey was not short and straightforward, and I would like to mention more people who made it possible. I am grateful to the staff of the Kelluke kindergarten, to the teachers of Annelinn school and to my former boss Madis Einasto for his patience and support.

I thank my family and friends who supported me and believed in me. My very special thanks to my dearest daughter Olja who found the word ‘compelling’ for my Introduction.

And, finally, I’m grateful to the city of Tartu which is a continuous source of inspiration for me.

The financial support was granted by the Estonian Research Council Grants (COVSG2, PRG1496, TK141, TK210) and the European Commission project STOP (Grant agreement ID: 101057961).

This work was financially supported by Estonian Research Council Grants (COVSG2, PRG1496, TK210), the European Commission project STOP (Grant agreement ID: 101057961). This work was also supported by The Centre of Excellence project TK141 (2014–2020.4.01.15-0011), Functional Materials and Technology Doctoral School (FMTDK) (2014–2020.4.01.16-0027) and Estonian Doctoral School (2021–2027.4.04.24-0003), all co-funded by the European Union.

# 9. REFERENCES


1. https://www.who.int/news-room/fact-sheets/detail/influenza-(seasonal).
2. https://data.who.int/dashboards/covid19/deaths.
3. Leung, N. H. L. (2021). Transmissibility and transmission of respiratory viruses. *Nature Reviews Microbiology*, *19*(8), 528–545. https://doi.org/10.1038/s41579-021-00535-6
4. Kutter, J. S., Spronken, M. I., Fraaij, P. L., Fouchier, R. A., & Herfst, S. (2018). Transmission routes of respiratory viruses among humans. *Current Opinion in Virology*, *28*, 142–151. https://doi.org/10.1016/j.coviro.2018.01.001
5. Rheinbaben, F. v., Schünemann, S., Groß, T., & Wolff, M. H. (2000). Transmission of viruses via contact in ahousehold setting: experiments using bacteriophage φX174 as a model virus. *Journal of Hospital Infection*, *46*(1), 61–66. https://doi.org/10.1053/jhin.2000.0794
6. Jin, T., Chen, X., Nishio, M., Zhuang, L., Shiomi, H., Tonosaki, Y., … Zhang, N. (2022). Interventions to prevent surface transmission of an infectious virus based on real human touch behavior: a case study of the norovirus. *International Journal of Infectious Diseases*, *122*, 83–92. https://doi.org/10.1016/j.ijid.2022.05.047
7. for the PANDHUB consortium, Ikonen, N., Savolainen-Kopra, C., Enstone, J. E., Kulmala, I., Pasanen, P., … Ruutu, P. (2018). Deposition of respiratory virus pathogens on frequently touched surfaces at airports. *BMC Infectious Diseases*, *18*(1), 437. https://doi.org/10.1186/s12879-018-3150-5
8. Fong, M. W., Leung, N. H. L., Xiao, J., Chu, D. K. W., Cheng, S. M. S., So, H. C., … Cowling, B. J. (2020). Presence of Influenza Virus on Touch Surfaces in Kindergartens and Primary Schools. *The Journal of Infectious Diseases*, *222*(8), 1329–1333. https://doi.org/10.1093/infdis/jiaa114
9. Sun, Z., & Ostrikov, K. (Ken). (2020). Future antiviral surfaces: Lessons from COVID-19 pandemic. *Sustainable Materials and Technologies*, *25*, e00203. https://doi.org/10.1016/j.susmat.2020.e00203
10. Rakowska, P. D., Tiddia, M., Faruqui, N., Bankier, C., Pei, Y., Pollard, A. J., … Gilmore, I. S. (2021). Antiviral surfaces and coatings and their mechanisms of action. *Communications Materials*, *2*(1), 53. https://doi.org/10.1038/s43246-021-00153-y
11. Koonin, E. V., Dolja, V. V., Krupovic, M., & Kuhn, J. H. (2021). Viruses Defined by the Position of the Virosphere within the Replicator Space. *Microbiology and Molecular Biology Reviews*, *85*(4), e00193-20. https://doi.org/10.1128/MMBR.00193-20
12. Wagner, E. K., Hewlett, M. J., & Hewlett, M. J. (2004). *Basic virology* (2nd ed.). Malden, Mass.: Blackwell Science.
13. Wisskirchen, K., Lucifora, J., Michler, T., & Protzer, U. (2014). New pharmacological strategies to fight enveloped viruses. *Trends in Pharmacological Sciences*, *35*(9), 470–478. https://doi.org/10.1016/j.tips.2014.06.004
14. https://ictv.global/about/taxonomy. (n.d.). Retrieved from https://ictv.global/about/taxonomy
15. Siddell, S. G., Smith, D. B., Adriaenssens, E., Alfenas-Zerbini, P., Dutilh, B. E., Garcia, M. L., … Zerbini, F. M. (2023). Virus taxonomy and the role of the International Committee on Taxonomy of Viruses (ICTV). *Journal of General Virology*, *104*(5). https://doi.org/10.1099/jgv.0.001840

16. Koonin, E. V., Krupovic, M., & Agol, V. I. (2021). The Baltimore Classification of Viruses 50 Years Later: How Does It Stand in the Light of Virus Evolution? *Microbiology and Molecular Biology Reviews*, *85*(3), e00053-21. https://doi.org/10.1128/MMBR.00053-21
17. Galdiero, S., Falanga, A., Vitiello, M., Cantisani, M., Marra, V., & Galdiero, M. (2011). Silver Nanoparticles as Potential Antiviral Agents. *Molecules*, *16*(10), 8894–8918. https://doi.org/10.3390/molecules16108894
18. Hussain, F. S., Abro, N. Q., Ahmed, N., Memon, S. Q., & Memon, N. (2022). Nano-antivirals: A comprehensive review. *Frontiers in Nanotechnology*, *4*, 1064615. https://doi.org/10.3389/fnano.2022.1064615
19. Liang, L., Ahamed, A., Ge, L., Fu, X., & Lisak, G. (2020). Advances in Antiviral Material Development. *ChemPlusChem*, *85*(9), 2105–2128. https://doi.org/10.1002/cplu.202000460
20. Balasubramaniam, B., Prateek, Ranjan, S., Saraf, M., Kar, P., Singh, S. P., … Gupta, R. K. (2021). Antibacterial and Antiviral Functional Materials: Chemistry and Biological Activity toward Tackling COVID-19-like Pandemics. *ACS Pharmacology & Translational Science*, *4*(1), 8–54. https://doi.org/10.1021/acsptsci.0c00174
21. Mouritz, A. P., Galos, J., Linklater, D. P., Ladani, R. B., Kandare, E., Crawford, R. J., & Ivanova, E. P. (2021). Towards antiviral polymer composites to combat COVID-19 transmission. *Nano Select*, *2*(11), 2061–2071. https://doi.org/10.1002/nano.202100078
22. https://eur-lex.europa.eu/legal-content/EN/TXT/?uri=CELEX:32011H0696. (n.d.). Retrieved from https://eur-lex.europa.eu/legal-content/EN/TXT/?uri=CELEX:32011H0696
23. Luceri, A., Francese, R., Lembo, D., Ferraris, M., & Balagna, C. (2023). Silver Nanoparticles: Review of Antiviral Properties, Mechanism of Action and Applications. *Microorganisms*, *11*(3), 629. https://doi.org/10.3390/microorganisms11030629
24. Tortella, G. R., Pieretti, J. C., Rubilar, O., Fernández-Baldo, M., Benavides-Mendoza, A., Diez, M. C., & Seabra, A. B. (2022). Silver, copper and copper oxide nanoparticles in the fight against human viruses: progress and perspectives. *Critical Reviews in Biotechnology*, *42*(3), 431–449. https://doi.org/10.1080/07388551.2021.1939260
25. Rios-Ibarra, C., Salinas-Santander, M., Orozco-Nunnelly, D., & Bravo-Madrigal, J. (2024). Nanoparticle-based antiviral strategies to combat the influenza virus (Review). *Biomedical Reports*, *20*(4), 65. https://doi.org/10.3892/br.2024.1753
26. Hmed, A. A., El-Gebaly, A. S., Refaey, E. E., Youssef, A. M., & Sofy, A. R. (2025). Antiviral potential of copper and titanium dioxide nanoparticles against H1N1, Adenovirus 40 and herpes simplex virus type-II. *Inorganic Chemistry Communications*, *171*, 113605. https://doi.org/10.1016/j.inoche.2024.113605
27. Lozovski, V., Lysenko, V., Piatnytsia, V., Scherbakov, O., Zholobak, N., & Spivak, M. (2012). Physical Point of View for Antiviral Effect Caused by the Interaction Between the Viruses and Nanoparticles. *Journal of Bionanoscience*, *6*(2), 109–112. https://doi.org/10.1166/jbns.2012.1084
28. Li, Y., Li, J., Li, M., Sun, J., Shang, X., & Ma, Y. (2024). Biological mechanism of ZnO nanomaterials. *Journal of Applied Toxicology*, *44*(1), 107–117. https://doi.org/10.1002/jat.4522

29. Bhatti, A., & DeLong, R. K. (2023). Nanoscale Interaction Mechanisms of Antiviral Activity. *ACS Pharmacology & Translational Science*, *6*(2), 220–228. https://doi.org/10.1021/acsptsci.2c00195
30. Mishra, Y. K., Adelung, R., Röhl, C., Shukla, D., Spors, F., & Tiwari, V. (2011). Virostatic potential of micro–nano filopodia-like ZnO structures against herpes simplex virus-1. *Antiviral Research*, *92*(2), 305–312. https://doi.org/10.1016/j.antiviral.2011.08.017
31. Abd-El-Aziz, A., Fouda, M. M. G., Sharaby, C. M., Xiao, O., Zhang, X., Alzahrany, Y. A., … Abd-El-Aziz, A. S. (2024). Recent Developments in Antimicrobial and Antiviral Agents Based on Natural/Synthetic Polymers and Dendrimers: Design and Therapeutic Applications. *Macromolecular Chemistry and Physics*, *225*(17), 2400123. https://doi.org/10.1002/macp.202400123
32. Gupta, C. K., & Krishnamurthy, N. (1992). Extractive metallurgy of rare earths. *International Materials Reviews*, *37*(1), 197–248. https://doi.org/10.1179/imr.1992.37.1.197
33. Scirè, S., & Palmisano, L. (2020). Cerium and cerium oxide: A brief introduction. In *Cerium Oxide ($CeO_2$): Synthesis, Properties and Applications* (pp. 1–12). Elsevier. https://doi.org/10.1016/B978-0-12-815661-2.00001-3
34. Trovarelli, A. (2014). *Catalysis by Ceria and Related Materials* (1st ed.). Singapore: Imperial College Press., Chapters 1 and 2
35. Schmitt, R., Nenning, A., Kraynis, O., Korobko, R., Frenkel, A. I., Lubomirsky, I., … Rupp, J. L. M. (2020). A review of defect structure and chemistry in ceria and its solid solutions. *Chemical Society Reviews*, *49*(2), 554–592. https://doi.org/10.1039/C9CS00588A
36. Montini, T., Melchionna, M., Monai, M., & Fornasiero, P. (2016). Fundamentals and Catalytic Applications of $CeO_2$ -Based Materials. *Chemical Reviews*, *116*(10), 5987–6041. https://doi.org/10.1021/acs.chemrev.5b00603
37. Mohamed, H. E. A., Afridi, S., Khalil, A. T., Ali, M., Zohra, T., Akhtar, R., … Maaza, M. (2020). Promising Antiviral, Antimicrobial and Therapeutic Properties of Green Nanoceria. *Nanomedicine*, *15*(5), 467–488. https://doi.org/10.2217/nnm-2019-0368
38. Pugazhendhi, A. S., Neal, C. J., Ta, K. M., Molinari, M., Kumar, U., Wei, F., … Coathup, M. J. (2024). A neoteric antibacterial ceria-silver nanozyme for abiotic surfaces. *Biomaterials*, *307*, 122527. https://doi.org/10.1016/j.biomaterials.2024.122527
39. Sun, C., Li, H., & Chen, L. (2012). Nanostructured ceria-based materials: synthesis, properties, and applications. *Energy & Environmental Science*, *5*(9), 8475. https://doi.org/10.1039/c2ee22310d
40. Baldim, V., Bedioui, F., Mignet, N., Margaill, I., & Berret, J.-F. (2018). The enzyme-like catalytic activity of cerium oxide nanoparticles and its dependency on $Ce^{3+}$ surface area concentration. *Nanoscale*, *10*(15), 6971–6980. https://doi.org/10.1039/C8NR00325D
41. Heckert, E. G., Karakoti, A. S., Seal, S., & Self, W. T. (2008). The role of cerium redox state in the SOD mimetic activity of nanoceria. *Biomaterials*, *29*(18), 2705–2709. https://doi.org/10.1016/j.biomaterials.2008.03.014
42. Yang, Y., Mao, Z., Huang, W., Liu, L., Li, J., Li, J., & Wu, Q. (2016). Redox enzyme-mimicking activities of $CeO_2$ nanostructures: Intrinsic influence of exposed facets. *Scientific Reports*, *6*(1), 35344. https://doi.org/10.1038/srep35344

43. Melchionna, M., Trovarelli, A., & Fornasiero, P. (2020). Synthesis and properties of cerium oxide-based materials. In *Cerium Oxide ($CeO_2$): Synthesis, Properties and Applications* (pp. 13–43). Elsevier. https://doi.org/10.1016/B978-0-12-815661-2.00002-5
44. André, R. F., Rousse, G., Sassoye, C., Avdeev, M., Lassalle-Kaiser, B., Baptiste, B., & Carenco, S. (2023). From $Ce(OH)_3$ to Nanoscaled $CeO_2$ : Identification and Crystal Structure of a Cerium Oxyhydroxide Intermediate Phase. *Chemistry of Materials*, *35*(13), 5040–5048. https://doi.org/10.1021/acs.chemmater.3c00486
45. Ivanov, V. K., Polezhaeva, O. S., Shcherbakov, A. B., Gil', D. O., & Tret'yakov, Yu. D. (2010). Microwave-hydrothermal synthesis of stable nanocrystalline ceria sols for biomedical uses. *Russian Journal of Inorganic Chemistry*, *55*(1), 1–5. https://doi.org/10.1134/S0036023610010018
46. Xie, A., Wang, S., Liu, W., Zhang, J., Yang, Y., & Han, J. (2015). Rapid hydro-thermal synthesis of $CeO_2$ nanoparticles with (220)-dominated surface and its CO catalytic performance. *Materials Research Bulletin*, *62*, 148–152. https://doi.org/10.1016/j.materresbull.2014.11.029
47. Hassan, M. S., Khan, R., Amna, T., Yang, J., Lee, I.-H., Sun, M.-Y., … Khil, M. S. (2016). The influence of synthesis method on size and toxicity of $CeO_2$ quantum dots: Potential in the environmental remediation. *Ceramics International*, *42*(1), 576–582. https://doi.org/10.1016/j.ceramint.2015.08.149
48. Henych, J., Šťastný, M., Ederer, J., Němečková, Z., Pogorzelska, A., Tolasz, J., … Janoš, P. (2022). How the surface chemical properties of nanoceria are related to its enzyme-like, antiviral and degradation activity. *Environmental Science: Nano*, *9*(9), 3485–3501. https://doi.org/10.1039/D2EN00173J
49. Sekiguchi, S., Umezawa, E., Yamanaka, H. I., Fujino, K., Motoshiromizu, T., Ouchi, M. K., … Taharaguchi, S. (2024). Efficient inactivation of influenza virus through adsorption of nanoceria and its oxidative power. *Chemistry Letters*, *53*(7), upae124. https://doi.org/10.1093/chemle/upae124
50. Zholobak, N. M., Olevinskaia, Z. M., Spivak, N. I., Shcherbakov, A. B., Ivanov, V. K., & Usatenko, A. V. (2010). [Antiviral effect of cerium dioxide nanoparticles stabilized by low-molecular polyacrylic acid]. *Mikrobiolohichnyi Zhurnal (Kiev, Ukraine: 1993)*, *72*(3), 42–47.
51. Umezawa, E., Fujino, K., Yamanaka, H. I., Sekiguchi, S., Motoshiromizu, T., Ouchi, M. K., … Taharaguchi, S. (2025). Nonwoven fabric coated with cerium oxide nanoparticles for viral inactivation and transmission Inhibition. *Scientific Reports*, *15*(1), 10340. https://doi.org/10.1038/s41598-025-94199-4
52. Dutta, P., Pal, S., Seehra, M. S., Shi, Y., Eyring, E. M., & Ernst, R. D. (2006). Concentration of $Ce^{3+}$ and Oxygen Vacancies in Cerium Oxide Nanoparticles. *Chemistry of Materials*, *18*(21), 5144–5146. https://doi.org/10.1021/cm061580n
53. Zhang, H., Qiu, J., Yan, B., Liu, L., Chen, D., & Liu, X. (2021). Regulation of Ce (III) / Ce (IV) ratio of cerium oxide for antibacterial application. *iScience*, *24*(3), 102226. https://doi.org/10.1016/j.isci.2021.102226
54. Xia, T., Kovochich, M., Liong, M., Mädler, L., Gilbert, B., Shi, H., … Nel, A. E. (2008). Comparison of the Mechanism of Toxicity of Zinc Oxide and Cerium Oxide Nanoparticles Based on Dissolution and Oxidative Stress Properties. *ACS Nano*, *2*(10), 2121–2134. https://doi.org/10.1021/nn800511k

55. Celardo, I., De Nicola, M., Mandoli, C., Pedersen, J. Z., Traversa, E., & Ghibelli, L. (2011). $Ce^{3+}$ Ions Determine Redox-Dependent Anti-apoptotic Effect of Cerium Oxide Nanoparticles. *ACS Nano*, *5*(6), 4537–4549. https://doi.org/10.1021/nn200126a
56. Hijaz, M., Das, S., Mert, I., Gupta, A., Al-Wahab, Z., Tebbe, C., … Rattan, R. (2016). Folic acid tagged nanoceria as a novel therapeutic agent in ovarian cancer. *BMC Cancer*, *16*(1), 220. https://doi.org/10.1186/s12885-016-2206-4
57. Kwon, H. J., Kim, D., Seo, K., Kim, Y. G., Han, S. I., Kang, T., … Hyeon, T. (2018). Ceria Nanoparticle Systems for Selective Scavenging of Mitochondrial, Intracellular, and Extracellular Reactive Oxygen Species in Parkinson's Disease. *Angewandte Chemie International Edition*, *57*(30), 9408–9412. https://doi.org/10.1002/anie.201805052
58. Ramos-Zúñiga, J., Bruna, N., & Pérez-Donoso, J. M. (2023). Toxicity Mechanisms of Copper Nanoparticles and Copper Surfaces on Bacterial Cells and Viruses. *International Journal of Molecular Sciences*, *24*(13), 10503. https://doi.org/10.3390/ijms241310503
59. Długosz, O., Żebracka, A., Sochocka, M., Franz, D., Ochnik, M., Chmielowiec-Korzeniowska, A., & Banach, M. (2025). Selective and complementary anti-microbial and antiviral activity of silver, copper, and selenium nanoparticle suspensions in deep eutectic solvent. *Environmental Research*, *264*, 120351. https://doi.org/10.1016/j.envres.2024.120351
60. Warnes, S. L., Little, Z. R., & Keevil, C. W. (2015). Human Coronavirus 229E Remains Infectious on Common Touch Surface Materials. *mBio*, *6*(6), e01697-15. https://doi.org/10.1128/mBio.01697-15
61. Foster, A. W., Osman, D., & Robinson, N. J. (2014). Metal Preferences and Metallation. *Journal of Biological Chemistry*, *289*(41), 28095–28103. https://doi.org/10.1074/jbc.R114.588145
62. Department of Textile Design, National Institute of Fashion Technology, Bhubaneswar, India, Bar, G., Biswas, D., Department of Textile Design, National Institute of Fashion Technology, Bhubaneswar, India, Pati, S., Department of Textile Design, National Institute of Fashion Technology, Bhubaneswar, India, … Laboratoire Génie de Production, LGP, Université de Toulouse, INP-ENIT, Tarbes, France. (2021). Anti viral Finishing on Texti les – An Overview. *Textile & Leather Review*, *4*(1), 5–22. https://doi.org/10.31881/TLR.2020.17
63. Miyauchi, M., Sunada, K., & Hashimoto, K. (2020). Antiviral Effect of Visible Light-Sensitive CuxO/TiO2 Photocatalyst. *Catalysts*, *10*(9), 1093. https://doi.org/10.3390/catal10091093
64. Mazurkova, N. A., Spitsyna, Yu. E., Shikina, N. V., Ismagilov, Z. R., Zagrebel'nyi, S. N., & Ryabchikova, E. I. (2010). Interaction of titanium dioxide nanoparticles with influenza virus. *Nanotechnologies in Russia*, *5*(5–6), 417–420. https://doi.org/10.1134/S1995078010050174
65. Biswas, A., Kar, U., & Jana, N. R. (2022). Cytotoxicity of ZnO nanoparticles under dark conditions *via* oxygen vacancy dependent reactive oxygen species generation. *Physical Chemistry Chemical Physics*, *24*(22), 13965–13975. https://doi.org/10.1039/D2CP00301E
66. Lekki-Porębski, S. A., Rakowski, M., & Grzelak, A. (2023). Free zinc ions, as a major factor of ZnONP toxicity, disrupts free radical homeostasis in CCRF-CEM cells. *Biochimica et Biophysica Acta (BBA) – General Subjects*, *1867*(10), 130447. https://doi.org/10.1016/j.bbagen.2023.130447

67. Siddiqi, K. S., Ur Rahman, A., Tajuddin, & Husen, A. (2018). Properties of Zinc Oxide Nanoparticles and Their Activity Against Microbes. *Nanoscale Research Letters*, *13*(1), 141. https://doi.org/10.1186/s11671-018-2532-3
68. Antoine, T. E., Mishra, Y. K., Trigilio, J., Tiwari, V., Adelung, R., & Shukla, D. (2012). Prophylactic, therapeutic and neutralizing effects of zinc oxide tetrapod structures against herpes simplex virus type-2 infection. *Antiviral Research*, *96*(3), 363–375. https://doi.org/10.1016/j.antiviral.2012.09.020
69. Ye, S., Shao, K., Li, Z., Guo, N., Zuo, Y., Li, Q., … Han, H. (2015). Antiviral Activity of Graphene Oxide: How Sharp Edged Structure and Charge Matter. *ACS Applied Materials & Interfaces*, *7*(38), 21571–21579. https://doi.org/10.1021/acsami.5b06876
70. Deokar, A. R., Nagvenkar, A. P., Kalt, I., Shani, L., Yeshurun, Y., Gedanken, A., & Sarid, R. (2017). Graphene-Based "Hot Plate" for the Capture and Destruction of the Herpes Simplex Virus Type 1. *Bioconjugate Chemistry*, *28*(4), 1115–1122. https://doi.org/10.1021/acs.bioconjchem.7b00030
71. Donskyi, I. S., Azab, W., Cuellar-Camacho, J. L., Guday, G., Lippitz, A., Unger, W. E. S., … Haag, R. (2019). Functionalized nanographene sheets with high antiviral activity through synergistic electrostatic and hydrophobic interactions. *Nanoscale*, *11*(34), 15804–15809. https://doi.org/10.1039/C9NR05273A
72. Park, S., Ko, Y.-S., Lee, S. J., Lee, C., Woo, K., & Ko, G. (2018). Inactivation of influenza A virus via exposure to silver nanoparticle-decorated silica hybrid composites. *Environmental Science and Pollution Research*, *25*(27), 27021–27030. https://doi.org/10.1007/s11356-018-2620-z
73. Martínez-Abad, A., Ocio, M. J., Lagarón, J. M., & Sánchez, G. (2013). Evaluation of silver-infused polylactide films for inactivation of Salmonella and feline calicivirus in vitro and on fresh-cut vegetables. *International Journal of Food Microbiology*, *162*(1), 89–94. https://doi.org/10.1016/j.ijfoodmicro.2012.12.024
74. Mori, Y., Ono, T., Miyahira, Y., Nguyen, V. Q., Matsui, T., & Ishihara, M. (2013). Antiviral activity of silver nanoparticle/chitosan composites against H1N1 influenza A virus. *Nanoscale Research Letters*, *8*(1), 93. https://doi.org/10.1186/1556-276X-8-93
75. Nguyen, V. Q., Ishihara, M., Kinoda, J., Hattori, H., Nakamura, S., Ono, T., … Matsui, T. (2014). Development of antimicrobial biomaterials produced from chitin-nanofiber sheet/silver nanoparticle composites. *Journal of Nanobiotechnology*, *12*(1), 49. https://doi.org/10.1186/s12951-014-0049-1
76. LaBauve, A. E., Rinker, T. E., Noureddine, A., Serda, R. E., Howe, J. Y., Sherman, M. B., … Negrete, O. A. (2018). Lipid-Coated Mesoporous Silica Nanoparticles for the Delivery of the ML336 Antiviral to Inhibit Encephalitic Alphavirus Infection. *Scientific Reports*, *8*(1), 13990. https://doi.org/10.1038/s41598-018-32033-w
77. Lee, E. C., Nguyen, C. T. H., Strounina, E., Davis-Poynter, N., & Ross, B. P. (2018). Structure–Activity Relationships of GAG Mimetic-Functionalized Mesoporous Silica Nanoparticles and Evaluation of Acyclovir-Loaded Antiviral Nanoparticles with Dual Mechanisms of Action. *ACS Omega*, *3*(2), 1689–1699. https://doi.org/10.1021/acsomega.7b01662
78. Otto, D. P., & De Villiers, M. M. (2020). Layer-by-Layer Nanocoating of Antiviral Polysaccharides on Surfaces to Prevent Coronavirus Infections. *Molecules*, *25*(15), 3415. https://doi.org/10.3390/molecules25153415

79. Erkoc, P., & Ulucan-Karnak, F. (2021). Nanotechnology-Based Antimicrobial and Antiviral Surface Coating Strategies. *Prosthesis*, *3*(1), 25–52. https://doi.org/10.3390/prosthesis3010005
80. Vasickova, P., Pavlik, I., Verani, M., & Carducci, A. (2010). Issues Concerning Survival of Viruses on Surfaces. *Food and Environmental Virology*, *2*(1), 24–34. https://doi.org/10.1007/s12560-010-9025-6
81. Huang, H., Fan, C., Li, M., Nie, H.-L., Wang, F.-B., Wang, H., … Huang, J. (2020). COVID-19: A Call for Physical Scientists and Engineers. *ACS Nano*, *14*(4), 3747–3754. https://doi.org/10.1021/acsnano.0c02618
82. Lishchynskyi, O., Shymborska, Y., Stetsyshyn, Y., Raczkowska, J., Skirtach, A. G., Peretiatko, T., & Budkowski, A. (2022). Passive antifouling and active self-disinfecting antiviral surfaces. *Chemical Engineering Journal*, *446*, 137048. https://doi.org/10.1016/j.cej.2022.137048
83. Linklater, D. P., Mah, S. Wl., Tzanov, V., Baulin, V., Borg, N. A., Moad, G., … Ivanova, E. P. (2023). Current perspectives on the development of virucidal nano surfaces. *Current Opinion in Colloid & Interface Science*, *67*, 101720. https://doi.org/10.1016/j.cocis.2023.101720
84. Wang, N., Ferhan, A. R., Yoon, B. K., Jackman, J. A., Cho, N.-J., & Majima, T. (2021). Chemical design principles of next-generation antiviral surface coatings. *Chemical Society Reviews*, *50*(17), 9741–9765. https://doi.org/10.1039/D1CS00317H
85. Behzadinasab, S., Williams, M. D., Hosseini, M., Poon, L. L. M., Chin, A. W. H., Falkinham, J. O., & Ducker, W. A. (2021). Transparent and Sprayable Surface Coatings that Kill Drug-Resistant Bacteria Within Minutes and Inactivate SARS-CoV-2 Virus. *ACS Applied Materials & Interfaces*, *13*(46), 54706–54714. https://doi.org/10.1021/acsami.1c15505
86. Bobrin, V. A., Chen, S.-P., Grandes Reyes, C. F., Sun, B., Ng, C. K., Kim, Y., … Monteiro, M. J. (2021). Water-Borne Nanocoating for Rapid Inactivation of SARS-CoV-2 and Other Viruses. *ACS Nano*, *15*(9), 14915–14927. https://doi.org/10.1021/acsnano.1c05075
87. Zhang, Y., Fan, W., Sun, Y., Chen, W., & Zhang, Y. (2021). Application of anti-viral materials in textiles: A review. *Nanotechnology Reviews*, *10*(1), 1092–1115. https://doi.org/10.1515/ntrev-2021-0072
88. Kumar, U., Fox, C. R., Feit, C., Kolanthai, E., Sheiber, J., Fu, Y., … Seal, S. (2022). ALD based nanostructured zinc oxide coated antiviral silk fabric. *RSC Advances*, *12*(30), 19327–19339. https://doi.org/10.1039/D2RA02653H
89. Prakash, J., Cho, J., & Mishra, Y. K. (2022). Photocatalytic TiO2 nanomaterials as potential antimicrobial and antiviral agents: Scope against blocking the SARS-COV-2 spread. *Micro and Nano Engineering*, *14*, 100100. https://doi.org/10.1016/j.mne.2021.100100
90. Bregnocchi, A., Jafari, R., & Momen, G. (2022). Design strategies for antiviral coatings and surfaces: A review. *Applied Surface Science Advances*, *8*, 100224. https://doi.org/10.1016/j.apsadv.2022.100224
91. Nicastro, F., Sironi, G., Antonello, E., Bianco, A., Biasin, M., Brucato, J. R., … Clerici, M. (2021). Solar UV-B/A radiation is highly effective in inactivating SARS-CoV-2. *Scientific Reports*, *11*(1), 14805. https://doi.org/10.1038/s41598-021-94417-9

92. Sagripanti, J., & Lytle, C. D. (2007). Inactivation of Influenza Virus by Solar Radiation. *Photochemistry and Photobiology*, *83*(5), 1278–1282. https://doi.org/10.1111/j.1751-1097.2007.00177.x
93. Li, W., Wang, Y., Tang, X., Yuen, T. T. T., Han, X., Li, J., … Wang, L. (2021). Liquid repellency enabled antipathogen coatings. *Materials Today Bio*, *12*, 100145. https://doi.org/10.1016/j.mtbio.2021.100145
94. Soni, R., Joshi, S. R., Karmacharya, M., Min, H., Kim, S.-K., Kumar, S., … Lee, C. Y. (2021). Superhydrophobic and Self-Sterilizing Surgical Masks Spray-Coated with Carbon Nanotubes. *ACS Applied Nano Materials*, *4*(8), 8491–8499. https://doi.org/10.1021/acsanm.1c01082
95. Ruz, J. J., Tamayo, J., Pini, V., Kosaka, P. M., & Calleja, M. (2014). Physics of Nanomechanical Spectrometry of Viruses. *Scientific Reports*, *4*(1), 6051. https://doi.org/10.1038/srep06051
96. Tarannum, T., & Ahmed, S. (2023). Recent development in antiviral surfaces: Impact of topography and environmental conditions. *Heliyon*, *9*(6), e16698. https://doi.org/10.1016/j.heliyon.2023.e16698
97. Harper, G. J. (1963). The influence of environment on the survival of airborne virus particles in the laboratory. *Archiv for die gesamte Virusforschung*, *13*(1–3), 64–71. https://doi.org/10.1007/BF01243824
98. Kaur, H., Rosenberg, M., Kook, M., Danilian, D., Kisand, V., & Ivask, A. (2024). Antibacterial activity of solid surfaces is critically dependent on relative humidity, inoculum volume, and organic soiling. *FEMS Microbes*, *5*, xtad022. https://doi.org/10.1093/femsmc/xtad022
99. Gonçalves, A., Bertrand, J., Ke, R., Comets, E., De Lamballerie, X., Malvy, D., … Guedj, J. (2020). Timing of Antiviral Treatment Initiation is Critical to Reduce SARS-CoV-2 Viral Load. *CPT: Pharmacometrics & Systems Pharmacology*, *9*(9), 509–514. https://doi.org/10.1002/psp4.12543
100. Fu, J., Liu, T., Binte Touhid, S. S., Fu, F., & Liu, X. (2023). Functional Textile Materials for Blocking COVID-19 Transmission. *ACS Nano*, *17*(3), 1739–1763. https://doi.org/10.1021/acsnano.2c08894
101. Iyigundogdu, Z. U., Demir, O., Asutay, A. B., & Sahin, F. (2017). Developing Novel Antimicrobial and Antiviral Textile Products. *Applied Biochemistry and Biotechnology*, *181*(3), 1155–1166. https://doi.org/10.1007/s12010-016-2275-5
102. Tang, P., Zhang, Z., El-Moghazy, A. Y., Wisuthiphaet, N., Nitin, N., & Sun, G. (2020). Daylight-Induced Antibacterial and Antiviral Cotton Cloth for Offensive Personal Protection. *ACS Applied Materials & Interfaces*, *12*(44), 49442–49451. https://doi.org/10.1021/acsami.0c15540
103. Zhong, H., Zhu, Z., Lin, J., Cheung, C. F., Lu, V. L., Yan, F., … Li, G. (2020). Reusable and Recyclable Graphene Masks with Outstanding Superhydrophobic and Photothermal Performances. *ACS Nano*, *14*(5), 6213–6221. https://doi.org/10.1021/acsnano.0c02250
104. Lee, S., Nam, J.-S., Han, J., Zhang, Q., Kauppinen, E. I., & Jeon, I. (2021). Carbon Nanotube Mask Filters and Their Hydrophobic Barrier and Hyperthermic Antiviral Effects on SARS-CoV-2. *ACS Applied Nano Materials*, *4*(8), 8135–8144. https://doi.org/10.1021/acsanm.1c01386
105. Issman, L., Graves, B., Terrones, J., Hosmillo, M., Qiao, R., Glerum, M., … Boies, A. (2021). Filtration of viral aerosols via a hybrid carbon nanotube active filter. *Carbon*, *183*, 232–242. https://doi.org/10.1016/j.carbon.2021.07.004

106. Borkow, G., Zhou, S. S., Page, T., & Gabbay, J. (2010). A Novel Anti-Influenza Copper Oxide Containing Respiratory Face Mask. *PLoS ONE*, *5*(6), e11295. https://doi.org/10.1371/journal.pone.0011295
107. Gabbay, J., Borkow, G., Mishal, J., Magen, E., Zatcoff, R., & Shemer-Avni, Y. (2006). Copper Oxide Impregnated Textiles with Potent Biocidal Activities. *Journal of Industrial Textiles*, *35*(4), 323–335. https://doi.org/10.1177/1528083706060785
108. Heine, E., Knops, H. G., Schaefer, K., Vangeyte, P., & Moeller, M. (2007). Antimicrobial Functionalisation of Textile Materials. In S. Duquesne, C. Magniez, & G. Camino (Eds.), *Multifunctional Barriers for Flexible Structure* (Vol. 97, pp. 23–38). Berlin, Heidelberg: Springer Berlin Heidelberg. https://doi.org/10.1007/978-3-540-71920-5_2
109. Damerchely, R., Mohammad Esmail Yazdanshenas, Rashidi, A.-S., & Khajavi, R. (2011). Morphology and mechanical properties of antibacterial nylon 6/nano-silver nano-composite multifilament yarns. *Textile Research Journal*, *81*(16), 1694–1701. https://doi.org/10.1177/0040517511410104
110. Kalaj, M., & Cohen, S. M. (2020). Postsynthetic Modification: An Enabling Technology for the Advancement of Metal–Organic Frameworks. *ACS Central Science*, *6*(7), 1046–1057. https://doi.org/10.1021/acscentsci.0c00690
111. Hebeish, A., El-Shafei, A., Sharaf, S., & Zaghloul, S. (2011). Novel precursors for green synthesis and application of silver nanoparticles in the realm of cotton finishing. *Carbohydrate Polymers*, *84*(1), 605–613. https://doi.org/10.1016/j.carbpol.2010.12.032
112. Imai, K., Ogawa, H., Bui, V. N., Inoue, H., Fukuda, J., Ohba, M., … Nakamura, K. (2012). Inactivation of high and low pathogenic avian influenza virus H5 subtypes by copper ions incorporated in zeolite-textile materials. *Antiviral Research*, *93*(2), 225–233. https://doi.org/10.1016/j.antiviral.2011.11.017
113. Gouda, M., Aljaafari, A., Al-Fayz, Y., & Boraie, W. E. (2015). Preparation and Characterization of Some Nanometal Oxides Using Microwave Technique and Their Application to Cotton Fabrics. *Journal of Nanomaterials*, *2015*(1), 586904. https://doi.org/10.1155/2015/586904
114. El-Rafie, M. H., Ahmed, H. B., & Zahran, M. K. (2014). Characterization of nanosilver coated cotton fabrics and evaluation of its antibacterial efficacy. *Carbohydrate Polymers*, *107*, 174–181. https://doi.org/10.1016/j.carbpol.2014.02.024
115. Ibrahim, N. A., Eid, B. M., Abd El-Aziz, E., & Abou Elmaaty, T. M. (2013). Functionalization of linen/cotton pigment prints using inorganic nano structure materials. *Carbohydrate Polymers*, *97*(2), 537–545. https://doi.org/10.1016/j.carbpol.2013.04.084
116. Ibrahim, N. A., Eid, B. M., Elmaaty, T. M. A., & El-Aziz, E. A. (2013). A smart approach to add antibacterial functionality to cellulosic pigment prints. *Carbohydrate Polymers*, *94*(1), 612–618. https://doi.org/10.1016/j.carbpol.2013.01.040
117. Zhang, Y., Xu, Q., Fu, F., & Liu, X. (2016). Durable antimicrobial cotton textiles modified with inorganic nanoparticles. *Cellulose*, *23*(5), 2791–2808. https://doi.org/10.1007/s10570-016-1012-0
118. Jiang, T., Liu, L., & Yao, J. (2011). In situ deposition of silver nanoparticles on the cotton fabrics. *Fibers and Polymers*, *12*(5), 620–625. https://doi.org/10.1007/s12221-011-0620-4

119. Yue, X., Lin, H., Yan, T., Zhang, D., Lin, H., & Chen, Y. (2014). Synthesis of silver nanoparticles with sericin and functional finishing to cotton fabrics. *Fibers and Polymers*, *15*(4), 716–722. https://doi.org/10.1007/s12221-014-0716-8
120. Cady, N. C., Behnke, J. L., & Strickland, A. D. (2011). Copper-Based Nano-structured Coatings on Natural Cellulose: Nanocomposites Exhibiting Rapid and Efficient Inhibition of a Multi-Drug Resistant Wound Pathogen, *A. baumannii*, and Mammalian Cell Biocompatibility In Vitro. *Advanced Functional Materials*, *21*(13), 2506–2514. https://doi.org/10.1002/adfm.201100123
121. Uğur, Ş. S., Sarıışık, M., Aktaş, A. H., Uçar, M. Ç., & Erden, E. (2010). Modifying of Cotton Fabric Surface with Nano-ZnO Multilayer Films by Layer-by-Layer Deposition Method. *Nanoscale Research Letters*, *5*(7), 1204–1210. https://doi.org/10.1007/s11671-010-9627-9
122. Shahidi, S., Ghoranneviss, M., Moazzenchi, B., Rashidi, A., & Mirjalili, M. (2007). Investigation of Antibacterial Activity on Cotton Fabrics with Cold Plasma in the Presence of a Magnetic Field. *Plasma Processes and Polymers*, *4*(S1), S1098–S1103. https://doi.org/10.1002/ppap.200732412
123. Perelshtein, I., Ruderman, Y., Perkas, N., Beddow, J., Singh, G., Vinatoru, M., … Gedanken, A. (2013). The sonochemical coating of cotton withstands 65 washing cycles at hospital washing standards and retains its antibacterial properties. *Cellulose*, *20*(3), 1215–1221. https://doi.org/10.1007/s10570-013-9929-z
124. Petkova, P., Francesko, A., Fernandes, M. M., Mendoza, E., Perelshtein, I., Gedanken, A., & Tzanov, T. (2014). Sonochemical Coating of Textiles with Hybrid ZnO/Chitosan Antimicrobial Nanoparticles. *ACS Applied Materials & Interfaces*, *6*(2), 1164–1172. https://doi.org/10.1021/am404852d
125. Aherne, D., Ledwith, D. M., Gara, M., & Kelly, J. M. (2008). Optical Properties and Growth Aspects of Silver Nanoprisms Produced by a Highly Reproducible and Rapid Synthesis at Room Temperature. *Advanced Functional Materials*, *18*(14), 2005–2016. https://doi.org/10.1002/adfm.200800233
126. Popov, A. L., Zaichkina, S. I., Popova, N. R., Rozanova, O. M., Romanchenko, S. P., Ivanova, O. S., … Ivanov, V. K. (2016). Radioprotective effects of ultra-small citrate-stabilized cerium oxide nanoparticles in vitro and in vivo. *RSC Advances*, *6*(108), 106141–106149. https://doi.org/10.1039/C6RA18566E
127. Guo, Q., Huang, D., Kou, X., Cao, W., Li, L., Ge, L., & Li, J. (2017). Synthesis of disperse amorphous $SiO_2$ nanoparticles via sol–gel process. *Ceramics International*, *43*(1), 192–196. https://doi.org/10.1016/j.ceramint.2016.09.133
128. Liu, X., Lu, X., Wen, P., Shu, X., & Chi, F. (2017). Synthesis of ultrasmall silica nanoparticles for application as deep-ultraviolet antireflection coatings. *Applied Surface Science*, *420*, 180–185. https://doi.org/10.1016/j.apsusc.2017.05.124
129. Agback, P., Agback, T., Dominguez, F., Frolova, E. I., Seisenbaeva, G. A., & Kessler, V. G. (2022). Site-specific recognition of SARS-CoV-2 nsp1 protein with a tailored titanium dioxide nanoparticle – elucidation of the complex structure using NMR data and theoretical calculation. *Nanoscale Advances*, *4*(6), 1527–1532. https://doi.org/10.1039/D1NA00855B
130. Seisenbaeva, G. A., Daniel, G., Nedelec, J.-M., & Kessler, V. G. (2013). Solution equilibrium behind the room-temperature synthesis of nanocrystalline titanium dioxide. *Nanoscale*, *5*(8), 3330. https://doi.org/10.1039/c3nr34068f

131. Sattar, S. A., Zargar, B., & Tetro, J. (2024). Methods to assess environmental surface disinfectants against viruses: the quest and recommendations for a globally harmonized approach to microbicide testing. *Infection Prevention in Practice*, *6*(4), 100395. https://doi.org/10.1016/j.infpip.2024.100395
132. https://eur-lex.europa.eu/legal-content/EN/TXT/HTML/?uri=CELEX:02012R0528-20220415. (n.d.).
133. European Chemicals Agency. (2018). *Guidance on the Biocidal Products Regulation. Volume II, Efficacy. Assessment and Evaluation (Parts B+C)*. LU: Publications Office. Retrieved from https://data.europa.eu/doi/10.2823/95242
134. Bhattacharjee, S. (2016). DLS and zeta potential – What they are and what they are not? *Journal of Controlled Release*, *235*, 337–351. https://doi.org/10.1016/j.jconrel.2016.06.017
135. Jia, Z., Li, J., Gao, L., Yang, D., & Kanaev, A. (2023). Dynamic Light Scattering: A Powerful Tool for In Situ Nanoparticle Sizing. *Colloids and Interfaces*, *7*(1), 15. https://doi.org/10.3390/colloids7010015
136. Asadi Asadabad, M., & Jafari Eskandari, M. (2015). Transmission Electron Microscopy as Best Technique for Characterization in Nanotechnology. *Synthesis and Reactivity in Inorganic, Metal-Organic, and Nano-Metal Chemistry*, *45*(3), 323–326. https://doi.org/10.1080/15533174.2013.831901
137. Aziz, A., Shaikh, H., Abbas, A., Zehra, K. E., & Javed, B. (2025). Microscopic Techniques for Nanomaterials Characterization: A Concise Review. *Microscopy Research and Technique*, *88*(5), 1599–1614. https://doi.org/10.1002/jemt.24799
138. Wilschefski, S., & Baxter, M. (2019). Inductively Coupled Plasma Mass Spectrometry: Introduction to Analytical Aspects. *Clinical Biochemist Reviews*, *40*(3), 115–133. https://doi.org/10.33176/AACB-19-00024
139. Maity, S., Gundampati, R. K., & Suresh Kumar, T. K. (2019). NMR Methods to Characterize Protein-Ligand Interactions. *Natural Product Communications*, *14*(5), 1934578X19849296. https://doi.org/10.1177/1934578X19849296
140. Ahlberg, S., Antonopulos, A., Diendorf, J., Dringen, R., Epple, M., Flöck, R., … Zellner, R. (2014). PVP-coated, negatively charged silver nanoparticles: A multi-center study of their physicochemical characteristics, cell culture and in vivo experiments. *Beilstein Journal of Nanotechnology*, *5*, 1944–1965. https://doi.org/10.3762/bjnano.5.205
141. Zhao, Y., Baeza, J. A., Koteswara Rao, N., Calvo, L., Gilarranz, M. A., Li, Y. D., & Lefferts, L. (2014). Unsupported PVA- and PVP-stabilized Pd nanoparticles as catalyst for nitrite hydrogenation in aqueous phase. *Journal of Catalysis*, *318*, 162–169. https://doi.org/10.1016/j.jcat.2014.07.011
142. Rajukkannu, S., Bunpheng, W., Dhairiyasamy, R., & Gopinath, V. (2025). Efficiency improvement in silicon and perovskite solar cells through nanofluid cooling using citrate and PVP stabilized silver nanoparticles. *Scientific Reports*, *15*(1), 833. https://doi.org/10.1038/s41598-025-85374-8
143. Calvache-Muñoz, J., Prado, F. A., & Rodríguez-Páez, J. E. (2017). Cerium oxide nanoparticles: Synthesis, characterization and tentative mechanism of particle formation. *Colloids and Surfaces A: Physicochemical and Engineering Aspects*, *529*, 146–159. https://doi.org/10.1016/j.colsurfa.2017.05.059
144. Mohan, J. C., Praveen, G., Chennazhi, K. P., Jayakumar, R., & Nair, S. V. (2013). Functionalised gold nanoparticles for selective induction of *in vitro* apoptosis among human cancer cell lines. *Journal of Experimental Nanoscience*, *8*(1), 32–45. https://doi.org/10.1080/17458080.2011.557841

145. Plakhova, T. V., Romanchuk, A. Yu., Yakunin, S. N., Dumas, T., Demir, S., Wang, S., … Kalmykov, S. N. (2016). Solubility of Nanocrystalline Cerium Dioxide: Experimental Data and Thermodynamic Modeling. *The Journal of Physical Chemistry C*, *120*(39), 22615–22626. https://doi.org/10.1021/acs.jpcc.6b05650
146. Rogers, J. V., Parkinson, C. V., Choi, Y. W., Speshock, J. L., & Hussain, S. M. (2008). A Preliminary Assessment of Silver Nanoparticle Inhibition of Monkeypox Virus Plaque Formation. *Nanoscale Research Letters*, *3*(4), 129–133. https://doi.org/10.1007/s11671-008-9128-2
147. Galdiero, S., Rai, M., Gade, A., Falanga, A., Incoronato, N., Russo, L., … Ingle, A. (2013). Antiviral activity of mycosynthesized silver nanoparticles against herpes simplex virus and human parainfluenza virus type 3. *International Journal of Nanomedicine*, 4303. https://doi.org/10.2147/IJN.S50070
148. Morris, D., Ansar, M., Speshock, J., Ivanciuc, T., Qu, Y., Casola, A., & Garofalo, R. (2019). Antiviral and Immunomodulatory Activity of Silver Nanoparticles in Experimental RSV Infection. *Viruses*, *11*(8), 732. https://doi.org/10.3390/v11080732
149. Martins Da Silva Filho, P., Higor Rocha Mariano, P., Lopes Andrade, A., Barros Arrais Cruz Lopes, J., De Azevedo Pinheiro, A., Itala Geronimo De Azevedo, M., … Longhinotti, E. (2023). Antibacterial and antifungal action of CTAB-containing silica nanoparticles against human pathogens. *International Journal of Pharmaceutics*, *641*, 123074. https://doi.org/10.1016/j.ijpharm.2023.123074
150. Lu, L., Sun, R. W.-Y., Chen, R., Hui, C.-K., Ho, C.-M., Luk, J. M., … Che, C.-M. (2008). Silver Nanoparticles Inhibit Hepatitis B virus Replication. *Antiviral Therapy*, *13*(2), 253–262. https://doi.org/10.1177/135965350801300210
151. Ren, X., Glende, J., Yin, J., Schwegmann-Wessels, C., & Herrler, G. (2008). Importance of cholesterol for infection of cells by transmissible gastroenteritis virus. *Virus Research*, *137*(2), 220–224. https://doi.org/10.1016/j.virusres.2008.07.023
152. Saud, Z., Tyrrell, V. J., Zaragkoulias, A., Protty, M. B., Statkute, E., Rubina, A., … Stanton, R. J. (2022). The SARS-CoV2 envelope differs from host cells, exposes procoagulant lipids, and is disrupted in vivo by oral rinses. *Journal of Lipid Research*, *63*(6), 100208. https://doi.org/10.1016/j.jlr.2022.100208
153. Doktorova, M., Heberle, F. A., Kingston, R. L., Khelashvili, G., Cuendet, M. A., Wen, Y., … Dick, R. A. (2017). Cholesterol Promotes Protein Binding by Affecting Membrane Electrostatics and Solvation Properties. *Biophysical Journal*, *113*(9), 2004–2015. https://doi.org/10.1016/j.bpj.2017.08.055
154. Bellmaine, S., Schnellbaecher, A., & Zimmer, A. (2020). Reactivity and degradation products of tryptophan in solution and proteins. *Free Radical Biology and Medicine*, *160*, 696–718. https://doi.org/10.1016/j.freeradbiomed.2020.09.002
155. Nakagawa, M., Kato, S., Nakano, K., & Hino, T. (1981). Dye-sensitized photooxygenation of tryptophan to give N′-formylkynurenine. *J. Chem. Soc., Chem. Commun.*, (16), 855–856. https://doi.org/10.1039/C39810000855
156. Govind, V., Bharadwaj, S., Sai Ganesh, M. R., Vishnu, J., Shankar, K. V., Shankar, B., & Rajesh, R. (2021). Antiviral properties of copper and its alloys to inactivate covid-19 virus: a review. *BioMetals*, *34*(6), 1217–1235. https://doi.org/10.1007/s10534-021-00339-4
157. Kampf, G. (2020). How long can nosocomial pathogens survive on textiles? A systematic review. *GMS Hygiene and Infection Control; 15:Doc10*. https://doi.org/10.3205/DGKH000345

158. Bäumler, W., Eckl, D., Holzmann, T., & Schneider-Brachert, W. (2022). Antimicrobial coatings for environmental surfaces in hospitals: a potential new pillar for prevention strategies in hygiene. *Critical Reviews in Microbiology*, *48*(5), 531–564. https://doi.org/10.1080/1040841X.2021.1991271
159. Klupp, E.-M., Knobling, B., Franke, G., Belmar Campos, C., Maurer, P. M., & Knobloch, J. K. (2023). Activity of antimicrobial examination gloves under realistic conditions: challenge not fulfilled. *Antimicrobial Resistance & Infection Control*, *12*(1), 116. https://doi.org/10.1186/s13756-023-01322-z
160. Pietsch, F., O'Neill, A. J., Ivask, A., Jenssen, H., Inkinen, J., Kahru, A., … Schreiber, F. (2020). Selection of resistance by antimicrobial coatings in the healthcare setting. *Journal of Hospital Infection*, *106*(1), 115–125. https://doi.org/10.1016/j.jhin.2020.06.006
161. Campos, M. D., Zucchi, P. C., Phung, A., Leonard, S. N., & Hirsch, E. B. (2016). The Activity of Antimicrobial Surfaces Varies by Testing Protocol Utilized. *PLOS ONE*, *11*(8), e0160728. https://doi.org/10.1371/journal.pone.0160728

# PUBLICATIONS

# CURRICULUM VITAE


| | |
|---|---|
| **Name:** | Alexandra Nefedova |
| **e-mail:** | alexandra.nefedova@gmail.com |
| **Born** | on 16.10.1977 in Moscow, former USSR |
| **Citizenship:** | Russian |
| **Current workplace:** | University of Tartu, Faculty of Science and Technology, Institute of Physics, X-Ray spectroscopy laboratory, Lab assistant |


**Education**

| | |
|---|---|
| 1994–1999 | Moscow State University, Chemistry department |
| 2016–present | University of Tartu, Institute of Physics, doctoral studies |

**Career**

| | |
|---|---|
| 1999–2003 | Scientific-production association "P&M-Invest", Moscow, Russia, Chemist |
| 2003–2004 | Chimmed Ltd, Moscow, Russia, Chemist |
| 2004–2016 | Renault Russia, Moscow, Russia, Technical documentation specialist |
| 2011–2015 | Parental leave |
| 2015–2020 | Evikontroll Systems OÜ, Tartu, Estonia, Technical documentation specialist |
| 2016–present | University of Tartu, Faculty of Science and Technology, Institute of Physics, Specialist/Lab assistant |

**Conference presentations:**

April 2017, Tartu, FMNT, poster "Solvothermal synthesis of $LaF_3$:$Nd^{3+}$ nanoparticles in comparison with hydrothermal-microwave treatment"

October 2024, Tartu, FMNT, oral presentation "Mechanism of tryptophan oxidation on metal oxide nanoparticles"

**Publications:**


2017 Kaldvee, K.; Nefedova, A.V.; Fedorenko, S.G.; Vanetsev, A.S.; Orlovskaya, E.O.; Puust, L.; Pärs, M.; Sildos, I.; Ryabova, A.V.; Orlovskii, Yu.V. Approaches to contactless optical thermometer in the NIR spectral range based on $Nd^{3+}$ doped crystalline nanoparticles, Journal of Luminescence, 183, 478–485. https://doi.org/10.1016/j.jlumin.2016.11.061.

Vanetsev, A.; Kaldvee, Kaarel; Puust, L.; Keevend, K.; Nefedova, A.; Fedorenko, S.; Baranchikov, A.; Sildos, I.; Rähn, M.; Sammelselg, V.; Orlovskii, Y. Relation of crystallinity and fluorescent properties of $LaF_3$:$Nd^{3+}$ nanoparticles synthesized with different water based techniques, ChemistrySelect, 2, 4874–4871. https://doi.org/10.1002/slct.201701075.

2022 Nefedova, A.; Rausalu, K.; Zusinaite, E.; Vanetsev, A.; Rosenberg, M.; Koppel, K.; Lilla, S.; Visnapuu, M.; Smits, K.; Kisand, V.; Tätte, T.; Ivask, A. Antiviral efficacy of cerium oxide nanoparticles, Scientific Reports, 12, 18746. https://doi.org/10.1038/s41598-022-23465-6.

2023 Nefedova, A.; Rausalu, K.; Zusinaite, E.; Kisand, V.; Kook, M.; Šmits, K.; Vanetsev, A.; Ivask, A., Antiviral efficacy of nanomaterial-treated textiles in real-life like exposure conditions, Heliyon, 9 (9), e20067. https://doi.org/10.1016/j.heliyon.2023.e20067.

2024 Nefedova, A.; Svensson, F. G.; Vanetsev, A. S.; Agback, P.; Agback, T.; Gohil, S.; Kloo, L.; Tätte, T.; Ivask, A.; Seisenbaeva, G. A.; Kessler, V. G., Molecular Mechanisms in Metal Oxide Nanoparticle-Tryptophan Interactions, Inorganic Chemistry, 63 (19), 8556–8566. https://doi.org/10.1021/acs.inorgchem.3c03674.

2025 Vihodceva, S.; Šutka, A.; Iesalnieks, M.; Orlova, L.; Pludonis, A.; Otsus, M.; Sihtmäe, M.; Vija, H.; Nefedova, A.; Ivask, A.; Kahru, A.e; Kasemets, K., Emerging investigator series: $CeO_2$/CuO nanostructured composite with enhanced antimicrobial properties and low cytotoxicity to human keratinocytes in vitro, Environmental Science Nano, 12 (1), 276–291. https://doi.org/10.1039/d4en00501e.

Greijer, B.; Nefedova, A.; Agback, T.; Agback, P.; Kisand, V.; Rausalu, K.; Vanetsev, A.; Seisenbaeva, G. A.; Ivask, A.; Kessler, V. G. Molecular mechanisms behind the anti corona virus activity of small metal oxide nanoparticles, Nanoscale, 17 (7), 3728–3738. https://doi.org/10.1039/d4nr03730h.

Vihodceva, S.; Šutka, A.; Iesalnieks, M.; Sihtmäe, M.; Nefedova, A.; Ivask, A.; Blinova, I.; Maiorov, M.; Vanags, M.; Eiduks, T. V.; Plūdons, A.; Kahru, A.; Kasemets, K., Synthesis and antimicrobial efficacy of magnetic CuO/$Fe_2O_3$/$CuFe_2O_4$ nanostructured composite: Mechanisms of action, cytotoxicity to human keratinocytes in vitro, and ecotoxicity towards *Vibrio fischeri* and *Daphnia magna,* Journal of Environmental Chemical Engineering, 13, (5), October 2025, 117991, https://doi.org/10.1016/j.jece.2025.117991

# ELULOOKIRJELDUS

**Nimi:** Alexandra Nefedova
**e-mail**: alexandra.nefedova@gmail.com
**Sündinud**: 16.10.1977 Moskvas, Venemaa (endine NSVL)
**Kodakondsus:** Venemaa
**Praegune töökoht:** Tartu Ülikool, Füüsika instituut, Röntgenspektroskoopia labor, laborant

**Haridustee**

| | |
|---|---|
| 1994–1999 | Moskva Ülikool, keemia osakond |
| 2016– | Tartu Ülikool, Füüsika instituut, doktorant |

**Töökogemus**

| | |
|---|---|
| 1999–2003 | "P&M-Invest" OÜ, Moskva, Venemaa, Keemik |
| 2003–2004 | Chimmed Ltd, Moskva, Venemaa, Keemik |
| 2004–2016 | Renault Russia, Moskva, Venemaa, Tehnilise dokumentatsiooni spetsialist |
| 2011–2015 | Emapuhkusel |
| 2015–2020 | Evikontroll Systems OÜ, Tartu, Eesti, Tehnilise dokumentatsiooni spetsialist |
| 2016– … | Tartu Ülikool, Füüsika instituut, spetsialist/laborant |

**Konverentsiettekanded:**

Aprill 2017, Tartu, FMNT, poster "Solvothermal synthesis of $LaF_3$:$Nd^{3+}$ nanoparticles in comparison with hydrothermal-microwave treatment"

Oktoober 2024, Tartu, FMNT, suuline ettekanne "Mechanism of tryptophan oxidation on metal oxide nanoparticles"

**Publikatsioonid:**

2017 Kaldvee, K.; Nefedova, A.V.; Fedorenko, S.G.; Vanetsev, A.S.; Orlovskaya, E.O.; Puust, L.; Pärs, M.; Sildos, I.; Ryabova, A.V.; Orlovskii, Yu.V. Approaches to contactless optical thermometer in the NIR spectral range based on $Nd^{3+}$ doped crystalline nanoparticles, Journal of Luminescence, 183, 478–485. https://doi.org/10.1016/j.jlumin.2016.11.061.

Vanetsev, A.; Kaldvee, Kaarel; Puust, L.; Keevend, K.; Nefedova, A.; Fedorenko, S.; Baranchikov, A.; Sildos, I.; Rähn, M.; Sammelselg, V.; Orlovskii, Y. Relation of crystallinity and fluorescent properties of $LaF_3$:$Nd^{3+}$ nanoparticles synthesized with different water based techniques, ChemistrySelect, 2, 4874–4871. https://doi.org/10.1002/slct.201701075.

2022 Nefedova, A.; Rausalu, K.; Zusinaite, E.; Vanetsev, A.; Rosenberg, M.; Koppel, K.; Lilla, S.; Visnapuu, M.; Smits, K.; Kisand, V.; Tätte, T.; Ivask, A. Antiviral efficacy of cerium oxide nanoparticles, Scientific Reports, 12, 18746. https://doi.org/10.1038/s41598-022-23465-6.

2023 Nefedova, A.; Rausalu, K.; Zusinaite, E.; Kisand, V.; Kook, M.; Šmits, K.; Vanetsev, A.; Ivask, A., Antiviral efficacy of nanomaterial-treated textiles in real-life like exposure conditions, Heliyon, 9 (9), e20067. https://doi.org/10.1016/j.heliyon.2023.e20067.

2024 Nefedova, A.; Svensson, F. G.; Vanetsev, A. S.; Agback, P.; Agback, T.; Gohil, S.; Kloo, L.; Tätte, T.; Ivask, A.; Seisenbaeva, G. A.; Kessler, V. G., Molecular Mechanisms in Metal Oxide Nanoparticle-Tryptophan Interactions, Inorganic Chemistry, 63 (19), 8556–8566. https://doi.org/10.1021/acs.inorgchem.3c03674.

2025 Vihodceva, S.; Šutka, A.; Iesalnieks, M.; Orlova, L.; Pludonis, A.; Otsus, M.; Sihtmäe, M.; Vija, H.; Nefedova, A.; Ivask, A.; Kahru, A.; Kasemets, K., Emerging investigator series: $CeO_2$/CuO nanostructured composite with enhanced antimicrobial properties and low cytotoxicity to human keratinocytes in vitro, Environmental Science Nano, 12 (1), 276–291. https://doi.org/10.1039/d4en00501e.

Greijer, B.; Nefedova, A.; Agback, T.; Agback, P.; Kisand, V.; Rausalu, K.; Vanetsev, A.; Seisenbaeva, G. A.; Ivask, A.; Kessler, V. G. Molecular mechanisms behind the anti corona virus activity of small metal oxide nanoparticles, Nanoscale, 17 (7), 3728–3738. https://doi.org/10.1039/d4nr03730h.

Vihodceva, S.; Šutka, A.; Iesalnieks, M.; Sihtmäe, M.; Nefedova, A.; Ivask, A.; Blinova, I.; Maiorov, M.; Vanags, M.; Eiduks, T. V.; Plūdons, A.; Kahru, A.; Kasemets, K., Synthesis and antimicrobial efficacy of magnetic CuO/$Fe_2O_3$/$CuFe_2O_4$ nanostructured composite: Mechanisms of action, cytotoxicity to human keratinocytes in vitro, and ecotoxicity towards *Vibrio fischeri* and *Daphnia magna,* Journal of Environmental Chemical Engineering, 13, (5), October 2025, 117991, https://doi.org/10.1016/j.jece.2025.117991

# DISSERTATIONES SCIENTIAE MATERIALIS UNIVERSITATIS TARTUENSIS

1. **Martin Järvekülg**. Tubular microstructures by Hf-, Zr- and Ti-butoxide gel sheet rolling. Tartu, 2011, 112 p.
2. **Sergei Vlassov**. Investigation of nanoscale interactions and mechanical properties of nanostructures using quartz tuning fork based real-time measurements. Tartu, 2011, 171 p.
3. **Margus Kodu**. Pulsed Laser Deposition of Magnesium Oxide and Barium Ternary Oxides for Plasma Display Protective Layers. Tartu, 2011, 89 p.
4. **Rainer Pärna**. Surface studies of some oxide films. Tartu, 2011, 129 p.
5. **Jevgeni Šulga**. Self-assembly and interaction of nanostructures. Tartu, 2011, 114 p.
6. **Wojciech Kuznik**. Quantum-chemical computer simulations of the linear and non-linear optical properties of pyrazoloquinoline and dicyanopyrazine derivatives. Tartu, 2012, 89 p.
7. **Leonid Dorogin**. Structural and tribological properties of zero- and one-dimensional nanocrystals. Tartu, 2012, 193 p.
8. **Viljar Palmre**. Fabrication and characterization of microporous carbon-based electroactive polymer actuators. Tartu, 2012, 99 p.
9. **Madis Paalo**. Synthesis of CNT-metal oxide nanocomposites: sol-gel process, rheology, structural and functional properties. Tartu, 2014, 175 p.
10. **Raul Välbe**. Developement of ionic liquid composites by sol-gel method for elaboration of industrial nano- and microstructures. Tartu, 2014, 97 p.
11. **Urmas Joost**. Impurity and preparation dependent properties of titania thin films. Tartu, 2014, 155 p.
12. **Madis Umalas**. Application of sol-gel technology for production of ceramic nanocomposites and functional coatings. Tartu, 2015, 136 p.
13. **Elena Samsonova**. Energy transfer probe as a tool to study morphological and structural origins of fluorescence quenching in rare-earth doped nanophosphors. Tartu, 2015, 114 p.
14. **Jay Mondal**. Novel Corrosion Protective Nanostructured Composite Coatings. Tartu, 2016, 104 p.
15. **Kathriin Utt**. Metal oxide mesostructures for optical applications. Tartu, 2016, 88 p.
16. **Kaido Siimon**. Electrospun gelatin cross-linked by glucose. Tartu, 2016, 84 p.
17. **Marko Part**. Combined three-dimensional sol-gel structures and atomic layer deposited thin films. Tartu, 2017, 162 p.
18. **Pejman Rasti**. Analysis of Remote Sensing Image Super Resolution using Fluid Lenses. Tartu, 2017, 188 p.
19. **Ivo Romet**. Recombination luminescence of doped borates: origin and application prospects in dosimetry. Tartu, 2017, 111 p.

20. **Vladimir I. Kondratiev**. Processing and characterization of transparent electrode materials. Tartu, 2017, 111 p.
21. **Taivo Jõgiaas**. Mechanical properties of atomic layer deposited thin films and nanocomposites. Tartu, 2017, 125 p.
22. **Lauri Aarik**. Atomic layer deposition and characterization of thin oxide films for application in protective coatings. Tartu, 2017, 180 p.
23. **Triin Kangur**. Preparation and functional properties of stochastic micro-structured sol-gel silica materials. Tartu, 2018, 96 p.
24. **Marta Berholts**. Fragmentation of ionic and hydrogen-bonded molecules induced by synchrotron radiation. Tartu, 2018, 126 p.
25. **Priit Priimägi**. Development and optimization of 3D-microbatteries. Tartu, 2018, 118 p.
26. **Siim Hödemann**. Residual stress determination in chemically strengthened and thermally tempered glass plates using scattered light method. Tartu, 2019, 146 p.
27. **Jekaterina Kozlova**. Complex characterization of graphene structures on nanometer level. Tartu, 2019, 206 p.
28. **Kristjan Kalam**. Magnetic, electric and structural properties of atomic layer deposited zirconia-based nanolaminates and mixtures. Tartu, 2020, 94 p.
29. **Triinu Vihmann**. Ionic liquids: synthesis and application in lubrication and lithography. Tartu, 2020, 102 p.
30. **Helina Seemen**. Atomic layer deposition and microscopic analysis of magnetically and electrically polarizable thin solid films. Tartu, 2021, 126 p.
31. **Ekaterina Vagapova**. Fluorescence quenching in inorganic crystalline solids activated by neodymium ions; from bulk to micro- and nanocrystals. Tartu, 2021, 116 p.
32. **Evgenii Strugovshchikov**. First-principles studies on rare-earth metal-hydride-based smart materials. Tartu, 2021, 166 p.
33. **Maido Merisalu**. Nanostructured Coatings for Car and Aerospace Industries. Tartu, 2022, 179 p.
34. **Elena Vinogradova**. Optical centers and quantum entangled states of Nd3+ ions in doped fluoride crystals. Tartu, 2023, 92 p.
35. **Dmytro Danilian**. “Photocatalytic materials for water treatment and antimicrobial applications”. Tartu, 2024, 139 p.
36. **Kristel Möls**. Metastable $TiO_2$-II in atomic layer deposited thin and ultrathin films: stabilization, properties and impact on film growth. Tartu, 2024, 112 p.
37. **Helle-Mai Piirsoo**. Mechanical Properties of Nanocomposites with Artificial Periodic Structure. Tartu, 2024, 144 p.
38. **Artjom Berholts**. Light-enhanced sensors of oxidizing gases based on single-layer CVD graphene. Tartu, 2024, 97 p.